

PROBING ENSEMBLE AND SINGLE-MOLECULE BEHAVIOR OF COCAINE-
SENSITIVE DOPAMINE TRANSPORTER WITH ANTAGONIST-CONJUGATED
QUANTUM DOTS

By

Oleg Kovtun

Dissertation

Submitted to the Faculty of the
Graduate School of Vanderbilt University
in partial fulfillment of the requirements

for the degree of

DOCTOR OF PHILOSOPHY

in

Chemistry

December, 2013

Nashville, Tennessee

Approved:

Sandra J. Rosenthal

Randy D. Blakely

Eva M. Harth

David W. Wright

Copyright © 2013 by Oleg Kovtun

All Rights Reserved

Dedicated to my grandfather Ivan Kovtun.

Your unbridled spirit, iron will, and
unquenchable thirst for life will always inspire me.

ACKNOWLEDGEMENTS

HUGE THANK YOU to my advisor and mentor Dr. Sandy Rosenthal for her patience, support, and understanding. Thank you for being by my side through all my ups and downs. Thank you to my co-advisor Dr. Randy Blakely for helping me to become a better scientist. Thank you to my committee members Dr. Eva Harth and Dr. David Wright for all their advice and guidance.

I would like to thank my family for their love, patience, and rock-solid support throughout all of my life and especially the final months of my Ph.D. pursuit. Huge thanks to my second set of parents, my aunt Natalie and my uncle Tudor – you made all of this possible, and for that I will be forever grateful. Thanks to my friends for sharing all those unforgettable experiences that helped me maintain a positive frame of mind in the toughest moments!

Thanks to my Vanderbilt colleagues and fellow Rosenthal group members for their help and support. Special thanks to Dr. Jerry Chang for mentoring me, teaching me everything, and being one of the most kind-hearted and hard-working individuals I have ever met. I miss you, man! Best wishes to you as you are advancing your scientific career – I am confident a GREAT future awaits you. Just make sure you stay true to yourself. Noah and Emily, thank you for being such amazing colleagues and friends. It has been a great pleasure to work with you two, and I will surely miss our engaging coffee dates and lunch breaks! DJ and Ian, thank you for your assistance and collaboration – you have been instrumental in helping me publish the key parts of this dissertation. Finally, I would like to thank the

Department of Chemistry at the Vanderbilt University, the Vanderbilt Institute of Nanoscale Science and Engineering (VINSE), and the National Institutes of Health (NIH) for funding.

TABLE OF CONTENTS

	Page
DEDICATION.....	III
ACKNOWLEDGMENTS	IV
LIST OF TABLES.....	IX
LIST OF FIGURES	X
LIST OF ABBREVIATIONS	XIII
Chapter	
1. INTRODUCTION.....	1
2. BIOLOGICAL APPLICATIONS OF PHOTOLUMINESCENT SEMICONDUCTOR QUANTUM DOTS.....	4
2.1. Introduction	4
2.2. Quantum Dot Material Composition.....	6
2.3. Quantum Dot Solubilization Strategies	7
2.4. Quantum Dot Functionalization Strategies.....	11
2.5. Quantum Dot Biological Applications: Cellular Labeling.....	17
2.6. Quantum Dot Biological Applications: Single QD Tracking.....	20
2.7. Quantum Dot Biological Applications: Intracellular Delivery and Therapeutics	24
2.8. Quantum Dot Biological Applications: FRET-Based Biosensing.....	27
2.9. Quantum Dot Biological Applications: In Vivo Deep Tissue Imaging.....	32
2.10. Quantum Dot Biological Applications: Multimodal Imaging	35
2.11. Quantum Dot Toxicity Concerns.....	36
2.12. Current Limitations of Quantum Dots.....	37
2.13. Summary.....	39
2.14. References	40
3. ENSEMBLE AND SINGLE QUANTUM DOT FLUORESCENCE METHODS IN NEUROTRANSMITTER TRANSPORTER RESEARCH	50
3.1. Introduction	50
3.2. Materials: HEK293 Cell Culture and Reagents.....	53
3.3. Equipment, Software, Accessories.....	55
3.4. Methods	55
3.4.1. Ensemble Microscopy Protocol.....	55
3.4.2. Flow Cytometry Protocol.....	56

3.4.3. Single-Molecule Microscopy Protocol.....	58
3.5. Troubleshooting Notes.....	60
3.6. References.....	64
4. VISUALIZATION OF THE COCAINE-SENSITIVE DOPAMINE TRANSPORTER WITH LIGAND-CONJUGATED QUANTUM DOTS.....	68
4.1. Introduction	68
4.2. Results and Discussion	71
4.2.1. Cocaine Analog Synthesis	72
4.2.2. DAT Visualization in Flp-In-293 Cells in Suspension.....	74
4.2.3. IDT444 and SavQD Dose Response	76
4.2.4. DAT Visualization in HeLa Cells <i>in situ</i>	78
4.2.5. Visualization of PKC-Dependent DAT Internalization.....	79
4.2.6. Quantum Dot Photostability	82
4.3. Conclusion.....	83
4.4. References.....	84
5. A FLOW CYTOMETRY-BASED DOPAMINE TRANSPORTER BINDING ASSAY USING ANTAGONIST-CONJUGATED QUANTUM DOTS	87
5.1. Introduction	87
5.2. Results and Discussion	89
5.3. Summary	93
5.4. References.....	94
6. SINGLE-QUANTUM DOT TRACKING OF DOPAMINE TRANSPORTER PLASMA MEMBRANE DYNAMICS: A LINK BETWEEN TRAFFICKING DYSREGULATION AND ATTENTION DEFICIT/HYPERACTIVITY DISORDER.....	97
6.1. Introduction	97
6.2. Results and Discussion	100
6.2.1. Tracking Single DAT-QD Complexes.....	100
6.2.2. DAT-QD Membrane Dynamics Reveals Confined Behavior.....	102
6.2.3. DAT-QD Lateral Diffusion is Highly Restricted in Two Heterologous Expression systems.....	104
6.2.4. Attention Deficit/Hyperactivity Disorder-Derived DAT Coding Variation Produces Altered Transporter Mobility	109
6.2.5. DAT-615R and DAT-615C Surface Mobility is Differentially Regulated by Methyl- β -Cyclodextrin and Amphetamine	113
6.3. Summary and Conclusion	117
6.4. Experimental Section	118
6.4.1. Materials	118
6.4.2. Cell Culture, Transfections, and Stable Cell Line Generation	118
6.4.3. QD Labeling of DAT-Expressing Flp-In-293 Cells	119
6.4.4. Ganglioside GM1-QD Tracking	120
6.4.5. High-Speed Confocal Microscopy.....	120

6.4.6. Data Analysis.....	120
6.5. References.....	122
7. SUMMARY AND FUTURE DIRECTIONS.....	125
Appendix	
A. QUANTUM DOT APPROACHES FOR TARGET-BASED DRUG SCREENING AND MULTIPLEXED ACTIVE BIOSENSING	127
A.1. Introduction	127
A.2. Quantum Dot Surface Functionalization.....	128
A.3. Quantum Dot-Based Pharmacological Assays.....	130
A.3.1. The Displacement Assay	135
A.3.2. The Active Endpoint Assay	138
A.3.3. The Passive Assay.....	139
A.4. Multiplex Quantum Dot-Based Biosensing via Förster Resonance Energy Transfer.....	141
A.5. Conclusion and Future Outlook	143
A.6. References.....	144

LIST OF TABLES

Table 2.1. Intracellular and extracellular components labeled with QDs	19
Table 3.1 Comparison of the photophysical properties of the commonly encountered fluorescent probes.....	51
Table 3.2. Methodological approaches that enable specific targeting of neurotransmitter transporters.	52
Table 3.3. Troubleshooting a single-QD imaging experiment.	64
Table 6.1. Comparison of median diffusion coefficients and explored areas at 1 s of QD-labeled DAT 615R and DAT 615C variants under basal, methyl- β -cyclodextrin-treated, and amphetamine-treated conditions in Flp-In 293 cells.	112
Table A.1. Quantum dots in biosensing applications of pharmacological relevance.	131

LIST OF FIGURES

Figure 2.1. List of ligands used in the ligand cap exchange solubilization approach.	8
Figure 2.2. List of polymers used in the polymer encapsulation approach.	9
Figure 2.3. QD functionalization strategies.....	12
Figure 2.4. Biomolecules covalently conjugated to the QD surface via EDC/SMCC methodology.	13
Figure 2.5. Quantum dots in cellular and whole animal in vivo imaging.	18
Figure 2.6. Scheme of data processing and analysis in the SQT experiment.	21
Figure 2.7. Single-quantum dot tracking (SQT) examples.	23
Figure 2.8. Achieving specific targeting in photodynamic therapy.	32
Figure 2.9. Sentinel lymph node mapping surgical procedure aided by NIR-emitting type II QDs.	35
Figure 2.10. Fluorescent intermittency of a single semiconductor nanocrystal.	39
Figure 3.1. Structure schematic of tailored organic ligands targeting plasma membrane monoamine transporters.	53
Figure 3.2. Labeling of dopamine transporter (DAT) with ligand-conjugated QDs in live cells. (left) streptavidin-conjugated QDs were used to label DATs previously exposed to a biotinylated, PEGylated cocaine analog.....	57
Figure 3.3. Flow cytometry-based screening of the inhibitory activity of GBR12909, a high-affinity DAT antagonist, using antagonist-conjugated QDs.....	59
Figure 3.4. Time-lapse image series depicting movement of cell surface QD-bound transporters.	60
Figure 3.5. Schematic illustrating trajectory data analysis in a typical single-QD tracking experiment.....	61
Figure 3.6. Comparison of nonspecific cell surface binding of 50 nM AMP TM Dots (A1-F1) and PEGylated AMP TM Dots (A2-F2).....	62
Figure 4.1. Structures of DAT and its relevant substrates.	69
Figure 4.2. (A) The synthetic route used to prepare IDT444 ⁶ . (B). Schematic representation of the two-step DAT labeling approach using IDT ligand and SavQDs.	73

Figure 4.3. Specific SavQD-IDT444 labeling of DAT stably expressed in Flp-In-293 cells. .74	74
Figure 4.4. IDT444 (A) and SavQD (B) dose response curves.....77	77
Figure 4.5. Specific SavQD-IDT444 labeling of DAT stably expressed in living HeLa cells <i>in situ</i>79	79
Figure 4.6. Visualization of DAT internalization in HeLa cells transiently expressing DAT using IDT444-SavQD conjugates.....80	80
Figure 4.7. Photostability comparison between QD655 and FITC.....82	82
Figure 5.1. Schematic of a QD-based assay that uses antagonist-conjugated QDs to determine inhibitory activity of DAT modulators.....90	90
Figure 5.2. Flow cytometry-based screening of the inhibitory activity of GBR12909, a high-affinity DAT antagonist, using antagonist-conjugated QDs.....91	91
Figure 5.3. Flow cytometry-based screening of the inhibitory activity of PMA using antagonist-conjugated QDs.93	93
Figure 6.1. Dopaminergic synapse and dopamine transporter two-dimensional topology.....98	98
Figure 6.2. Time-lapse imaging of DAT in the plasma membrane of stably-transfected Flp-In 293 cells.102	102
Figure 6.3. Single-quantum dot tracking of AMP TM QDs nonspecifically bound to the membrane of Flp-In 293 cells and SavQDs specifically bound to membrane DATs expressed in Flp-In 293 cells.103	103
Figure 6.4. Instantaneous velocity and diffusion behavior of single DAT-QD complexes in HeLa and Flp-In 293 cells.106	106
Figure 6.5. Diffusion behavior of single ganglioside GM1-QD complexes in HeLa and Flp-In 293 cells.....108	108
Figure 6.6. Single-quantum dot tracking of the wildtype DAT 615R variant and the attention deficit/hyperactivity-derived DAT 615C variant in Flp-In 293 cells.....111	111
Figure 6.7. DAT 615R and DAT 615C membrane diffusion after M β CD-mediated cholesterol depletion and amphetamine treatment in Flp-In 293 cells.115	115
Figure A.1. Biologically active, serotonin-conjugated QDs for serotonin transporter (SERT) labeling in living HEK cells.....133	133
Figure A.2. Structure schematic of tailored organic ligands targeting plasma membrane monoamine transporters.134	134

Figure A.3. Possible configurations of a target-based drug screening assay employing QDs.	136
Figure A.4. QD-based fluorescence displacement assay aimed at the discovery of allosteric antidepressants.	137
Figure A.5. High-content screening of the agonist-induced internalization of κ -opioid receptor in human osteocarcinoma cells.....	140
Figure A.6. Schematic of a time-gated FRET relay for multiplexed protease sensing.....	142

LIST OF KEY ABBREVIATIONS

5-HT – serotonin, 5-hydroxytryptamine

ADHD – attention deficit/hyperactivity disorder

AMPH – amphetamine

BirA – biotin ligase

β -CFT - 2- β -carbomethoxy-3- β -(4-fluorophenyl)tropane

CaMKII – calcium/calmodulin-dependent protein kinase II

CtxB – cholera toxin subunit B

DA – dopamine

DAT – dopamine transporter

DHLA – dihydrolipoic acid

EGF – epidermal growth factor

FLIM – fluorescence lifetime imaging microscopy

FRET – fluorescence resonance energy transfer

FWHM – full width at half-max

GlyR – glycine receptor

HD – hydrodynamic diameter

HDA - hexadecylamine

HPLC – high-pressure liquid chromatography

LCE – ligand cap exchange

MALDI – matrix-assisted laser desorption ionization

MBCD – methyl-beta-cyclodextrin

MFI – median fluorescence intensity

MSD – mean-square displacement
NET – norepinephrine transporter
NIR – near-infrared
NTT – neurotransmitter transporter
PDT – photodynamic therapy
PEG – polyethylene glycol
PI – percent inhibition
PKC – protein kinase C
PL – photoluminescence
PMA – phorbol 12-myristate 13-acetate
QD – quantum dot
QY – quantum yield
SAV - streptavidin
SERT – serotonin transporter
SNR – signal-to-noise ratio
SPT – single-particle tracking
SQDT – single quantum dot tracking
TOPO – trioctylphosphonic oxide
WT – wildtype

CHAPTER I

INTRODUCTION

Mental illness incidence rates have skyrocketed in the United States and globally over the past decade. According to the latest statistics of the National Institute of Mental Health, over 26 percent of Americans ages 18 and older suffer from a diagnosable mental disorder in a given year. Evidence from the World Health Organization suggests that nearly half the world's population are affected by mental illness, with a negative impact on self-esteem, interpersonal relationships, and ability to function in daily life. Moreover, emotional health directly influences individual's physical health and can lead to increased crime rates and substance abuse. Mental illness has become the leading cause of disability worldwide – the total costs of brain disorders exceed \$3 trillion. It is apparent that the global community is facing a socioeconomic “ticking bomb” as people succumb to brain disorders. This becomes particularly relevant in times of global economic downturn. In a globalized world, recession-associated increased unemployment, stagnant wages, poverty, and economic distress tightly correlate with increased suicide rates and the prevalence of mental illness. Therefore, appropriate diagnosis and treatment are critical components in the global fight against mental illness. Adequate mental health care is primarily complicated by poor access and ever-increasing complexity of molecular mechanisms underlying mental illness. Indeed, the breakneck pace of technological progress has revolutionized our understanding and perception of mental illness and permitted us to take a deeper look into the intrinsic complexity of the brain at the nanoscale. Our outdated static view of the brain is no longer applicable, and we only begin our journey of uncovering the dynamic image of the brain, a

collection of billions of dynamic interneuron connections that are subject to active remodeling due to internal and external inputs. The recently announced Brain Activity Mapping (BAM) project seeks to apply novel, high-resolution, nanoscale approaches to advance our understanding of the complexity of neural circuits.¹⁻⁴ Since 2002, the mission of our lab has been just that – the development of targeted molecular probes based on semiconductor nanocrystals to aid in the quest of elucidating molecular mechanisms underlying mental illness and discovering novel, more effective therapeutics. We have focused our research efforts on the family of integral membrane monoamine transporters (serotonin transporter, SERT; dopamine transporter, DAT; norepinephrine transporter, NET). To date, we have been pursuing the following goals: (i) synthesis of small-molecule organic ligands that allow non-invasive recognition of monoamine transporters at the surface of live cells, (ii) single-molecule investigation of the role of membrane dynamic nanoscale compartmentalization and dysregulated protein-protein interactions in the onset and progression of mental illness, particularly major depression and attention deficit/hyperactivity disorder, and (iii) development and validation of fluorescence-based drug discovery assays that may aid in high-throughput screening of antidepressant and antipsychotic drug candidates. My own efforts have revolved around the dopamine transporter protein, which has been implicated in psychostimulant abuse, clinical depression, attention deficit/hyperactivity disorder, and Parkinson's disease, and culminated in the development of dopamine transporter-specific, fluorescence-based, high-resolution labeling protocol (Chapter IV), validation of flow cytometry-based, high-content screening assay aimed at discovery of novel dopamine transporter modulators (Chapter V), and single-particle visualization of cell surface dopamine transporters as well as investigation of molecular mechanisms controlling dopamine transporter membrane dynamics (Chapter VI).

I open this dissertation with a thorough overview of the chemical/photophysical properties of semiconductor nanocrystals and their utility in biological research (Chapter II) and a collection of ensemble and single-particle labeling protocols that I have developed and validated over the past few years (Chapter III). I will close with a brief summary of my research accomplishments and offer a glimpse into the future research topics that will be tackled in the Rosenthal lab (Chapter VII).

REFERENCES

- (1) Alivisatos, A. P.; Andrews, A. M.; Boyden, E. S.; Chun, M.; Church, G. M.; Deisseroth, K.; Donoghue, J. P.; Fraser, S. E.; Lippincott-Schwartz, J.; Looger, L. L.; Masmanidis, S.; McEuen, P. L.; Nurmikko, A. V.; Park, H.; Peterka, D. S.; Reid, C.; Roukes, M. L.; Scherer, A.; Schnitzer, M.; Sejnowski, T. J.; Shepard, K. L.; Tsao, D.; Turrigiano, G.; Weiss, P. S.; Xu, C.; Yuste, R.; Zhuang, X., Nanotools for Neuroscience and Brain Activity Mapping. *ACS Nano* 2013, 7 (3), 1850-1866.
- (2) Alivisatos, A. P.; Chun, M.; Church, G. M.; Deisseroth, K.; Donoghue, J. P.; Greenspan, R. J.; McEuen, P. L.; Roukes, M. L.; Sejnowski, T. J.; Weiss, P. S.; Yuste, R., The Brain Activity Map. *Science* 2013, 339 (6125), 1284-1285.
- (3) Alivisatos, A. P.; Chun, M.; Church, George M.; Greenspan, Ralph J.; Roukes, Michael L.; Yuste, R., The Brain Activity Map Project and the Challenge of Functional Connectomics. *Neuron* 2012, 74 (6), 970-974.
- (4) Andrews, A. M.; Weiss, P. S., Nano in the Brain: Nano-Neuroscience. *ACS Nano* 2012, 6 (10), 8463-8464.

CHAPTER II

BIOLOGICAL APPLICATIONS OF PHOTOLUMINESCENT SEMICONDUCTOR QUANTUM DOTS.

2.1. Introduction

Recent advances in photoluminescence-based techniques for molecular biology have allowed investigators to study fundamental biological processes in living systems with unprecedented spatiotemporal resolution in real time. The dynamic nature of biological processes in conjunction with instrumentation progress demanded that new classes of improved probes be developed to allow access to spatial and temporal scales that have largely remained undisturbed by scientific inquiry with conventional biochemical means.¹⁻⁵ Currently, there are several classes of photoluminescent probes available to biologists including, but not limited to, small organic dyes^{5,6}, genetically encoded fluorescent proteins^{7,8}, metal-ligand complexes^{9,10}, silver^{11,12}, carbon^{13,14}, and silicon¹⁵ nanoparticles, and semiconductor nanocrystals¹⁶⁻²¹, termed as quantum dots (QDs). Among these, QDs have already proven to be valuable tools in biological inquiry since their introduction to the field in 1998.^{18,19}

QDs are nanometer-sized semiconductor nanocrystals with the exciton Bohr radius on the order of or smaller than that of the bulk semiconductor material.²² The quantum confinement effects lead to the increase of band gap and the appearance of discrete energy states, and together with the robust inorganic nature of the QDs give rise to their unique photophysical properties.²² QDs are characterized by excellent brightness that is a product of large molar absorption coefficients, typically ranging between 100,000-1,000,000 M⁻¹cm⁻¹ at the first excitonic absorption band, and high photoluminescence (PL) quantum yields (QYs), with values reported close to unity for CdSe/CdZnS nanocrystals emitting in the visible

range (400-700 nm).^{16,23-25} They have broad absorption spectra that gradually decrease towards longer wavelengths and narrow, Gaussian, emission spectra independent of excitation wavelength. The full width at half maximum (FWHM) of the emission spectra are ~ 25-40 nm in the case of CdS, CdSe, CdTe QDs and slightly higher values of ~70-90 nm for PbS and PbSe QDs.^{26,29} The position of the emission peak is size-dependent and shifts to longer wavelengths as the QD size increases. Size tunability of the emission spectra combined with broad absorption spectra enables and considerably simplifies multiplexing, simultaneous imaging of several fluorophores using a single excitation source.³⁰⁻³³ The robust inorganic nature of QDs and effective surface passivation strategies render them resistant to photodegradation under continuous illumination and physiological conditions.^{29,31} Long-term dynamic imaging at high frame rates fully takes advantage of their excellent photostability. PL lifetime of QDs (>10 ns) is significantly longer than conventional organic dyes lifetimes (1-4 ns).^{6,34} Time-gated imaging and fluorescence lifetime imaging microscopy (FLIM) techniques exploit such lifetime differences to achieve higher contrast and signal-to-noise ratio (SNR).³⁵⁻³⁷ However, the complicated multi-exponential fluorescence decay behavior of QDs and significant variations of QD spectral properties within a single batch are intrinsic limitations for fluorescence lifetime-based imaging techniques.^{34,38} Also, with the two-photon absorption cross sections larger than those of any other photoluminescent probe, QDs are an attractive choice for multiphoton in vivo imaging applications.³⁹ Overall, it is the ability to tune QD photophysical properties through synthetic control and surface modification that makes them an exciting class of photoluminescent probes for biological applications.

2.2. Quantum Dot Material Composition

The peak emission wavelength of QDs depends on the material composition in addition to nanocrystal size and the degree of dispersity. Therefore, it is possible to obtain desirable QD optical properties for a given biological application by varying the material constituents of the semiconductor nanocrystal. Cadmium selenide (CdSe) is the most commonly used material for QD preparation. CdSe-based QDs are characterized by high quantum yields and effectively span the entire visible light range (420-660 nm).^{24,26,29,40-42} Other QDs include CdS (II/VI type) that feature blue-shifted peak emission wavelengths extending into the near-ultraviolet region (350-400 nm) and CdTe (II/IV type) that allow biological investigation in the far-red and near-infrared (NIR) spectrum regions (660-750 nm).^{29,43-46} III/V and I-IV-VI₂ QDs such as InP, ternary In_xGa_{1-x}P, and CuInS₂/ZnS have been prepared in attempt to develop more environmentally friendly alternatives to Cd-based semiconductor nanocrystals.⁴⁷⁻⁵² Also, syntheses of NIR-emitting PbS and PbSe QDs (≥700 nm) have been reported.^{26,27} NIR QD probes offer a promising potential in deep tissue and in vivo imaging by dramatically improving tissue penetration depth and minimizing cellular damage from the excitation source.

All of the QD materials mentioned above suffer from low quantum yield and poor thermal and photochemical stability under physiologically relevant conditions if not properly surface-passivated. Encapsulation of a core particle in a shell of wider-bandgap semiconductor material significantly improves QD PL QY and stability by eliminating the presence of reactive surface trap states that induce unfavorable non-radiative relaxation processes and physical degradation.^{26,40-42} A one- or two-layer inorganic shell was shown to increase photoluminescence quantum yield by up to 300%.⁴⁰ As the thickness of the inorganic shell increases, the core particle exhibits higher resistance to degradation. In the

case of CdSe cores, CdS/ZnS is the surface-passivating material of choice to give CdSe/CdZnS core/shell QDs a reported photoluminescence quantum yield in excess of 85%.²³

2.3 Quantum Dot Solubilization Strategies

QDs must satisfy several requirements to be compatible with biological systems. They must be rendered water-soluble and stable in physiologically relevant pH and ionic strength ranges, possess functional surface elements that confer biological specificity, display minimal nonspecific interactions, and retain their optical properties after post-preparative surface modifications. Since core/shell semiconductor nanocrystal synthesis typically takes place in high-temperature, organic, nonpolar solvents, the as-prepared nanocrystals have no intrinsic water solubility due to the hydrophobic nature of the organic capping ligands (trioctylphosphine oxide, TOPO; hexadecylamine, HDA).^{29,42} Currently, the main approaches to rendering as-prepared QDs water-soluble are (i) ligand cap exchange, (ii) encapsulation in a heterobifunctional polymer shell, and (iii) encapsulation in a silica shell. In the ligand cap exchange (LCE) approach, bifunctional ligands, which contain a point of attachment to the core/shell nanocrystal surface and a hydrophilic moiety to aid in aqueous dispersion, displace native organic capping ligands. Surface attachment of the ligand occurs via a thiol (-SH), amine (-NH₂), or phosphine (-PH₂) functionality, and such groups as hydroxyl (-OH), carboxyl (-COOH), methoxy (-OCH₃), and polyethylene glycol [(-OCH₂CH₂)_n] provide the hydrophilic interface that is necessary to render QD water-soluble. Representative examples of the ligands used in LCE approach are demonstrated in Figure 2.1. Thiolated carboxylic acids are commonly chosen as the capping ligands due to the

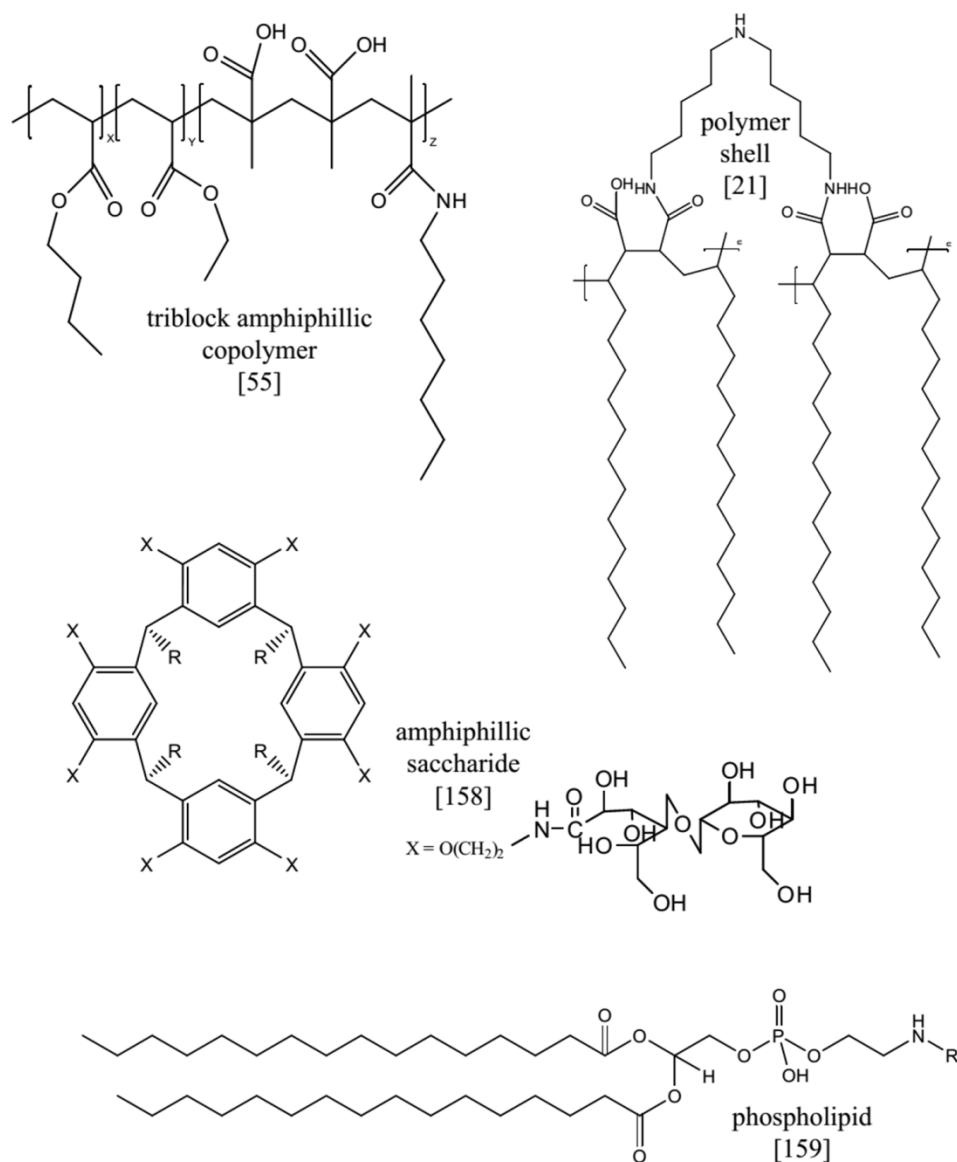


Figure 2.2. List of polymers used in the polymer encapsulation approach.

protrude into the surrounding environment and tightly interdigitate with the aliphatic chains of the added amphiphilic polymer, phospholipid, or amphiphilic polysaccharide through hydrophobic interactions (Figure 2.2). The outer hydrophilic backbone of the resulting polymer shell aids in the aqueous dispersity and colloidal stability of the encapsulated QD water-soluble and presents functionalities necessary for further conjugation (e.g., -COOH).

In the silica encapsulation approach, as-prepared core/shell nanocrystals are coated with an inert silica shell via techniques based on the adapted Stöber method or the water-in-oil reverse microemulsion method.⁵⁶⁻⁶³ The Stöber method is based on the alkaline hydrolysis and condensation of tetraethyl orthosilicate (TEOS) in ethanol:water mixtures and involves surface exchange of the native QD capping ligands with a silane coupling agent such as 3-mercaptopropyl sulfonic acid (MPS). In the microemulsion approach QDs do not act as seeds for silica growth but are instead incorporated into silica spheres formed by the hydrolysis and condensation of TEOS at the water/oil interface.

Each of the QD solubilization approaches mentioned above is associated with distinct advantages and drawbacks and may be chosen depending on the requirements a particular biological system imposes on the photoluminescent probe. Ligand-exchanged QDs are known to suffer from significant quantum yield loss and poor long-term colloidal stability in aqueous buffers due to the surface-altering nature of the ligand-exchange process and the dynamic character of QD-ligand bonds.²⁰ QD stability may be improved through the use of polydentate ligands with multiple attachment sites to the nanocrystal surface. For example, dihydrolipoic acid (DHLA) and oligomeric phosphines were reported to dramatically prolong the shelf life of QDs in comparison to monodentate thiol ligands.^{64,65} In addition, the lack of tools to determine the efficiency of the LCE process and the final surface coverage remains a significant obstacle to broader use of ligand-exchanged QDs in biological applications.²⁰ Amphiphillic polymer encapsulation has thus far been the preferred solubilization strategy since polymer-coated QDs retain the native passivating ligands and do not exhibit significant loss of photoluminescence quantum yield. In addition, the use of an amphiphillic polymer shell results in excellent QD stability over a wide range of pH and aqueous buffer concentrations.⁶⁶ Similar to the polymer shell, silica shell provides QDs with

improved colloidal stability and preserves QD optical properties. However, in contrast to LCE approach, a silica shell and polymer encapsulation significantly increase hydrodynamic diameter (HD) of QDs, with typical HD values of 30-40 nm.^{53,66} Increased post-encapsulation QD size places limits on the applicability of QDs to size-sensitive biological applications such as single-QD tracking (SQT), intracellular delivery, and fluorescence resonance energy transfer (FRET).

An alternative approach to prepare water-soluble QDs is synthesis directly in aqueous medium.⁶⁷⁻⁶⁹ This allows avoiding any post-preparative solubilization modifications and possibly eliminating large decreases in QY associated with such processing. There have been a few reports of aqueous preparations of QDs capped with 3-mercaptopropanol, thioglycerol, thioglycolic acid (TGA), and glutathione.^{69,70} Although a water-based approach is simpler and cost-effective in comparison to the traditional TOPO synthetic methodology, QDs prepared in water tend to suffer from lower quantum yields and broad emission spectra, which severely limits their utility in biology.

2.4. Quantum Dot Functionalization Strategies

QDs must be rendered water-soluble in such a way that they contain or allow subsequent conjugation of functional surface elements, which enable specific recognition of biological targets. In addition, it is desirable to obtain QD conjugates that display minimal nonspecific interaction with the surrounding biological environment. Several methodologies have been developed to confer biological specificity to QDs and can be grouped into covalent conjugation and noncovalent interaction strategies (Figure 2.3).

In covalent conjugation strategy, a reactive group (-COOH, -NH₂, -SH) at the QD surface is coupled to a biomolecule containing a compatible reactive group with the use of a

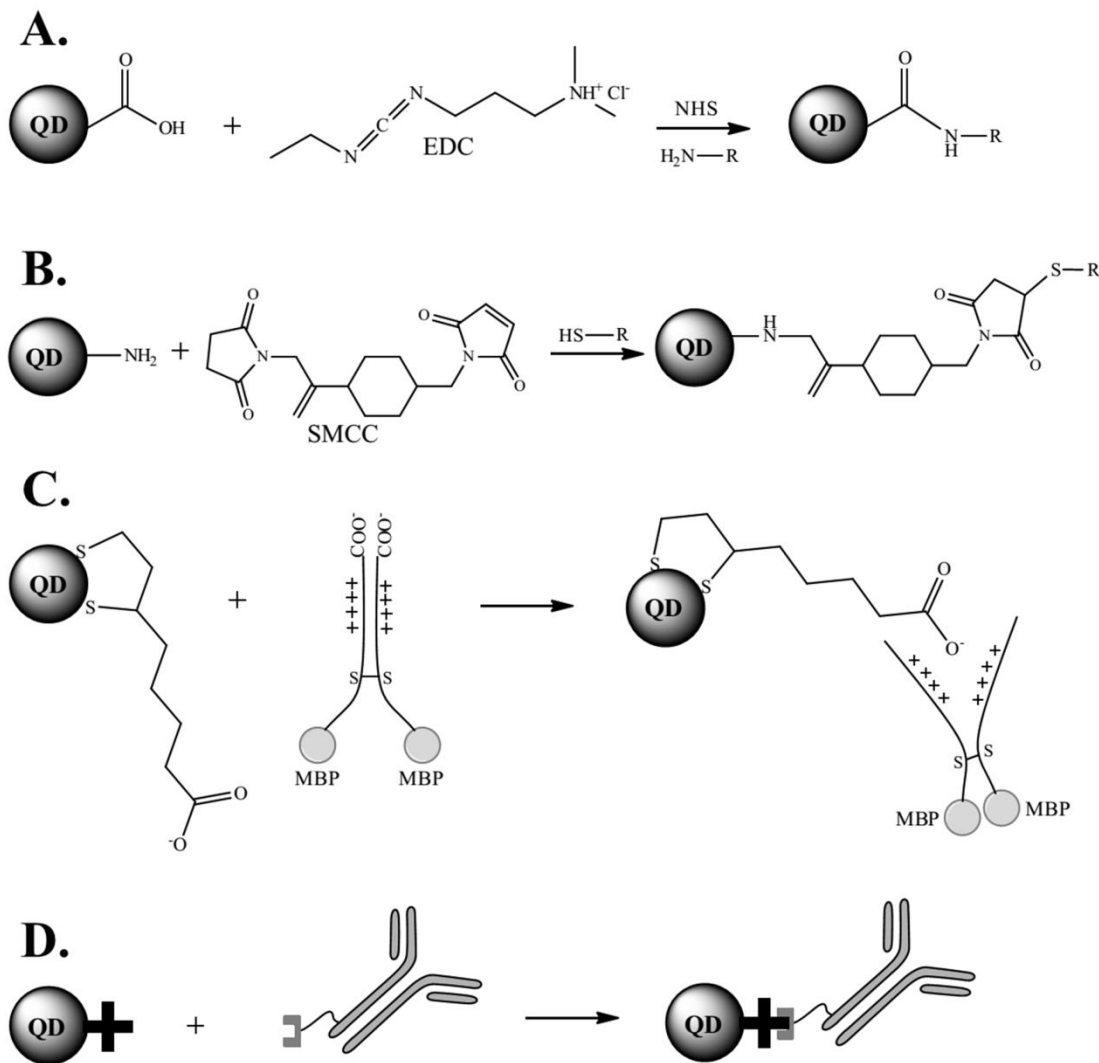


Figure 2.3. QD functionalization strategies. EDC/SMCC covalent conjugation strategies are shown in A and B. Electrostatic assembly of MBP protein on DHLA-capped QDs is shown in C.⁶⁴ Conjugation of streptavidin-conjugated QDs to biotinylated antibody to give an immunofluorescent probe is shown in D.

carbodiimide (EDC) and succinimidyl-4-(N-maleimidomethyl) cyclohexane-1-carboxylate (SMCC) are commonly used to conjugate $-\text{COOH}$ and $-\text{NH}_2$ groups and $-\text{NH}_2$ and $-\text{SH}$ groups respectively (Figure 2.3:A,B). Such covalent conjugation methodology has been employed to couple a variety of biomolecules to QDs including proteins, peptides, nucleic acids, and small molecules (Figure 2.4). Also, direct attachment of biologically active molecules to the QD surface during ligand exchange may also be used to impart QDs with

biological specificity. For example, Pinaud et al. coated CdSe/ZnS core/shell QDs with synthetic phytochelatin-related α peptides that contained a cysteine-rich adhesive domain for direct conjugation to QD surface Zn atoms.⁷¹ Gomez et al. used a combination of mercaptopropionic acid and thiolated RGD peptide to modify the surface of CdS QDs and subsequently target $\alpha v\beta 3$ integrin receptors in rat neuroblastoma PC12 and rat neonatal cortical cells.⁷² In another example, Mitchell and colleagues used alkylthiol-capped oligonucleotides to functionalize CdSe/ZnS core/shell nanocrystals and study their interactions with complementary Au-DNA hybrids.⁷³

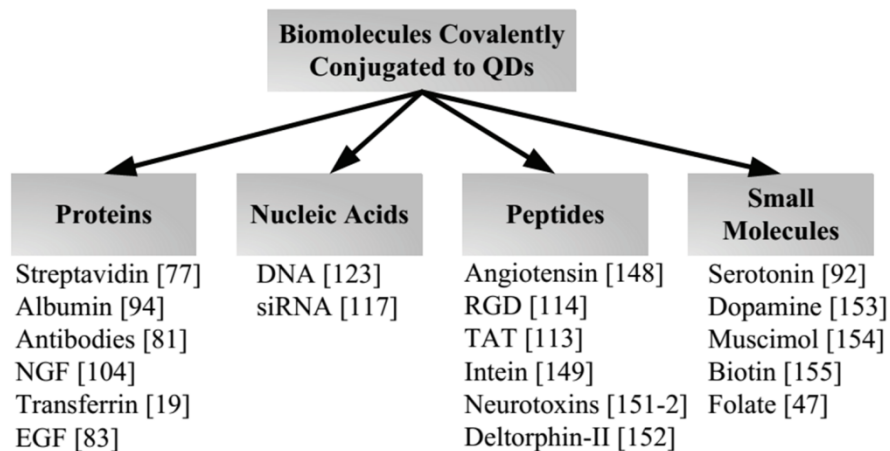


Figure 2.4. Biomolecules covalently conjugated to the QD surface via EDC/SMCC methodology.

Among all the classes of biomolecules successfully conjugated to QDs, polyethylene glycol (PEG) and tetrameric protein streptavidin (Sav) deserve a special mention. PEG is a water-soluble, flexible, organic polymer and is generally considered to be chemically inert and have low toxicity.⁷⁴ Due to their excellent biocompatibility, PEG groups were utilized to address the issue of nonspecific binding to the surrounding environment reported for QDs, especially those functionalized with carboxylic acid groups. Bentzen et al. conjugated PEG chains with average molecular weight of 2000 Da to amphiphilic polyacrylic acid-coated

QDs functionalized with carboxylic acid groups (AMP-QDs).⁷⁵ PEG surface modification significantly reduced nonspecific interactions of AMP-QDs with different cell lines used in the study. In another study, Chattopadhyay et al. observed that PEGylated QDs effectively address the issue of poor separation of dimly and brightly staining cell populations in flow cytometry.³³ Also, passivation with PEG was reported to minimize nonspecific complexation of bovine serum albumin (BSA) with QDs.⁷⁶ Currently, surface passivation with PEG has been employed in a large variety of QD architectures including QDs commercially available from Invitrogen® (Carlsbad, CA).

In 2002, Goldman et al. prepared avidin-conjugated QDs and used them in fluoroimmunoassays in conjunction with antibodies chemically tagged with biotin (biotinylation), a small organic molecule with a high affinity for avidin.⁷⁷ The authors emphasized the general utility and large potential of such mixed covalent conjugation approach whereby avidin is used as a bridge between inorganic semiconductor fluorophores and biotinylated probes. Streptavidin is a homotetrameric protein with a molecular mass of ~52.8 kDa.⁷⁸ Each streptavidin tetramer is capable of binding four biotins, and streptavidin-biotin interaction is one of the strongest and most stable noncovalent interactions known in nature (dissociation constant, $K_D \sim 10^{-15}$ M; half-life, greater than several days).⁷⁹ Glycosylated, positively charged avidin and deglycosylated neutravidin are similar, evolutionary unrelated biotin-binding proteins that may be used instead of streptavidin.⁸⁰ Due to excellent stability, tight interaction, and minimal nonspecific binding, streptavidin-biotin assembly has become a very popular basis for QD biological targeting approach. In 2002, Wu et al. targeted the breast cancer marker Her2 with the QD-streptavidin (QD-strep) conjugates together with humanized anti-Her2 antibody and biotinylated goat anti-human IgG.⁸¹ They also used the multicolored QD-streptavidin conjugates to visualize actin

filaments, microtubules, and nuclear antigens in 3T3 mouse fibroblast cells. In both cases, little to no nonspecific binding was observed when the streptavidin-conjugated QDs were incubated with the cells only. Dahan et al. used the QD-strep conjugates to investigate the diffusion dynamics of individual glycine receptors (GlyR) in the neuronal plasma membrane in a single QD tracking (SQT) experiment.⁸² Again, specific labeling was achieved through the use of a QD-strep conjugate, a biotinylated secondary antibody (Fab fragment), and a GlyR-specific primary antibody. In another example, Lidke et al. relied on biotinylated epidermal growth factor (EGF) and the QD-strep conjugates to elucidate a previously unreported mechanism of retrograde transport to the cell body of the erbB1 receptor tyrosine kinase.⁸³

Although biotinylated antibodies are frequently used in conjunction with QD-strep conjugates for immunofluorescent staining, there are several drawbacks associated with the antibody-based labeling strategy (Figure 2.3 D; Figure 2.5 A).^{84,85} In particular, the final size of the QD-antibody conjugate is large (~50 nm) compared to the labeling target, and the antibody-target interaction often suffers from poor stability. It should also be noted that the generation of an efficient antibody against the extracellular epitope of the biological target of interest is typically a costly and complicated procedure that does not ensure a high-affinity final product. In an attempt to address the weaknesses of the antibody-based labeling, Howarth et al. developed a direct, enzymatic, site-specific cell surface protein targeting strategy.⁸⁶ In this strategy, a fifteen amino acid acceptor peptide sequence (AP) is genetically fused to either C- or N-terminus of the protein, and biotin ligase (BirA) is used to biotinylate a lysine side chain within the AP sequence. The attached biotin then serves as a handle for streptavidin-conjugated QDs. Such strategy was employed by Howarth et al. to label α -amino-3-hydroxy-5-methyl-4-isoxazolepropionate (AMPA) receptors in neurons and

subsequently observe plasma membrane trafficking of the AMPA-QD complex in the crowded synaptic cleft. In a more recent example, Sun et al. utilized BirA to biotinylate calmodulin subunits of myosin X molecular motor and subsequently visualized the movement of myosin X along actin filaments and bundles with QD-strep conjugates.⁸⁷

Alternative specific targeting approaches have recently emerged and are based on the expression of high-affinity fusion tags (CrAsH, Halotag, polyhistidine) by the cellular target.⁸⁸⁻⁹¹ QDs are directed to the target by conjugation with the complementary fusion tag-recognition elements. Our group relies on conjugation of small-molecule ligands to confer biological specificity to QDs.⁸⁵⁻⁹² In 2002, we conjugated serotonin (5-HT), a monoamine neurotransmitter, to CdSe/ZnS core/shell nanocrystals and measured the electrophysiological response of the interactions between QD-5-HT conjugates and 5-HT₃ receptor (Figure 2.5 B). Also, we utilized the QD conjugates to visualize human serotonin transporter protein (hSERT) transiently expressed in human embryonic kidney (HEK) cells. The small-molecule strategy is a cost-effective alternative to antibody-based immunofluorescent labeling that results in significantly smaller final QD size. However, one must ensure that the site of attachment on the small molecule does not alter its biological function.

Biological specificity can also be introduced to QDs via adsorption and electrostatic self-assembly in addition to covalent coupling. Mattoussi et al. constructed two-domain maltose-binding protein-basic leucine zipper (MBP-zp) fusion protein and conjugated it to dihydrolipoic acid (DHLLA)-capped CdSe/ZnS core/shells (Figure 2.3 D).⁶⁴ The MBP-zp fusion protein self-assembled on the surface of DHLLA-capped QDs through electrostatic interactions between negatively charged DHLLA carboxyl groups and positively charged leucine zippers of the MBP-zp fusion protein. Goldman et al. used the highly basic leucine

zipper domain as the basis for the engineered molecular adaptor PG-zb protein, which served as a bridge for subsequent conjugation of IgG antibody to DHLA-capped CdSe/ZnS core/shell nanocrystals.⁹³ In the report by Hanaki et al., a series of ten serum albumins were nonspecifically adsorbed on the surface of CdSe/ZnS core/shells coated with 11-mercaptoundecanoic acid (MUA).⁹⁴ QDs complexed with sheep serum albumin (SSA) were found to be the most stable in aqueous solution.

To sum up, there exist several surface modification strategies that render QDs water-soluble and biocompatible. Each strategy is associated with distinct advantages and disadvantages. Therefore, the surface modification approach must be carefully chosen as it determines photophysical properties of solubilized and functionalized QDs and ultimately the outcome of the experiment. In addition, rigorous control experiments must be performed to determine whether the biological activity of the molecule conjugated to QDs is retained.

2.5. Quantum Dot Biological Applications: Cellular Labeling

Fluorescent labeling of extra- and intracellular components is the area in which QDs excel. Their high brightness ensures cellular component visualization with high signal-to-noise ratio (SNR) and eliminates the need for a large number of fluorophores to produce a pronounced signal.⁹⁵ As a consequence, QDs have been successfully used to label a tremendous number of cellular components both external and internal to the plasma membrane in various types of fixed and live cells (Figure 2.5 A,B; Table 2.1). Their excellent resistance to degradation and photobleaching in physiologically relevant conditions enables microscopy image acquisition for extended periods of time under constant illumination

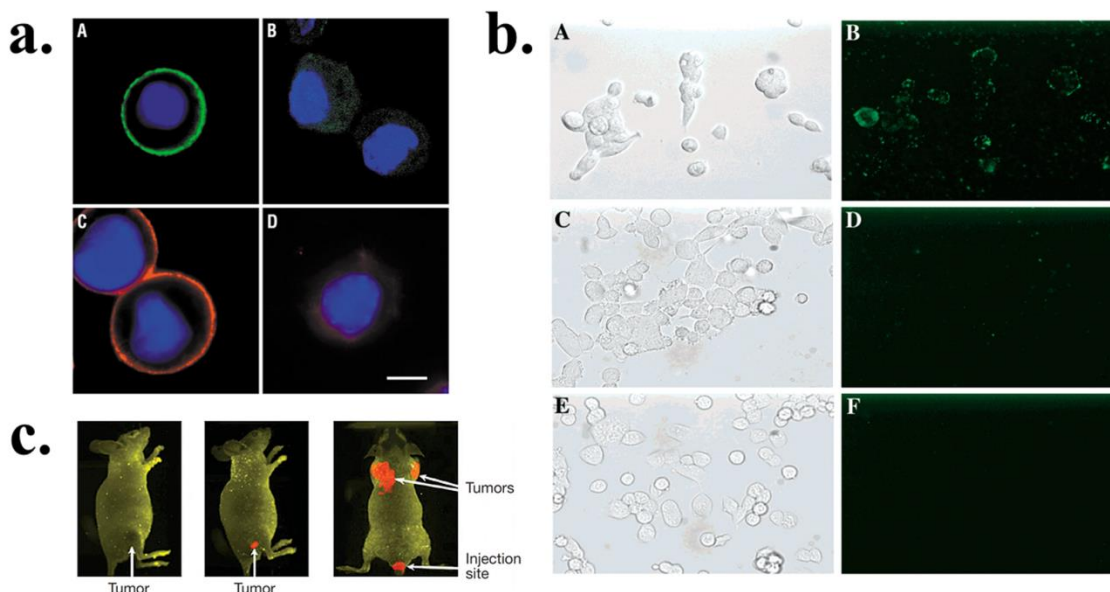


Figure 2.5. Quantum dots in cellular and whole animal in vivo imaging. Immunofluorescent labeling of extracellular Her2 cancer marker with antibody-conjugated QDs is shown in A. Reprinted from reference 81 by permission from MacMillan Publishers Ltd:Nature Biotechnology, copyright 2003. Visualization of hSERT in HEK-293T cells with serotonin-conjugated CdSe/ZnS core/shell nanocrystals is shown in B. Reprinted with permission from reference 92. Copyright 2002, American Chemical Society. The use of QDs to target cancer tumors in living mice is shown in C. Reprinted from reference 55 by permission from MacMillan Publishers Ltd:Nature Biotechnology, copyright 2004.

three-dimensional spatial and temporal resolution. The ability to visualize and analyze the dynamic interactions between viruses and host cells was recently demonstrated by Joo et al. who tagged human immunodeficiency virus (HIV) with QD-strep conjugates via site-specific BirA biotinylation and examined the kinetics of QD-HIV complex internalization into mammalian cells.⁹⁶ Single virus tracking experiments offer an opportunity to visualize and elucidate the molecular details of the viral infection process. In the case of whole cell tracking, QDs may be used to monitor transplanted and stem cell location, survival, and differentiation. For example, Schormann et al. attempted to track and examine metastatic behavior of QD-tagged MCF-7 human breast cancer cells transplanted into healthy mice. Tracking studies at the single QD level will be described in detail in the SQT section.⁹⁷

In contrast to conventional photoluminescent probes, QDs are ideal candidates for multiplexing labeling experiments owing to their broad absorption spectra and size-tunable, narrow, Gaussian emission spectra. They effectively eliminate the need for multiple excitation sources and convoluted spectral compensation algorithms. In 2007,

Table 2.1. Intracellular and extracellular components labeled with QDs.

Internal Cellular Components	
Nucleus [55]	prominent membrane-bounded organelle that contains DNA organized into chromosomes
Mitochondria [81]	membrane-bounded organelle that carries out oxidative phosphorylation and produces most of the ATP in eukaryotic cells
Synaptic vesicles [105]	50-nm spherical membrane-bounded organelles, storing neurotransmitter molecules and mediating neuronal signaling at chemical synapses
Actin filaments [81]	helical protein filament formed by polymerization of globular actin molecules that determines cell shape and is necessary for whole-cell locomotion
Microtubules [81]	long hollow cylindrical structures composed of the protein tubulin, controlling intracellular transport
Kinesin, myosin [87, 155]	molecular motor proteins that use the energy of ATP hydrolysis to move along cytoskeletal filaments
External Cellular Components	
SERT [92]	plasma membrane transporter protein that is responsible for reuptake of serotonin from the synaptic space into the presynaptic neuron and is a major target for selective serotonin reuptake inhibitors (SSRIs)
erbB/HER [83]	receptor protein kinases that are central to cellular signaling and are upregulated in certain cancer types
AMPA [86]	plasma membrane ionotropic glutamate receptor that mediates fast excitatory synaptic transmission in the central nervous system (CNS)
GlyR [82]	transmembrane inhibitory glycine receptor in CNS
K ⁺ channel [156]	transmembrane protein that controls a wide variety of cell functions
PSMA [55]	transmembrane glycoprotein that is a marker of prostate cancer

Chattopadhyay et al. were able to resolve seventeen fluorescence emissions including eight QD emissions in a polychromatic flow cytometry experiment, the most impressive

demonstration of QD multiplexing abilities to date.³³ In this study, nine antibody-conjugated organic dyes and eight pMHC1 antigen- and antibody-conjugated QDs were featured in a seventeen-color staining panel to immunophenotype antigen-specific T cells. The resolution of the eight QD emissions was achieved with minimal spectral compensation requirements.

2.6. Quantum Dot Biological Applications: Single-QD Tracking

SQT has emerged as a powerful technique to investigate individual dynamics rather than an ensemble average behavior of QD-tagged single molecules. Careful analysis of SQT data allows elucidation of the molecular details of various biological processes, in particular membrane trafficking of cell surface proteins.⁹⁵ The visualization and interpretation of the dynamic interaction with the biological surroundings have been reported for QD-labeled growth factors, cell surface receptors, membrane lipids, molecular motors, and synaptic vesicles. In a typical SQT experiment, one must label the biological target of interest with a QD, introduce a biological stimulus, observe the effect via image time-series acquisition, apply an algorithm to identify and locate single QD positions in each frame, link QD positions in successive frames to generate trajectories, and analyze the obtained trajectories (Figure 2.6). The x-y position of the diffraction-limited QD spot can be located by two-dimensional Gaussian fitting of its point spread function (PSF) via fluorescence imaging with one nanometer accuracy (the FIONA technique).⁹⁸⁸ The localization accuracy is dependent upon the standard deviation of the PSF and the number of photons detected from a single QD. Very bright particles like QDs significantly improve SNR image profile and can be located with high accuracy (as low as ~ 10 nm for a single QD).⁹⁵ The next step is to link the centers of single QD spots across adjacent frames of the entire image time-series to generate QD trajectories. The overwhelming majority of studies so far focused on particle dynamics

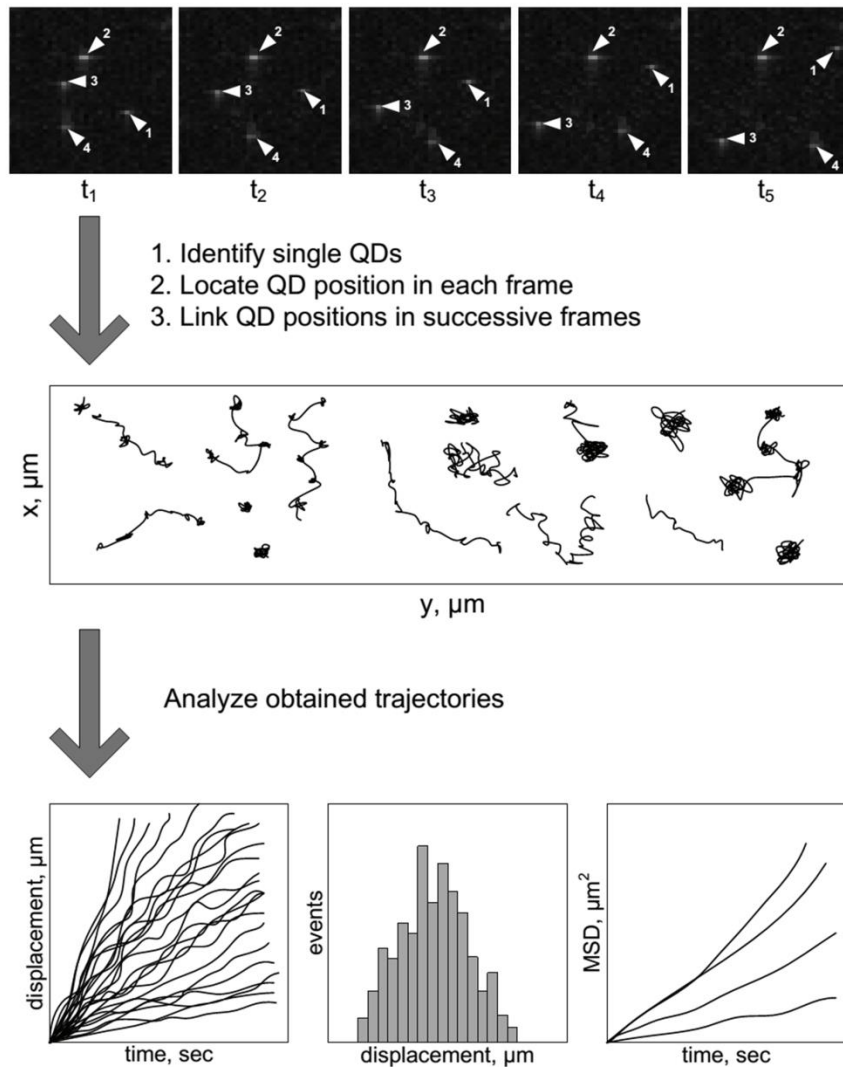


Figure 2.6. Scheme of data processing and analysis in the SQT experiment.

in an XY coordinate system. However, it will not be long before three-dimensional (3D) SQT will become the norm, with the emergence of 3D tracking techniques.⁹⁹⁻¹⁰¹ There are several tracking software packages available online that can be used as a starting point to develop a QD tracking algorithm and obtain individual trajectories.

When the tracking portion of the SQT experiment is completed, generated trajectories are analyzed to extract information about the QD dynamic behavior including displacement, velocity, and diffusion coefficient. Generally, QD mean-square displacement

(MSD) is calculated as a function of time to reduce the noise of the experimental trajectory.¹⁰² The resulting MSD curve is used to determine whether the QD-tagged biological target undergoes Brownian, directed, confined, or anomalous diffusive behavior.¹⁰³ The extracted mode of motion parameters are subjected to rigorous statistical analysis and subsequent biological interpretation. Several examples that clearly demonstrate the utility of SQT for elucidating the molecular mechanisms underlying the dynamic behavior of QD-tagged biological structures are described below.

In 2007, Cui et al. observed unidirectional retrograde transport of endosomes, containing QDs conjugated to nerve growth factor (NGF) dimer, along the neuronal axon (Figure 2.7 A).¹⁰⁴ The QD-NGF complexes were internalized by endosomes at the distal axon in a 1:1 stoichiometry and subsequently transported to the cell body in a characteristic stop-and-go movement pattern. In 2009, Zhang et al. published a controversial report on the mechanism of presynaptic neuronal transmission in which they subjected single QD-loaded individual synaptic vesicles to external stimulus and then observed vesicular response.¹⁰⁵ As a result, it was established that the transient vesicular fusion and reuse (kiss-and-run) is the preferred mechanism for presynaptic transmission as opposed to the full-collapse vesicular fusion. SQT is a particularly useful technique for elucidating dynamics of cell surface-associated proteins such as potassium and CFTR channels, GABA, NMDA, Gly, and AMPA neurotransmitter receptors, and integrins.⁹⁵ In a specific example, Heine et al. showed that postsynaptic AMPA glutamate receptors (AMPA) undergo fast lateral diffusion ($>0.25 \mu\text{m}^2/\text{s}$) which permits efficient replacement of desensitized receptors with the new, functional ones.¹⁰⁶ Such AMPAR exchange facilitates rapid recovery of the

depressed synaptic transmission that can be slowed down by constraining the movement of

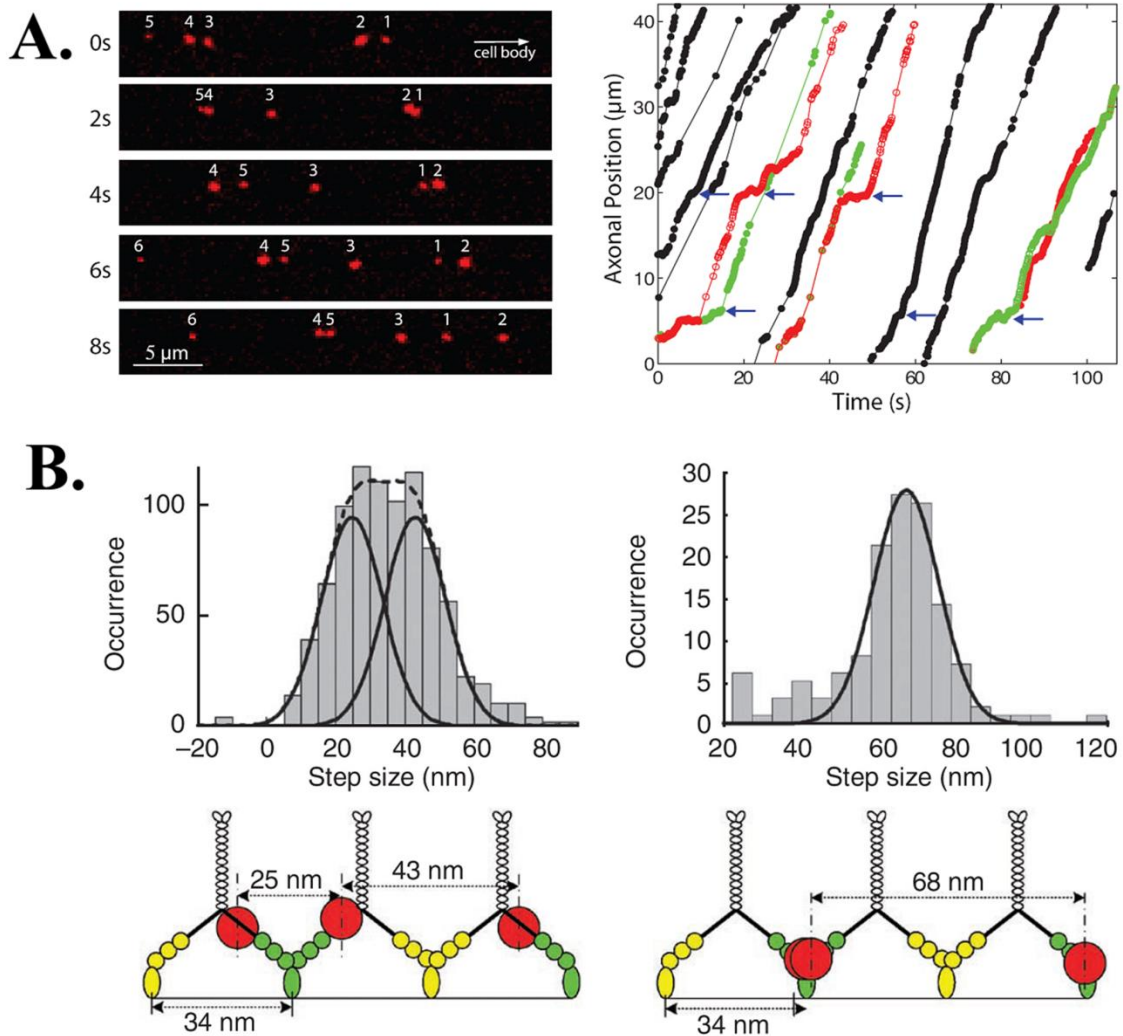


Figure 2.7. Single-quantum dot tracking (SQT) examples. A. Cui et al. observed unidirectional retrograde transport of endosomes, containing QDs conjugated to nerve growth factor (NGF) dimer, along the neuronal axon. Reprinted from reference 104 by permission from PNAS, copyright 2007. B. Sun et al. visualized the movement of biotinylated myosin X along actin filaments and bundles with QD-streptavidin conjugates. Reprinted from reference 87 by permission from MacMillan Publishers Ltd:Nature Structural and Molecular Biology, copyright 2010.

AMPA within the synapse. Clearly, SQT allows detailed investigation of the aspects of neurotransmission with unprecedented spatial and temporal resolution.

In another remarkable display of their utility to the field of single-particle tracking, QDs were used to reveal the details of intracellular movement of kinesin and myosin motor proteins along cytoskeletal microtubules and actin filaments respectively. In particular, Pierobon *et al.* visualized and determined the size of individual steps myosin V takes in the hand-over-hand walking motion along the cytoplasmic actin filaments in living HeLa cells.¹⁰⁷ To observe this phenomenon, Myosin-QD constructs were loaded into the cytoplasm of live HeLa cells via nonspecific endocytosis technique and imaged with a wide-field epifluorescence microscope (Figure 2.7 B). Molecular motor tracking experiments clearly demonstrated that QDs offer a promising potential in reporting intracellular dynamic activity of endogenous molecules. Existing strategies for intracellular delivery of QDs will be discussed in the following section.

2.7. Quantum Dot Biological Applications: Intracellular Delivery and Therapeutics

Successful use of QDs to probe membrane dynamics of extracellular proteins and intracellular motion of individual molecular motors in the cytoplasm of live cells leaves no doubt that QDs have a large potential to become intracellular activity photoluminescent reporters of choice. In addition to intracellular SQT and imaging various disease markers, QDs may be utilized as drug delivery vehicles or tags of conventional drug carriers. For example, Manabe *et al.* studied the effects of QD-conjugated captopril, an antihypertensive drug, on the blood pressure of hypertensive rats. QD-captopril conjugates and captopril alone were reported to decrease rat blood pressure to similar degree 30 min after administration.¹⁰⁸ However, the hypotensive effect of the conjugates disappeared after the initial 60-min window. Additional experiments are required to shed light on the mechanism of therapeutic action of QD-conjugates. Recently, Bagalkot *et al.* demonstrated parallel

combination disease marker- and drug release-sensing elements in QD architecture. QDs were covalently conjugated with RNA aptamers (A10) which contained an intercalated chemotherapeutic agent doxorubicin.¹⁰⁹ The A10 RNA aptamer enabled specific targeting of prostate specific membrane antigen (PSMA), while RNA-associated doxorubicin quenched fluorescence. Restored QD fluorescence due to the slow release of doxorubicin in the intracellular environment provided the means to monitor the therapeutic process in real time. Treatment of PSMA-positive cells with the QD-RNA-doxorubicin conjugates induced apoptosis and resulted in significant decrease of cell viability. In another instance, small interfering RNA (siRNA) molecules were covalently linked to the QD surface in an attempt to silence eGFP protein expression.⁷³ QDs may also be used to visualize drug delivery via other drug carriers as demonstrated by Jia et al. They used QDs to visualize intracellular delivery of polyethyleneimine (PEI)-coated carbon nanotubes that served as a vector for an antisense oligodeoxynucleotide sequence, a hydrophilic therapeutic agent.¹¹⁰

The future of intracellular applications of QDs depends on the efficient cytoplasmic delivery. Delehanty et al. group QD intracellular delivery strategies into three broad categories: (i) passive delivery, (ii) facilitated delivery, and (iii) active delivery.¹¹¹ In passive delivery, hydrophilic QDs undergo nonspecific endosomal sequestration due to electrostatic QD-membrane interactions. Jaiswal et al. visualized nonspecific endocytosis that occurred when HeLa cells were incubated with ~500 nM DHLA-coated QDs for several hours.¹¹² Although passive delivery is attractive in terms of simplicity, the cell type-independent internalization and the inability to escape endosomal sequestration remain significant challenges.

Facilitated delivery is based upon QD functionalization with peptides, proteins, small molecules, lipids, and polymers. Typically, intracellular delivery is achieved through the initial

interaction of the QD conjugate with a specific receptor and the subsequent QD-receptor complex endosomal sequestration. Alternatively, QD conjugates undergo endocytosis due to electrostatic interactions between charged surface groups and plasma membrane. The positively charged TAT peptide and the arginine-glycine-aspartate (RGD) tripeptide are two prominent examples of peptides that mediate intracellular delivery of QDs. High positive charge of the TAT peptide due to the presence of a linear polyarginine (lysine) chain permits electrostatic interaction with negatively charged receptors and subsequent receptor-mediated endocytosis.¹¹³ On the other hand, the RGD peptide was reported to mediate QD delivery via binding to the membrane receptors known as integrins.^{114,115} Similarly to peptide-QD conjugates, protein- and small molecule-QD conjugates take advantage of receptor endocytosis, with QD specificity for a given cell membrane marker introduced by protein (small molecule). Antibodies, cholera toxin B, transferrin, and folate conjugated to QDs have all been reported to undergo endocytosis after binding to the corresponding cell membrane proteins.^{19,47,111,116}

Lipids and polymers have also been used to deliver QDs into cells. Derfus et al. reported the internalization of the liposomes containing commercial transfection agent Lipofectamine 2000 self-assembled on the surface of negatively charged QDs.¹¹⁷ Several reports describe the use of phospholipid-based micelles engulfing QDs in the central pocket.¹¹¹ Bruchez et al. anchored the endosomal-disrupting PEG-PEI copolymers on the QD surface and observed subsequent cytoplasmic release of the QD-conjugates.¹⁸ While lipid- and polymer-mediated delivery usually results in a higher degree of uptake, the relatively large size of the final QD conjugate and the inability to control QD concentration and loading efficiency are likely to prevent this strategy from wide utilization.

In contrast to passive and facilitated delivery, active delivery techniques such as electroporation and microinjection rely on the application of mechanical stress to the cell membrane. In the electroporation technique, a brief electric pulse applied to the membrane temporarily permeabilizes the lipid bilayer and results in the influx of QDs into the cytoplasm. The advantages of electroporation are that a large number of cells can be processed simultaneously in a relatively inexpensive procedure. However, the QDs tend to aggregate near the membrane entry, which is undesirable for intracellular reporting applications. Also, a strong electrical shock applied to the cell suspension may result in reduced cell viability. In the microinjection technique, cells are first visualized with a fluorescent microscope, and then a thin-glass tube is used to inject a QD solution either into the nucleus or the cytoplasm of the cell.¹¹⁹ While QDs are typically dispersed at the injection site and diminished cell mortality is reported, microinjection is associated with high cost and low potential for high throughput. However, both active delivery techniques enable one to escape endosomal sequestration that typically occurs in other strategies.

Overall, it is evident the intracellular fate of QDs depends on the QD size, surface coating, ability to escape endosomal capture, and specific intracellular localization. Much progress remains to be made in the field of intracellular delivery of QDs as the existing strategies are largely inadequate to meet the requirements for efficient drug delivery and intracellular dynamics sensing.

2.8. Quantum Dot Biological Applications: FRET-based Biosensing

Förster or fluorescence resonance energy transfer (FRET) has emerged as a powerful technique for monitoring biological events at the nanometer scale (1-10 nm) including ligand-receptor binding, protein-protein interactions, and biomolecular conformational

changes.^{120,121} FRET-based applications require a short distance between donor (D) and acceptor (A) molecules and finite spectral overlap between the emission spectrum of D and the absorption spectrum of A. In their extensive review, Medintz and Mattoussi discuss the utility of QD photophysical properties to FRET-based biosensing applications.¹²² In particular, the size dependency of the QD emission profiles allows tuning the D-A spectral overlap and maximizing energy transfer efficiency. Another useful property of QDs is the ability to form multivalent constructs. This becomes useful when several A molecules are attached to one QD, thereby improving FRET signal. While broad absorption profiles of QDs allow multiplexing experiments and significantly improve SNR in the FRET experiment by reducing direct excitation contribution to the FRET signal, they render QDs ineffective acceptor fluorophores.¹²² Therefore, a typical QD-FRET configuration includes an organic dye molecule serving as the acceptor fluorophore. Another serious limitation associated with QD-based FRET is the QD size. The energy transfer efficiency has a 6th order dependence on the D-A separation distance and is defined as:

$$E = \frac{k_{D-A}}{k_{D-A} + \tau_D^{-1}} = \frac{R_0^6}{R_0^6 + r^6} \quad [1]$$

where k_{D-A} is the rate of energy transfer between D and A, τ_D is the exciton radiative lifetime of D, R_0 is the Förster radius, and r is the center-to-center separation distance between D and A. Surface modification and functionalization of QDs significantly increases the final conjugate size and results in large D-A separation distances leading to poor FRET rates and low energy transfer efficiency. Nevertheless, QD-dye FRET pairs have been successfully utilized by many groups to sense nucleic acid hybridization, detect presence of ions in solution, monitor enzyme activity, and assess competitive receptor binding kinetics. Several biosensing applications of QD-FRET are discussed below.

In the first example, Zhang and Johnson used QD-FRET to study an aspect of the HIV-1 virus replication.¹²³ Specifically, they attempted to monitor sequence-driven interaction between the arginine-rich fragment of Rev, a HIV-1 regulatory protein, and the RNA-based Rev responsive element, RRE IIB RNA. The experimental setup included streptavidin-coated QDs conjugated with biotinylated RRE and the Rev fragment labeled with the Cy5 dye. To monitor RRE-Rev interactions, QD PL was recorded as function of Rev peptide concentration, and significant QD quenching was reported with increasing peptide concentration. The disruptive effect of neomycin B presence on the RRE-Rev association translated into significantly lower FRET rates. Such a QD-FRET configuration may be used as a template for FRET-based drug discovery platform targeting viral replication. In the second example of DNA sensing, Gill et al. attempted to detect a Texas Red-labeled DNA sequence with a thiolated complementary DNA sequence conjugated to CdSe/ZnS core/shell nanocrystals.¹²⁴ Measurements of QD PL quenching and Texas Red PL were used to detect the hybridization process between the labeled complementary DNA. When DNase I enzyme was added to the solution, QD PL partial recovery was observed as the result of DNA hybrid degradation and simultaneous Texas Red separation.

By coupling a dye with the pH-sensitive absorption profile to QDs, it is possible to accurately monitor pH changes in real time. In the report by Snee et al., squaraine dye was covalently conjugated to polymer-encapsulated QDs, and the FRET interactions were measured as a function of the solution pH.¹²⁵ As a result, the ratiometric dependence of the QD and dye emission peaks were revealed and demonstrated the utility of such QD-dye assembly. In another example, Medintz et al. were able to detect the presence of the maltose sugar in solution with positively charged maltose-binding proteins (MBP) self-assembled on the DHLA-capped QD surface.¹²⁶ Cy3-labeled MBP was specifically prebound to maltose

analog β -cyclodextrin (BCD) tagged with Cy3.5 dark quencher prior to self-assembly. Excitation of the QD resulted in Cy3 FRET-excitation that was then fully quenched by the BCD-Cy3.5 complex. Addition of maltose to the solution resulted in the displacement of BCD-Cy3.5 complex, with Cy3 PL recovery measured in a dose-dependent manner. Thus, it is possible to develop QD-protein biosensors for FRET-based sensitive nutrient detection.

One of the most exciting QD-FRET applications to date is the use of QDs in photodynamic therapy (PDT). PDT has emerged as a cancer therapeutic tool alternative to surgical treatment and is widely used as treatment for several types of cancer, in particular basal cell carcinoma. In a general PDT process, a photosensitizing agent (PS) is photoexcited, and its excitation energy is transferred to a proximal triplet oxygen molecule to generate singlet oxygen. Singlet oxygen belongs to the family of reactive oxygen species (ROS) that are able to induce apoptotic damage of the cells in the immediate vicinity of ROS generation. By coupling the PS molecules to QDs in the QD-FRET-enhanced PDT, singlet oxygen generation quantum yield can be significantly increased as a result of the excellent UV or IR energy-harvesting capability of QDs and subsequent FRET excitation of the PSs.¹²⁷⁻¹²⁹ In addition, it is possible to anchor several membrane cancer marker-specific antibodies and PSs to the QD surface to achieve specific targeting and imaging of cancer cells along with highly localized therapeutic action of PSs (Figure 2.8).¹²⁷ In the most recent proof-of-concept experiment, Tsay et al. conjugated two PSs, Rose Bengal and chlorine e6, to CdSe/ZnS QDs, with lysine-terminated phytochelatin-related peptides serving as a rigid linker between the QD surface and the PS molecule.¹²⁹ Singlet oxygen generation was achieved either by indirect FRET-based excitation (355 nm) or direct laser excitation of PSs on the QD surface (532 nm) and detected spectroscopically at 1270 nm by measuring oxygen phosphorescence at 1270 nm. Singlet oxygen quantum yields as high as 0.17 and 0.31

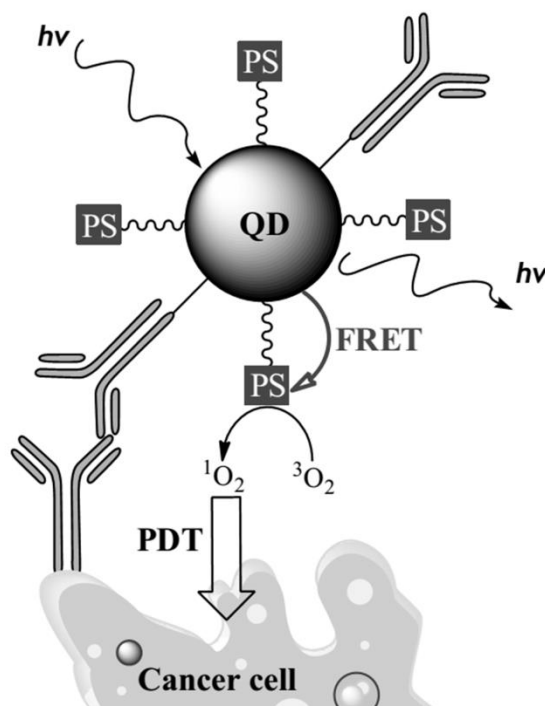


Figure 2.8. Achieving specific targeting in photodynamic therapy. A cancer cell is first exposed to a primary antibody that specifically binds to an extracellular cancer marker. Then the cancer cell is incubated with multivalent QDs conjugated to secondary antibody and photosensitizer molecule¹²⁸

were reported for QD-Rose Bengal conjugates and QD-chlorin e6 conjugates respectively. Interestingly, quantum yields from indirect excitation were much higher for QD-Rose Bengal complexes suggesting FRET is the primary mechanism of singlet oxygen generation. The opposite was true for QD-chlorin e6 complexes, indicating that FRET-based excitation of chlorine e6 was considerably lower. Further experiments are needed to pinpoint the basis for such differences between the QD-PS conjugates.

Performing FRET at the single molecule level offers the ability to monitor individual molecular interactions with increased sensitivity and temporal resolution when compared to ensemble experiments. In a general solution-phase single QD FRET experiment, emission intensity bursts of the donor and acceptor molecules are measured after the defined focal

volume of the solution is excited through a high numerical aperture objective.¹³⁰ Zhang et al. utilized a single QD-FRET biosensor for accurate and highly sensitive detection of DNA sequences in solution.¹³¹ The Cy5-labeled target DNA sequence was captured by hybridization with the biotinylated complementary DNA sequence introduced into the solution. The Cy5- and biotin-terminated DNA hybrid was then mixed with streptavidin-conjugated QDs, and the resulting solution with QD-DNA complexes was delivered into a glass microcapillary to minimize the sample volume for FRET analysis. The sensing responsivity of the QD-FRET DNA biosensor was determined to be several orders of magnitude higher than that of the dye-based molecular beacon.

Once again, the unique photophysical properties make QDs an attractive choice for the FRET-based biosensing and therapeutics applications. Clearly, there are significant challenges associated with QD-FRET, specifically QD-acceptor separation distances and QD-acceptor association multivalency. Addressing these issues will ensure that QD-FRET continues to be actively explored in a biological setting.

2.9. Quantum Dot Biological Applications: *In Vivo* Deep Tissue Imaging

Until recently, *in vivo* deep tissue fluorescence imaging relied on conventional dyes and suffered from poor tissue penetration depth, low SNR intensity profiles, and short-lived fluorescence signal. QDs offer several distinct advantages to the field of deep tissue imaging.^{21,55} First, their high brightness and the ability to shift their peak emission wavelengths to the far red and near-infrared (NIR) regions of the EM spectrum result in dramatic reduction of cellular autofluorescence, significant improvement of the SNR intensity profiles and tissue penetration depth. Second, their excellent photostability enables longer circulation times in the endothelial system and allows long-term imaging without the

significant image quality loss. Third, their large two-photon absorption cross sections permit the use of low-energy NIR excitation sources minimizing tissue damage and improving SNR profiles. Fourth, QD-based in vivo deep tissue imaging is a safer, cost-effective alternative to radiation-based imaging modalities. So far, intravitally injected QDs have been successfully used to image blood vessels, detect cancer tumors, and map lymph nodes in live animals.

In work by Smith J. D. et al., a series of QDs of varying sizes and surface coatings were intravitally injected into the chick chorioallantoic membrane (CAM) blood vessels, a model system developed for studying angiogenesis and blood vessel formation in vivo.¹³² Visualization of the chick blood vessels with NIR-emitting QDs produced a stronger, more uniform signal and eliminated virtually all of the background fluorescence compared to FITC-dextran, a dye-based vasculature visualization agent. It should also be noted that multiple QD injections produced no deleterious effects on the development of the chick embryo. In a more recent example, Smith B. R. et al. covalently attached ~30-50 RGD peptides to NIR-emitting QDs and injected QD-RGD complexes into the tail vein of live mice.¹³³ The authors exploited intravital microscopy to monitor QD-RGD binding to integrins $\alpha v \beta 3$ within the tumor neovasculature in real time. Interestingly, only QD-RGD aggregates and no single QD-RGD complexes were observed to bind to the tumor neovasculature. Also, it was reported that QDs were cleared from the vasculature via reticuloendothelial system within 1.5 hours post-administration. In another study describing the utility of QDs to the field of angiography, Larson et al. administered water-soluble QDs into living mice via tail vein injection and were able to clearly visualize QD-containing vasculature at a skin depth of $\sim 100 \mu\text{m}$ via two-photon (900 nm) excitation microscopy.³⁹

In 2004, Gao et al. described the use of amphiphilic triblock copolymer-encapsulated QDs to visualize human prostate cancer tumors in living nude mice (Figure 2.5 C).⁵⁵ PEG

chains and PSMA-specific antibody were conjugated to polymer-coated QDs to achieve passive and active targeting of cancer cells respectively. QD complexes were administered into living animals via tail vein injection and were allowed a 24-hour circulation period for QD accumulation in the tumor. The acquired spectral fluorescence images of whole animals clearly demonstrated QD accumulation in the prostate cancer tumors. Nonspecific activity of QD-PSMA Ab conjugates was determined by histological examination of six different host organs, showing nonspecific QD uptake in the liver and the spleen. The rate of uptake and retention of QD-PEG conjugates was significantly lower and was attributed to small hydrodynamic diameter of the conjugate.

Kim et al. utilized type II NIR-emitting (840-860 nm) QDs as surgical aids during the sentinel lymph node (SLN) mapping procedure in the mouse and pig (Figure 2.9).¹³⁵ After subcutaneous administration of 400 pmol of QDs on the thigh of the pig, it was possible to quickly localize the position of the SLN at the depth of ~ 1 cm in real time. The localization was achieved using a low fluence rate of 5 mW/cm^2 of NIR excitation light. According to Kim et al., NIR QDs considerably simplify surgeon's task of indentifying the SNL and performing complete resection during the cancer surgery.

Despite multiple successful demonstrations of their use in vivo, QDs face significant challenges before they can be approved for clinical use. The large size of QD-conjugates promotes QD retention in the liver and the spleen and prevents renal clearance, which imposes a 5-6 nm maximum size requirement.¹³⁵ In addition, toxicity remains a widely discussed issue and will be addressed in a separate section.

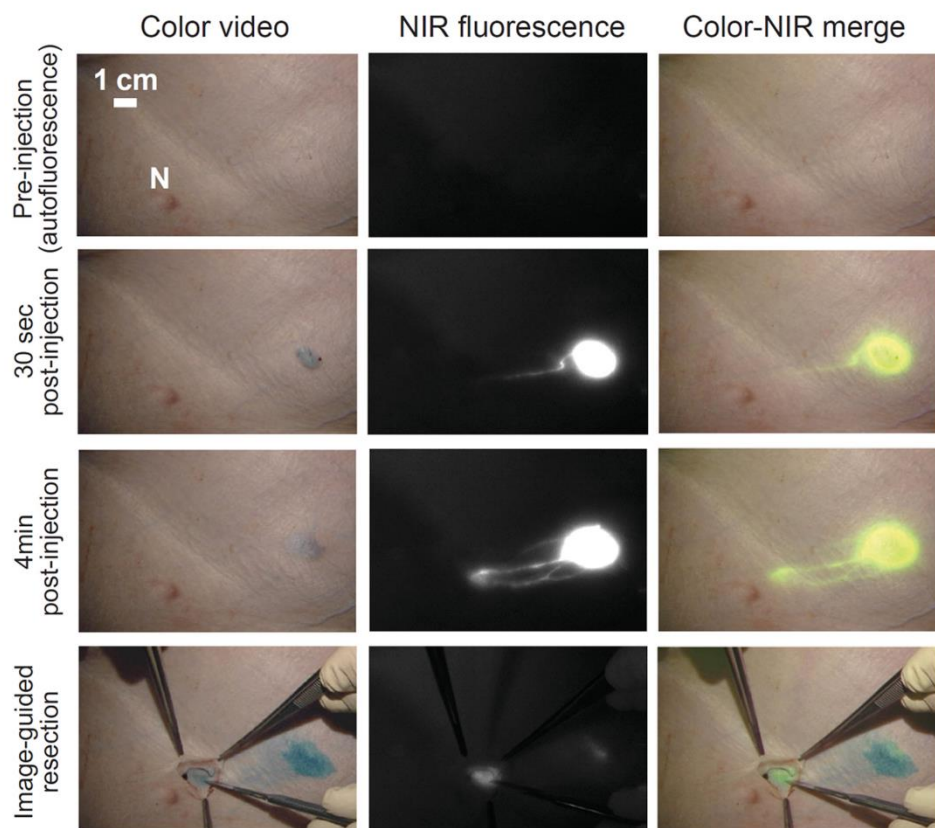


Figure 2.9. Sentinel lymph node mapping surgical procedure aided by NIR-emitting type II QDs. Reprinted from reference 134 by permission from MacMillan Publishers Ltd:Nature Biotechnology, copyright 2004.

2.10. Quantum Dot Biological Applications: Multimodal Imaging

Although QD-based fluorescence microscopy has demonstrated potential for in vivo molecular imaging, the tissue penetration depth is limited by the working distance of the microscope objective and excitation light scattering.¹³⁶ However, it is possible to enhance the visualization of QDs in vivo by introducing an additional property, such as paramagnetism, which allows molecular imaging in multiple modes. Paramagnetic QDs can serve as both photoluminescent probes and magnetic resonance imaging (MRI) contrast agents in a highly complementary bimodal molecular imaging mode. Several paramagnetic QD architectures have been developed. Yi et al. reported the synthesis of silica-coated nanocomposites of magnetic nanoparticles and QDs.⁶³ γ -Fe₂O₃ nanoparticles and CdSe QDs were prepared

separately and then encapsulated in a silica shell via reverse microemulsion. The resulting nanocomposites retained the paramagnetic properties of $\gamma\text{-Fe}_2\text{O}_3$ and the optical properties of CdSe. Mulder and colleagues prepared paramagnetic QDs by coating CdSe/ZnS core/shells with a phospholipid micelle composed of a pegylated phospholipid, PEG-DSPE, and a Gd-containing paramagnetic lipid, Gd-DTPA-BSA.¹³⁷ Chelated complexes of Gd are widely used as MRI contrast agents. The paramagnetic QDs were then functionalized with integrin-specific RGD peptide and were used to image human umbilical vein endothelial cells. In another example, Yang et al. functionalized silica-coated Mn-doped CdS/ZnS core/shells with Gd via capture of GdIII ions by TSPETE, a metal-chelating silane.¹³⁸ Inductively coupled plasma (ICP) analysis was utilized to determine the average number of Gd III ions on the QD surface to be ~ 107 . QD-Gd complexes possessed large proton relaxivities and retained yellow PL emission of the original QDs. In conclusion, the bimodal character of paramagnetic QDs makes them useful MRI contrast agents with the capability of parallel optical detection.

2.11. Quantum Dot Toxicity Concerns

QD core semiconductor constituents, such as Cd, Se, and Te, are highly toxic in their bulk form, and their adverse effects have been well documented. In particular, Cd exposure is associated with the increased rates of cancer, birth defects, and endocrine disruption.¹³⁹ In addition, Cd is known to facilitate the formation of reactive oxygen species, causing subsequent oxidative damage. Recently, several reports presented evidence that Cd expresses genotoxic activities in mammalian cells and animals, specifically chromosomal damage and gene expression modulation.¹⁴⁰ There is sufficient evidence establishing the toxic effects of

II-IV bulk semiconductors to raise concerns about possible deleterious impact of their nanoscale counterparts on the biological systems.

Numerous reports on the cytotoxicity associated with the utilization of QDs in biological setting have been published to date. In his comprehensive review in 2006, Hardman et al. summarized the existing state of knowledge on in vivo toxicity and biological fate of QDs.¹³⁵ Hardman concluded that QD toxicity ultimately depends on the effectiveness of the nanocrystal surface passivation, which directly influences QD size, charge, and stability. Indeed, several recently published toxicity studies have shown that QD toxicity can be minimized through complete surface passivation with an appropriate choice of inorganic shell or surface coating. In 2009, Pelley et al. published another extensive review, in which they updated, expanded and put Hardman's 2006 review in a regulatory context.¹⁴¹ Particular attention was paid to biological and environmental fate of QDs and a striking lack of studies showing QD long-term effects. Currently, QD toxicity still remains a widely discussed issue with many questions remaining to be answered.

Inherent toxicity of traditional QD core material constituents is a serious obstacle to the clinical utilization of QDs. To address this issue, III-V and I-III-VI₂ materials have been employed to replace toxic II-IV semiconductor elements in the QD architecture. Unfortunately, new materials suffer from sub-par performance compared to their traditional counterparts, and there have not been any reports establishing their reduced toxicity until recently.

2.12. Current Limitations of Quantum Dots

QDs have undoubtedly demonstrated their utility to the field of biological investigation. However, there several distinct limitations associated with QDs that must be

overcome before QDs can become the routine biological photoluminescent probes of first choice. First, the final size of biocompatible, water-soluble, functionalized QD conjugates can easily exceed 20 nm in diameter and several hundred kDa in molecular mass.^{95,142} This is especially true in the case of polymer-encapsulated streptavidin-coated QDs conjugated to large biotinylated antibodies. The large size of QD probes may impair labeled protein trafficking in SQT, causes reduced FRET efficiency between donor and acceptor molecules, and restricts access to crowded cellular locations. In addition, large hydrodynamic diameter precludes QDs from being cleared from the body via renal filtration or urinary excretion.^{135,141} Current strategies to reduce QD size are aimed at the development of new compact surface encapsulants, shorter linkers, and conjugation strategies as well as the reduction of QD multivalency.

Although multivalency has been successfully used in several instances to maximize the utility of QDs, it can cause QD aggregation due to cross-linking during conjugation and impair receptor mobility by cross-linking cell surface proteins. The ability to synthetically control QD valency will effectively eliminate issues due to cross-linking and significantly reduce the hydrodynamic diameter of QD conjugates. In an attempt to generate monovalent QDs, Howarth et al. conjugated single monovalent streptavidin (mSa) with a femtomolar biotin binding site to core/shells coated with DHLA-PEG₈-COOH and used the QD-mSa conjugates to visualize membrane mobility of individual LDL receptors.¹⁴³

Single QD photoluminescence emission intensity alternates between dark and bright states, and such fluorescent intermittency has been referred to as blinking (Figure 2.10 A). Several models have been proposed to explain the mechanistic basis underlying the blinking phenomenon of single QDs.^{144,145} Although blinking may be used to distinguish single fluorophores from aggregates, it significantly complicates trajectory reconstruction in SQT

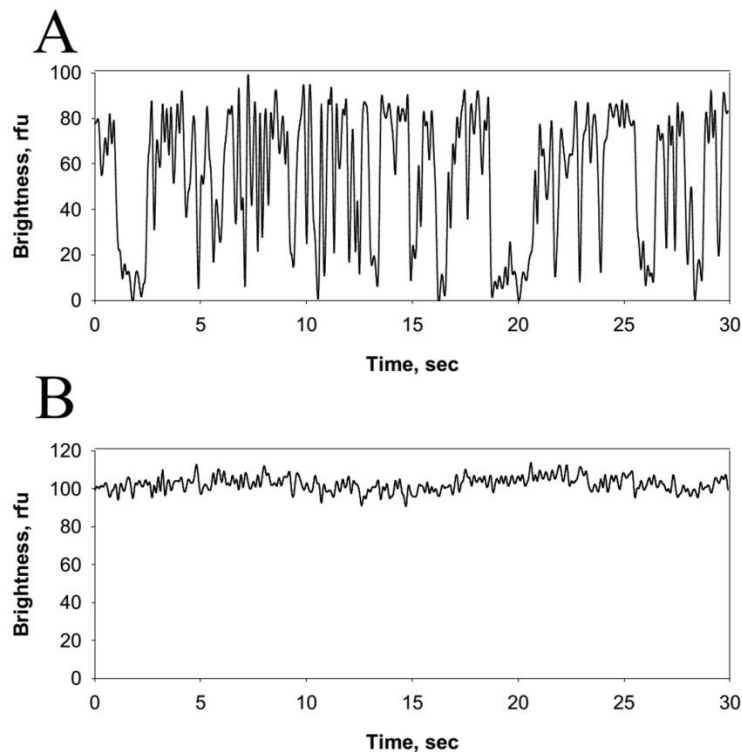


Figure 2.10. Fluorescent intermittency of a single semiconductor nanocrystal. Typical fluorescence spectrum of a single QD is shown in A. Random alterations between dark and bright states constitute blinking. A fluorescence spectrum for a single, non-blinking CdSe core nanocrystal coated with a 14-layer thick CdS shell is shown in B. Here, the QD spends the entire time interval in the bright state.

and may not be a reliable indicator of single molecule fluorophores due to the dependence of the intermittency rate on experimental parameters and biological environment.⁹⁵ To reduce “blinking”, a thick inorganic shell (CdS, CdZnS) with reduced lattice mismatch is grown around the QD core (Figure 2.10 B).^{146,147} Although these thick shells dramatically reduce fluorescent intermittency of QDs, they result in the hydrodynamic diameter increase, which is undesirable for biological applications.

2.13. Summary

It is clear that QDs have emerged as an attractive class of photoluminescent probes since their introduction to the field in 1998. Recent advances in nanocrystal surface

chemistry resulted in more compact and more stable QDs. Their relatively small size, excellent stability at physiologically relevant conditions, and unique optical properties permit biological investigation of cellular processes with unprecedented spatio-temporal resolution in real time. While QDs have already been established as powerful biological imaging agents, their use in the fields of diagnostics and targeted drug delivery is being actively explored. Utilizing their spectral characteristics, QDs can potentially form the basis of multiplexed fluorescence assays that examine individual protein-protein interactions and ultimately interrogate cell signaling pathways. Also, their robust inorganic nature renders QDs resistant to degradation and photobleaching for long periods of time and thereby guarantees a bright future for QDs as reporters of dynamic activity of biological molecules at the single-molecule level.

2.14. References

- (1) Fernandez-Suarez, M. and A. Y. Ting (2008). "Fluorescent probes for super-resolution imaging in living cells." *Nat Rev Mol Cell Biol* 9(12): 929-943.
- (2) Haraguchi, T. (2002). "Live cell imaging: approaches for studying protein dynamics in living cells." *Cell Struct Funct* 27(5): 333-4.
- (3) Lippincott-Schwartz, J. and G. H. Patterson (2003). "Development and Use of Fluorescent Protein Markers in Living Cells." *Science* 300(5616): 87-91.
- (4) Sako, Y. and T. Yanagida (2003). "Single-molecule visualization in cell biology." *Nat Rev Mol Cell Biol Suppl*: SS1-5.
- (5) Zhang, J., R. E. Campbell, et al. (2002). "Creating new fluorescent probes for cell biology." *Nat Rev Mol Cell Biol* 3(12): 906-918.
- (6) Resch-Genger, U., M. Grabolle, et al. (2008). "Quantum dots versus organic dyes as fluorescent labels." *Nat Meth* 5(9): 763-775.
- (7) Heim, R. and R. Y. Tsien (1996). "Engineering green fluorescent protein for improved brightness, longer wavelengths and fluorescence resonance energy transfer." *Current Biology* 6(2): 178-182.
- (8) Shaner, N. C., P. A. Steinbach, et al. (2005). "A guide to choosing fluorescent proteins." *Nat Meth* 2(12): 905-909.
- (9) Piszczek, G. (2006). "Luminescent metal-ligand complexes as probes of macromolecular interactions and biopolymer dynamics." *Arch Biochem Biophys* 453(1): 54-62.
- (10) Terpetschnig, E., H. Szmecinski, et al. (1995). "Metal-ligand complexes as a new class of long-lived fluorophores for protein hydrodynamics" *Biophys J* 68(1): 342-50.

- (11) Maretta, L., P. S. Billone, et al. (2009). "Facile photochemical synthesis and characterization of highly fluorescent silver nanoparticles." *J Am Chem Soc* 131(39): 13972-80.
- (12) Patel, S. A., C. I. Richards, et al. (2008). "Water-soluble Ag nanoclusters exhibit strong two-photon-induced fluorescence." *J Am Chem Soc* 130(35): 11602-3.
- (13) Barnard, A. S. (2009). "Diamond standard in diagnostics: nanodiamond biolabels make their mark." *Analyst* 134(9): 1751-64.
- (14) Yang, S. T., X. Wang, et al. (2009). "Carbon Dots as Nontoxic and High-Performance Fluorescence Imaging Agents." *J Phys Chem C Nanomater Interfaces* 113(42): 18110-18114.
- (15) Ow, H., D. R. Larson, et al. (2005). "Bright and stable core-shell fluorescent silica nanoparticles." *Nano Lett* 5(1): 113-7.
- (16) Alivisatos, A. P. (1996). "Semiconductor Clusters, Nanocrystals, and Quantum Dots." *Science* 271(5251): 933-937.
- (17) Alivisatos, A. P., W. Gu, et al. (2005). "Quantum dots as cellular probes." *Annu Rev Biomed Eng* 7: 55-76.
- (18) Bruchez, M., Jr., M. Moronne, et al. (1998). "Semiconductor Nanocrystals as Fluorescent Biological Labels." *Science* 281(5385): 2013-2016.
- (19) Chan, W. C., et al. (1998). "Quantum Dot Bioconjugates for Ultrasensitive Nonisotopic Detection." *Science* 281(5385): 2016-2018.
- (20) Medintz, I. L., H. T. Uyeda, et al. (2005). "Quantum dot bioconjugates for imaging, labelling and sensing." *Nat Mater* 4(6): 435-446.
- (21) Michalet, X., F. F. Pinaud, et al. (2005). "Quantum Dots for Live Cells, in Vivo Imaging, and Diagnostics." *Science* 307(5709): 538-544.
- (22) Brus, L. E. (1984). "Electron--electron and electron-hole interactions in small semiconductor crystallites: The size dependence of the lowest excited electronic state." *The Journal of Chemical Physics* 80(9): 4403-4409.
- (23) McBride, J., J. Treadway, et al. (2006). "Structural Basis for Near Unity Quantum Yield Core/Shell Nanostructures." *Nano Letters* 6(7): 1496-1501.
- (24) Yu, W. W., L. Qu, et al. (2003). "Experimental Determination of the Extinction Coefficient of CdTe, CdSe, and CdS Nanocrystals." *Chemistry of Materials* 15(14): 2854-2860.
- (25) Kucur, E., F. M. Boldt, et al. (2007). "Quantitative Analysis of Cadmium Selenide Nanocrystal Concentration by Comparative Techniques." *Analytical Chemistry* 79(23): 8987-8993.
- (26) Dabbousi, B. O., J. Rodriguez-Viejo, et al. (1997). "(CdSe)ZnS Core-Shell Quantum Dots: Synthesis and Characterization of a Size Series of Highly Luminescent Nanocrystallites." *The Journal of Physical Chemistry B* 101(46): 9463-9475.
- (27) Du, H., C. Chen, et al. (2002). "Optical Properties of Colloidal PbSe Nanocrystals." *Nano Letters* 2(11): 1321-1324.
- (28) Brumer, M., A. Kigel, et al. (2005). "PbSe/PbS and PbSe/PbSe Core/Shell Nanocrystals." *Advanced Functional Materials* 15(7): 1111-1116.
- (29) Murray, C. B., D. J. Norris, et al. (1993). "Synthesis and characterization of nearly monodisperse CdE (E = sulfur, selenium, tellurium) semiconductor nanocrystallites." *Journal of the American Chemical Society* 115(19): 8706-8715.
- (30) Chan, W. C. W., D. J. Maxwell, et al. (2002). "Luminescent quantum dots for multiplexed biological detection and imaging." *Current Opinion in Biotechnology* 13(1): 40-46.

- (31) Jaiswal, J. K., H. Mattoussi, et al. (2003). "Long-term multiple color imaging of live cells using quantum dot bioconjugates." *Nat Biotech* 21(1): 47-51.
- (32) Stroh, M., J. P. Zimmer, et al. (2005). "Quantum dots spectrally distinguish multiple species within the tumor milieu in vivo." *Nat Med* 11(6): 678-682.
- (33) Chattopadhyay, P. K., D. A. Price, et al. (2006). "Quantum dot semiconductor nanocrystals for immunophenotyping by polychromatic flow cytometry." *Nat Med* 12(8): 972-977.
- (34) Grecco, H. E., K. A. Lidke, et al. (2004). "Ensemble and single particle photophysical properties (two-photon excitation, anisotropy, FRET, lifetime, spectral conversion) of commercial quantum dots in solution and in live cells." *Microsc Res Tech* 65(4-5): 169-79.
- (35) Bastiaens, P. I. H. and A. Squire (1999). "Fluorescence lifetime imaging microscopy: spatial resolution of biochemical processes in the cell." *Trends in Cell Biology* 9(2): 48-52.
- (36) Dahan, M., T. Laurence, et al. (2001). "Time-gated biological imaging by use of colloidal quantum dots." *Opt. Lett.* 26(11): 825-827.
- (37) Gadella Jr, T. W. J., T. M. Jovin, et al. (1993). "Fluorescence lifetime imaging microscopy (FLIM): Spatial resolution of microstructures on the nanosecond time scale." *Biophysical Chemistry* 48(2): 221-239.
- (38) Schlegel, G., J. Bohnenberger, et al. (2002). "Fluorescence decay time of single semiconductor nanocrystals." *Phys Rev Lett* 88(13): 137401.
- (39) Larson, D. R., W. R. Zipfel, et al. (2003). "Water-Soluble Quantum Dots for Multiphoton Fluorescence Imaging in Vivo." *Science* 300(5624): 1434-1436.
- (40) Markus, G., Z. Jan, et al. (2008). "Stability and Fluorescence Quantum Yield of CdSe/ZnS Quantum Dots. Influence of the Thickness of the ZnS Shell" *Annals of the New York Academy of Sciences* 1130(Fluorescence Methods and Applications: Spectroscopy, Imaging, and Probes): 235-241.
- (41) Talapin, D. V., I. Mekis, et al. (2004). "CdSe/CdS/ZnS and CdSe/ZnSe/ZnS Core/Shell/Shell Nanocrystals." *The Journal of Physical Chemistry B* 108(49): 18826-18831.
- (42) Talapin, D. V., A. L. Rogach, et al. (2001). "Highly Luminescent Monodisperse CdSe and CdSe/ZnS Nanocrystals Synthesized in Hexadecylamine/Trioctylphosphine Oxide/Trioctylphosphine Mixture." *Nano Letters* 1(4): 207-211.
- (43) Bao, H., Y. Gong, et al. (2004). "Enhancement Effect of Illumination on the Photoluminescence of Water-Soluble CdTe Nanocrystals: Toward Highly Fluorescent CdTe/CdS Core-Shell Structure." *Chemistry of Materials* 16(20): 3853-3859.
- (44) Chen, Y. and Z. Rosenzweig (2002). "Luminescent CdS Quantum Dots as Selective Ion Probes." *Analytical Chemistry* 74(19): 5132-5138.
- (45) Lemon, B. I. and R. M. Crooks (2000). "Preparation and Characterization of Dendrimer-Encapsulated CdS Semiconductor Quantum Dots." *Journal of the American Chemical Society* 122(51): 12886-12887.
- (46) Mews, A., A. V. Kadavanich, et al. (1996). "Structural and spectroscopic investigations of CdS/HgS/CdS quantum-dot quantum wells." *Physical Review B* 53(20): R13242.

- (47) Bharali, D. J., D. W. Lucey, et al. (2005). "Folate-Receptor-Mediated Delivery of InP Quantum Dots for Bioimaging Using Confocal and Two-Photon Microscopy." *Journal of the American Chemical Society* 127(32): 11364-11371.
- (48) Kim, S.-W., J. P. Zimmer, et al. (2005). "Engineering InAs_xP_{1-x}/InP/ZnSe III⁺V Alloyed Core/Shell Quantum Dots for the Near-Infrared." *Journal of the American Chemical Society* 127(30): 10526-10532.
- (49) Micic, O. I., J. R. Sprague, et al. (1995). "Synthesis and Characterization of InP, GaP, and GaInP₂ Quantum Dots." *The Journal of Physical Chemistry* 99(19): 7754-7759.
- (50) Xie, R., D. Battaglia, et al. (2007). "Colloidal InP Nanocrystals as Efficient Emitters Covering Blue to Near-Infrared." *Journal of the American Chemical Society* 129(50): 15432-15433.
- (51) Pons, T., E. Pic, et al. "Cadmium-Free CuInS₂/ZnS Quantum Dots for Sentinel Lymph Node Imaging with Reduced Toxicity." *ACS Nano* 4(5): 2531-2538.
- (52) Torimoto, T., T. Adachi, et al. (2007). "Facile synthesis of ZnS-AgInS₂ solid solution nanoparticles for a color-adjustable luminophore." *J Am Chem Soc* 129(41): 12388-9.
- (53) Hezinger, A. F., J. Tessmar, et al. (2008). "Polymer coating of quantum dots--a powerful tool toward diagnostics and sensorics." *Eur J Pharm Biopharm* 68(1): 138-52.
- (54) Pellegrino, T., L. Manna, et al. (2004). "Hydrophobic Nanocrystals Coated with an Amphiphilic Polymer Shell: A General Route to Water Soluble Nanocrystals." *Nano Letters* 4(4): 703-707.
- (55) Gao, X., Y. Cui, et al. (2004). "In vivo cancer targeting and imaging with semiconductor quantum dots." *Nat Biotech* 22(8): 969-976.
- (56) Darbandi, M., R. Thomann, et al. (2005). "Single Quantum Dots in Silica Spheres by Microemulsion Synthesis." *Chemistry of Materials* 17(23): 5720-5725.
- (57) Gerion, D., F. Pinaud, et al. (2001). "Synthesis and Properties of Biocompatible Water-Soluble Silica-Coated CdSe/ZnS Semiconductor Quantum Dots" *The Journal of Physical Chemistry B* 105(37): 8861-8871.
- (58) Hu, X., P. Zrazhevskiy, et al. (2009). "Encapsulation of Single Quantum Dots with Mesoporous Silica." *Annals of Biomedical Engineering* 37(10): 1960-1966.
- (59) Ow, H., D. R. Larson, et al. (2005). "Bright and stable core-shell fluorescent silica nanoparticles." *Nano Lett* 5(1): 113-7.
- (60) Rong, H. and et al. (2007). "Core/shell fluorescent magnetic silica-coated composite nanoparticles for bioconjugation." *Nanotechnology* 18(31): 315601.
- (61) Selvan, S. T., T. T. Tan, et al. (2005). "Robust, Non-Cytotoxic, Silica-Coated CdSe Quantum Dots with Efficient Photoluminescence." *Advanced Materials* 17(13): 1620-1625.
- (62) Thomas, N. and M. Paul (2004). "Single Quantum Dots in Spherical Silica Particles13." *Angewandte Chemie International Edition* 43(40): 5393-5396.
- (63) Yi, D. K., S. T. Selvan, et al. (2005). "Silica-Coated Nanocomposites of Magnetic Nanoparticles and Quantum Dots." *Journal of the American Chemical Society* 127(14): 4990-4991.
- (64) Mattoussi, H., J. M. Mauro, et al. (2000). "Self-Assembly of CdSe/ZnS Quantum Dot Bioconjugates Using an Engineered Recombinant Protein." *Journal of the American Chemical Society* 122(49): 12142-12150.

- (65) Kim, S. and M. G. Bawendi (2003). "Oligomeric Ligands for Luminescent and Stable Nanocrystal Quantum Dots." *Journal of the American Chemical Society* 125(48): 14652-14653.
- (66) Sonal Mazumder, Rajib Dey, M. K. Mitra, S. Mukherjee, and G. C. Das (2009). "Biofunctionalized Quantum Dots in Biology and Medicine." *Journal of Nanomaterials*, Article ID 815734, 17 pages.
- (67) Bao, H., Y. Gong, et al. (2004). "Enhancement Effect of Illumination on the Photoluminescence of Water-Soluble CdTe Nanocrystals: Toward Highly Fluorescent CdTe/CdS Core/Shell Structure." *Chemistry of Materials* 16(20): 3853-3859.
- (68) Peng, H., L. Zhang, et al. (2007). "Preparation of water-soluble CdTe/CdS core/shell quantum dots with enhanced photostability." *Journal of Luminescence* 127(2): 721-726.
- (69) Wuister, S. F., I. Swart, et al. (2003). "Highly Luminescent Water-Soluble CdTe Quantum Dots." *Nano Letters* 3(4): 503-507.
- (70) Zheng, Y., Z. Yang, et al. (2007). "Aqueous Synthesis of Glutathione-Capped ZnSe and ZnCdSe Alloyed Quantum Dots." *Advanced Materials* 19(11): 1475-1479.
- (71) Pinaud, F., D. King, et al. (2004). "Bioactivation and Cell Targeting of Semiconductor CdSe/ZnS Nanocrystals with Phytochelatin-Related Peptides." *Journal of the American Chemical Society* 126(19): 6115-6123.
- (72) Gomez, N., J. O. Winter, et al. (2005). "Challenges in quantum dot-neuron active interfacing." *Talanta* 67(3): 462-471.
- (73) Mitchell, G. P., C. A. Mirkin, et al. (1999). "Programmed Assembly of DNA Functionalized Quantum Dots." *Journal of the American Chemical Society* 121(35): 8122-8123.
- (74) Brannon-Peppas, L. (2000). "Poly(ethylene glycol): Chemistry and Biological Applications: J.M. Harris and S. Zalipsky, editors, American Chemical Society, Washington DC, 1997, 489 pp." *Journal of Controlled Release* 66(2-3): 321-326.
- (75) Bentzen, E. L., I. D. Tomlinson, et al. (2005). "Surface Modification To Reduce Nonspecific Binding of Quantum Dots in Live Cell Assays." *Bioconjugate Chemistry* 16(6): 1488-1494.
- (76) Warnement, M. R., I. D. Tomlinson, et al. (2008). "Controlling the Reactivity of Amphiphilic Quantum Dots in Biological Assays through Hydrophobic Assembly of Custom PEG Derivatives." *Bioconjugate Chemistry* 19(7): 1404-1413.
- (77) Goldman, E. R., E. D. Balighian, et al. (2002). "Avidin: A Natural Bridge for Quantum Dot-Antibody Conjugates." *Journal of the American Chemical Society* 124(22): 6378-6382.
- (78) Chalet, L. and F. J. Wolf (1964). "The properties of streptavidin, a biotin-binding protein produced by Streptomycetes." *Archives of Biochemistry and Biophysics* 106: 1-5.
- (79) Weber, P. C., D. H. Ohlendorf, et al. (1989). "Structural origins of high-affinity biotin binding to streptavidin." *Science* 243(4887): 85-88.
- (80) Wilchek, M. and E. A. Bayer (1990). "Introduction to avidin-biotin technology." *Methods Enzymol* 184: 5-13.
- (81) Wu, X., H. Liu, et al. (2003). "Immunofluorescent labeling of cancer marker Her2 and other cellular targets with semiconductor quantum dots." *Nat Biotech* 21(1): 41-46.

- (82) Dahan, M., S. Levi, et al. (2003). "Diffusion Dynamics of Glycine Receptors Revealed by Single-Quantum Dot Tracking." *Science* 302(5644): 442-445.
- (83) Lidke, D. S., P. Nagy, et al. (2004). "Quantum dot ligands provide new insights into erbB/HER receptor-mediated signal transduction." *Nat Biotech* 22(2): 198-203.
- (84) George, N., H. Pick, et al. (2004). "Specific Labeling of Cell Surface Proteins with Chemically Diverse Compounds." *Journal of the American Chemical Society* 126(29): 8896-8897.
- (85) Warnement, M. R., I. D. Tomlinson, et al. (2007). "Fluorescent Imaging Applications of Quantum Dot Probes." *Current Nanoscience* 3: 273-284.
- (86) Howarth, M., K. Takao, et al. (2005). "Targeting quantum dots to surface proteins in living cells with biotin ligase." *Proceedings of the National Academy of Sciences of the United States of America* 102(21): 7583-7588.
- (87) Sun, Y., O. Sato, et al. "Single-molecule stepping and structural dynamics of myosin X." *Nat Struct Mol Biol* 17(4): 485-491.
- (88) Genin, E., O. Carion, et al. (2008). "CrAsH-Quantum Dot Nanohybrids for Smart Targeting of Proteins." *Journal of the American Chemical Society* 130(27): 8596-8597.
- (89) Yan, Z., S. Min-kyung, et al. (2006). "HaloTag Protein-Mediated Site-Specific Conjugation of Bioluminescent Proteins to Quantum Dots." *Angewandte Chemie International Edition* 45(30): 4936-4940.
- (90) Hauser, C. T. and R. Y. Tsien (2007). "A hexahistidine-Zn²⁺-dye label reveals STIM1 surface exposure." *Proceedings of the National Academy of Sciences* 104(10): 3693-3697.
- (91) Roullier, V., S. Clarke, et al. (2009). "High-Affinity Labeling and Tracking of Individual Histidine-Tagged Proteins in Live Cells Using Ni²⁺ Tris-nitrilotriacetic Acid Quantum Dot Conjugates." *Nano Letters* 9(3): 1228-1234.
- (92) Rosenthal, S. J., I. Tomlinson, et al. (2002). "Targeting Cell Surface Receptors with Ligand-Conjugated Nanocrystals." *Journal of the American Chemical Society* 124(17): 4586-4594.
- (93) Goldman, E. R., G. P. Anderson, et al. (2002). "Conjugation of Luminescent Quantum Dots with Antibodies Using an Engineered Adaptor Protein To Provide New Reagents for Fluoroimmunoassays." *Analytical Chemistry* 74(4): 841-847.
- (94) Hanaki, K.-i., A. Momo, et al. (2003). "Semiconductor quantum dot/albumin complex is a long-life and highly photostable endosome marker." *Biochemical and Biophysical Research Communications* 302(3): 496-501.
- (95) Pinaud, F., S. Clarke, et al. "Probing cellular events, one quantum dot at a time." *Nat Meth* 7(4): 275-285.
- (96) Joo, K.-I., Y. Lei, et al. (2008). "Site-Specific Labeling of Enveloped Viruses with Quantum Dots for Single Virus Tracking." *ACS Nano* 2(8): 1553-1562.
- (97) Schormann, W., F. Hammersen, et al. (2008). "Tracking of human cells in mice." *Histochemistry and Cell Biology* 130(2): 329-338.
- (98) Yildiz, A. and P. R. Selvin (2005). "Fluorescence imaging with one nanometer accuracy: application to molecular motors." *Acc Chem Res* 38(7): 574-82.
- (99) McHale, K., A. J. Berglund, et al. (2007). "Quantum Dot Photon Statistics Measured by Three-Dimensional Particle Tracking." *Nano Letters* 7(11): 3535-3539.
- (100) Pavani, S. R. P., M. A. Thompson, et al. (2009). "Three-dimensional, single-molecule fluorescence imaging beyond the diffraction limit by using a double-helix point

- spread function." *Proceedings of the National Academy of Sciences* 106(9): 2995-2999.
- (101) Toprak, E., H. Balci, et al. (2007). "Three-Dimensional Particle Tracking via Bifocal Imaging." *Nano Letters* 7(7): 2043-2045.
 - (102) Saxton, M. J. and K. Jacobson (2003). "SINGLE-PARTICLE TRACKING: Applications to Membrane Dynamics." *Annual Review of Biophysics and Biomolecular Structure* 26(1): 373-399.
 - (103) Saxton, M. J. (2007). "A Biological Interpretation of Transient Anomalous Subdiffusion. I. Qualitative Model." 92(4): 1178-1191.
 - (104) Cui, B., C. Wu, et al. (2007). "One at a time, live tracking of NGF axonal transport using quantum dots." *Proceedings of the National Academy of Sciences* 104(34): 13666-13671.
 - (105) Zhang, Q., Y. Li, et al. (2009). "The Dynamic Control of Kiss-And-Run and Vesicular Reuse Probed with Single Nanoparticles." *Science* 323(5920): 1448-1453.
 - (106) Heine, M., L. Groc, et al. (2008). "Surface Mobility of Postsynaptic AMPARs Tunes Synaptic Transmission." *Science* 320(5873): 201-205.
 - (107) Pierobon, P., S. Achouri, et al. (2009). "Velocity, Processivity, and Individual Steps of Single Myosin V Molecules in Live Cells." 96(10): 4268-4275.
 - (108) Manabe, N., A. Hoshino, et al. (2005). *Toward the in vivo study of captopril-conjugated quantum dots. Nanobiophotonics and Biomedical Applications II*, San Jose, CA, USA, SPIE.
 - (109) Bagalkot, V., L. Zhang, et al. (2007). "Quantum Dot-Aptamer Conjugates for Synchronous Cancer Imaging, Therapy, and Sensing of Drug Delivery Based on Bi-Fluorescence Resonance Energy Transfer." *Nano Letters* 7(10): 3065-3070.
 - (110) Jia, N., Q. Lian, et al. (2007). "Intracellular Delivery of Quantum Dots Tagged Antisense Oligodeoxynucleotides by Functionalized Multiwalled Carbon Nanotubes." *Nano Letters* 7(10): 2976-2980.
 - (111) Delehanty, J., H. Mattoussi, et al. (2009). "Delivering quantum dots into cells: strategies, progress and remaining issues." *Analytical and Bioanalytical Chemistry* 393(4): 1091-1105.
 - (112) Jaiswal, J. K., E. R. Goldman, et al. (2004). "Use of quantum dots for live cell imaging." *Nat Methods* 1(1): 73-8.
 - (113) Ruan, G., A. Agrawal, et al. (2007). "Imaging and Tracking of Tat Peptide-Conjugated Quantum Dots in Living Cells: New Insights into Nanoparticle Uptake, Intracellular Transport, and Vesicle Shedding." *Journal of the American Chemical Society* 129(47): 14759-14766.
 - (114) Cheng, Z., Y. Wu, et al. (2005). "Near-Infrared Fluorescent RGD Peptides for Optical Imaging of Integrin $\alpha_5\beta_1$ Expression in Living Mice." *Bioconjugate Chemistry* 16(6): 1433-1441.
 - (115) Cai, W., D.-W. Shin, et al. (2006). "Peptide-Labeled Near-Infrared Quantum Dots for Imaging Tumor Vasculature in Living Subjects." *Nano Letters* 6(4): 669-676.
 - (116) Chakraborty, S. K., J. A. J. Fitzpatrick, et al. (2007). "Cholera Toxin B Conjugated Quantum Dots for Live Cell Labeling." *Nano Letters* 7(9): 2618-2626.
 - (117) Derfus, A. M., A. A. Chen, et al. (2007). "Targeted Quantum Dot Conjugates for siRNA Delivery." *Bioconjugate Chemistry* 18(5): 1391-1396.
 - (118) Chen, F. and D. Gerion (2004). "Fluorescent CdSe/ZnS nanocrystal-peptide conjugates for long-term, nontoxic imaging and nuclear targeting in living cells." *Nano Letters* 4(10): 131-141.

- (119) Derfus, A. M., W. C. W. Chan, et al. (2004). "Intracellular Delivery of Quantum Dots for Live Cell Labeling and Organelle Tracking." *Advanced Materials* 16(12): 961-966.
- (120) Sekar, R. B. and A. Periasamy (2003). "Fluorescence resonance energy transfer (FRET) microscopy imaging of live cell protein localizations." *J Cell Biol* 160(5): 629-33.
- (121) Selvin, P. R. (2000). "The renaissance of fluorescence resonance energy transfer." *Nat Struct Biol* 7(9): 730-4.
- (122) Medintz, I. L. and H. Mattoussi (2009). "Quantum dot-based resonance energy transfer and its growing application in biology." *Phys Chem Chem Phys* 11(1): 17-45.
- (123) Zhang, C. Y. and L. W. Johnson (2006). "Quantum-dot-based nanosensor for RRE IIB RNA-Rev peptide interaction assay." *J Am Chem Soc* 128(16): 5324-5.
- (124) Gill, R., I. Willner, et al. (2005). "Fluorescence Resonance Energy Transfer in CdSe/ZnS DNA Conjugates: Probing Hybridization and DNA Cleavage." *The Journal of Physical Chemistry B* 109(49): 23715-23719.
- (125) Snee, P. T., R. C. Somers, et al. (2006). "A ratiometric CdSe/ZnS nanocrystal pH sensor." *J Am Chem Soc* 128(41): 13320-1.
- (126) Medintz, I. L., A. R. Clapp, et al. (2003). "Self-assembled nanoscale biosensors based on quantum dot FRET donors." *Nat Mater* 2(9): 630-638.
- (127) Bakalova, R., H. Ohba, et al. (2004). "Quantum dots as photosensitizers?" *Nat Biotechnol* 22(11): 1360-1.
- (128) Bakalova, R., H. Ohba, et al. (2004). "Quantum Dot anti-CD Conjugates: Are They Potential Photosensitizers or Potentiators of Classical Photosensitizing Agents in Photodynamic Therapy of Cancer?" *Nano Letters* 4(9): 1567-1573.
- (129) Tsay, J. M., M. Trzoss, et al. (2007). "Singlet oxygen production by Peptide-coated quantum dot-photosensitizer conjugates." *J Am Chem Soc* 129(21): 6865-71.
- (130) Pons, T., I. L. Medintz, et al. (2006). "Solution-Phase Single Quantum Dot Fluorescence Resonance Energy Transfer." *Journal of the American Chemical Society* 128(47): 15324-15331.
- (131) Zhang, C.-Y., H.-C. Yeh, et al. (2005). "Single-quantum-dot-based DNA nanosensor." *Nat Mater* 4(11): 826-831.
- (132) Smith, J. D., G. W. Fisher, et al. (2007). "The use of quantum dots for analysis of chick CAM vasculature." *Microvascular Research* 73(2): 75-83.
- (133) Smith, B. R., Z. Cheng, et al. (2008). "Real-time intravital imaging of RGD-quantum dot binding to luminal endothelium in mouse tumor neovasculature." *Nano Lett* 8(9): 2599-606.
- (134) Kim, S., Y. T. Lim, et al. (2004). "Near-infrared fluorescent type II quantum dots for sentinel lymph node mapping." *Nat Biotechnol* 22(1): 93-7.
- (135) Hardman, R. (2006). "A toxicologic review of quantum dots: toxicity depends on physicochemical and environmental factors." *Environ Health Perspect* 114(2): 165-72.
- (136) Evans, C. L., E. O. Potma, et al. (2005). "Chemical imaging of tissue in vivo with video-rate coherent anti-Stokes Raman scattering microscopy." *Proceedings of the National Academy of Sciences of the United States of America* 102(46): 16807-16812.
- (137) Mulder, W. J., R. Koole, et al. (2006). "Quantum dots with a paramagnetic coating as a bimodal molecular imaging probe." *Nano Lett* 6(1): 1-6.
- (138) Yang, H., S. Santra, et al. (2006). "Gd^{III}-Functionalized Fluorescent Quantum Dots as Multimodal Imaging Probes." *Advanced Materials* 18(21): 2890-2894.

- (139) Flick, D. F., H. F. Kraybill, et al. (1971). "Toxic effects of cadmium: A review." *Environmental Research* 4(2): 71-85.
- (140) Bertin, G. and D. Averbeck (2006). "Cadmium: cellular effects, modifications of biomolecules, modulation of DNA repair and genotoxic consequences (a review)." *Biochimie* 88(11): 1549-59.
- (141) Pelley, J. L., A. S. Daar, et al. (2009). "State of academic knowledge on toxicity and biological fate of quantum dots." *Toxicol Sci* 112(2): 276-96.
- (142) Jaiswal, J. K. and S. M. Simon (2004). "Potentials and pitfalls of fluorescent quantum dots for biological imaging." *Trends in Cell Biology* 14(9): 497-504.
- (143) Howarth, M., D. J. F. Chinnapen, et al. (2006). "A monovalent streptavidin with a single femtomolar biotin binding site." *Nat Meth* 3(4): 267-273.
- (144) Nirmal, M., B. O. Dabbousi, et al. (1996). "Fluorescence intermittency in single cadmium selenide nanocrystals." *Nature* 383(6603): 802-804.
- (145) Frantsuzov, P. A., S. Volkán-Kacsó, et al. (2009). "Model of Fluorescence Intermittency of Single Colloidal Semiconductor Quantum Dots Using Multiple Recombination Centers." *Physical Review Letters* 103(20): 207402.
- (146) Mahler, B., P. Spinicelli, et al. (2008). "Towards non-blinking colloidal quantum dots." *Nat Mater* 7(8): 659-664.
- (147) Wang, X., X. Ren, et al. (2009). "Non-blinking semiconductor nanocrystals." *Nature* 459(7247): 686-689.
- (148) Tomlinson, I. D., J. N. Mason, et al. (2005). "Peptide-conjugated quantum dots: imaging the angiotensin type 1 receptor in living cells." *Methods Mol Biol* 303: 51-60.
- (149) Charalambous, A., M. Andreou, et al. (2009). "Intein-mediated site-specific conjugation of Quantum Dots to proteins in vivo." *Journal of Nanobiotechnology* 7(1): 9.
- (150) Orndorff, R. L. and S. J. Rosenthal (2009). "Neurotoxin quantum dot conjugates detect endogenous targets expressed in live cancer cells." *Nano Lett* 9(7): 2589-99.
- (151) Orndorff, R. L., M. R. Warnement, et al. (2008). "Quantum Dot Ex Vivo Labeling of Neuromuscular Synapses." *Nano Letters* 8(3): 780-785.
- (152) Zhou, M., E. Nakatani, et al. (2007). "Peptide-labeled quantum dots for imaging GPCRs in whole cells and as single molecules." *Bioconjug Chem* 18(2): 323-32.
- (153) Clarke, S. J., C. A. Hollmann, et al. (2006). "Photophysics of dopamine-modified quantum dots and effects on biological systems." *Nat Mater* 5(5): 409-417.
- (154) Gussin, H. I. n. A., I. D. Tomlinson, et al. (2006). "Binding of Muscimol-Conjugated Quantum Dots to GABAC Receptors." *Journal of the American Chemical Society* 128(49): 15701-15713.
- (155) Courty, S. b., C. Luccardini, et al. (2006). "Tracking Individual Kinesin Motors in Living Cells Using Single Quantum-Dot Imaging." *Nano Letters* 6(7): 1491-1495.
- (156) O'Connell, K. M. S., A. S. Rolig, et al. (2006). "Kv2.1 Potassium Channels Are Retained within Dynamic Cell Surface Microdomains That Are Defined by a Perimeter Fence." *J. Neurosci.* 26(38): 9609-9618.
- (157) Pathak, S., S.-K. Choi, et al. (2001). "Hydroxylated Quantum Dots as Luminescent Probes for in Situ Hybridization." *Journal of the American Chemical Society* 123(17): 4103-4104.
- (158) Osaki, F., T. Kanamori, et al. (2004). "A Quantum Dot Conjugated Sugar Ball and Its Cellular Uptake. On the Size Effects of Endocytosis in the Subviral Region." *Journal of the American Chemical Society* 126(21): 6520-6521.

- (159) Dubertret, B., P. Skourides, et al. (2002). "In Vivo Imaging of Quantum Dots Encapsulated in Phospholipid Micelles." *Science* 298(5599): 1759-1762.

CHAPTER III

ENSEMBLE AND SINGLE QUANTUM DOT FLUORESCENCE METHODS IN NEUROTRANSMITTER TRANSPORTER RESEARCH

3.1. Introduction

Traditional biochemical and genetic approaches have contributed the majority of the existing research knowledge on NTT structure, function, and regulation. It is now apparent that NTT function is tightly regulated through multiple posttranslational mechanisms including interactions with a plethora of kinases, receptors, and scaffolding elements.¹⁻⁵ Consequent dynamic changes in NTT subcellular localization fundamentally impact the amplitude, duration, and specificity of NTT-mediated neurotransmitter signaling. Therefore, ability to “see” NTTs with subcellular resolution and to monitor dynamic trafficking pathways involved in NTT regulation becomes a critical tool in advancing our understanding of the molecular mechanisms underlying NTT signaling network.

Recent advances in fluorescence-based techniques for molecular biology permitted investigation of cellular signal transduction cascades with unprecedented spatiotemporal resolution.^{6,7} Currently, there are several classes of fluorescent probes available to investigators. Among these, the most prevalent fluorophores are organic, dyes, genetically encoded fluorescent proteins, and semiconductor nanocrystals, colloquially known as quantum dots (QDs).⁸⁻¹⁵ General properties, advantages, and drawbacks of the aforementioned fluorophores are summarized in Table 3.1. Our group is primarily focused on exploiting the unique photophysical properties of QDs (excellent brightness, narrow

Table 3.1 Comparison of the photophysical properties of the commonly encountered fluorescent probes.

Property	Cy5	EGFP	QD655
Size	~0.5 nm; 792 Da	~5 nm; ~27 kDa	15-25 nm; >1000 kDa
Quantum Yield	0.3	0.6	0.5
Molar Absorption Coefficient	$2.5 \times 10^5 \text{ M}^{-1}\text{cm}^{-1}$	$5.6 \times 10^4 \text{ M}^{-1}\text{cm}^{-1}$	$>2 \times 10^6 \text{ M}^{-1}\text{cm}^{-1}$
Excitation/Emission Maxima	649/670 nm	488/509 nm	steady increase toward UV wavelengths starting from absorption onset; emission max at 655 nm, with FWHM ~30 nm
Photostability	5-10 s	5-10 s	minutes
Applicability to Single-Molecule Imaging	moderate; limited by poor photostability	moderate; limited by poor photostability	excellent; complicated by blinking

emission spectra, broad excitation spectra, and superior photostability) to study subcellular distribution and dynamic regulation of NTTs.¹⁶⁻²³

There are several methodological approaches to enable specific targeting of membrane proteins in live cells with the aforementioned fluorescent probes (Table 3.2). Most commonly, (1) a fluorescent protein (e.g., EGFP) is fused to the terminus of the target protein and expressed in the cell of interest, or (2) a fluorophore is attached to an antibody targeting the extracellular domain of the target protein. Unfortunately, limited availability of such extracellular antibodies for NTTs and lack of suitable extracellular epitopes within the NTT structure have significantly hampered fluorescence-based investigation of NTT localization and regulation, particularly in endogenous systems. To this end, we pioneered a ligand-conjugated QD-based approach that utilizes a transporter-specific organic ligand composed of (1) a high-affinity parent drug that enables recognition of specific binding sites within the transporter structure and facilitates pseudo-irreversible binding, (2) a hydrophobic

Table 3.2. Methodological approaches that enable specific targeting of neurotransmitter transporters.

Approach	Advantages\Disadvantages	References
Genetic Fusion (XFP; Hemagglutinin fusion peptide)	Pros: perfect specificity, biocompatibility, retention of the XFP-target protein construct; Cons: incompatibility with endogenous expression systems, misfolding, failure to localize properly, altered activity compared to the wildtype protein	25-31
Antibody	Pros: excellent specificity, biocompatibility, low cytotoxicity, compatibility with endogenous expression systems; Cons: lack of efficient external antibodies, large size, prone to chemical degradation	32
Organic Ligand	Pros: targeting specificity and selectivity, binding stability, compatibility with endogenous expression systems, biological activity; Cons: sophisticated organic chemistry and rigorous analytical characterization required for preparation, primary binding site occupied	16-24, 33-36
Covalent Modification	Pros: excellent selectivity, possibility of an inert functional tag, small size Cons: potentially deleterious effects on protein structure and function, organic chemistry knowledge required	37, 38

alkyl spacer which permits sufficient flexibility and provides a hydrophobic interface for a successful drug-binding pocket interaction, (3) a PEG polymer that aids in aqueous solubility and abolishes possible nonspecific interactions with the plasma membrane, and (4) a biotin moiety that allows subsequent streptavidin-conjugated QD recognition upon the transporter binding event (Figure 3.1).¹⁶⁻²³

In this chapter, we outline three fluorescence-based techniques that have been successfully applied to measure spatiotemporal changes in NTT localization and to establish dynamic imaging of individual NTT molecules using our ligand-conjugated QD approach.

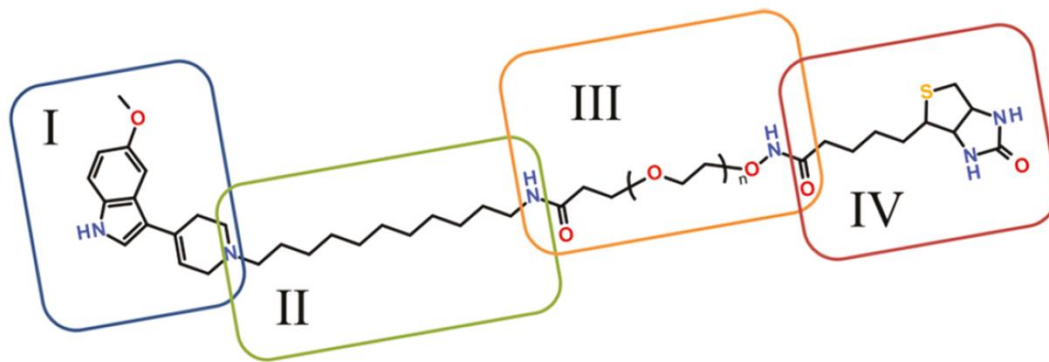


Figure 3.1. Structure schematic of tailored organic ligands targeting plasma membrane monoamine transporters. Reprinted with permission from Ref 21. Copyright 2011 American Chemical Society.

First, we discuss how to label and image membrane NTTs in live cells using QD probes in conjunction with ensemble fluorescence microscopy. Second, we present a more quantitative, flow cytometry-based protocol, particularly useful for assessing transporter internalization and recycling. Third, as dynamic trafficking of NTTs in the plasma membrane appears to be an important posttranslational regulatory mechanism, we describe a single-molecule microscopy protocol for determining the mobility of QD-bound transporters in the plasma membrane of live cells.

3.2. Materials: HEK293 Cell Culture and Reagents

1. DMEM medium (Gibco, Invitrogen Life Science, Bethesda, MD).
3. Phenol Red-free DMEM medium (Gibco, Invitrogen Life Science, Bethesda, MD).
4. Fetal bovine serum (FBS) (Gemini Bio-Products, West Sacramento, CA).
5. 0.05% Trypsin/EDTA (Cellgro, Mediatech).
6. L-Glutamine (Gibco, Invitrogen Life Science, Bethesda, MD).

7. T25/T75 flasks; 24-well or 96-well culture plates (BD Biosciences, Falcon).
8. Penicillin (10,000 U/mL) and streptomycin (10 mg/mL) solutions are frozen at -20°C (Gibco, Invitrogen Life Science); 5 mL is added to 0.5 L of DMEM complete culture medium.
9. Cell line: HEK293 cells transiently or stably expressing NTT of interest.
10. 0.1 mg/mL poly-D-lysine solution in sterile H_2O .
11. Lab-Tek chambered #1.0 borosilicate cover glass (eight-well chamber).
12. Biotinylated ligand (1 mM stock solution in sterile H_2O stored desiccated at -20°C).
13. Bovine serum albumin (BSA).
14. Streptavidin-conjugated quantum dots (SavQD605), with the emission maximum at 605 nm (Invitrogen Life Science, Bethesda, MD). Optimal filter is HQ 605/20 emission for QD605. QDs can be excited at any wavelengths, but 488-nm is a commonly utilized excitation line to minimize photodamage, QD blinking, and spectral cross-talk.
15. Cell Stripper, non-enzymatic dissociation buffer (Gibco, Invitrogen Life Science, Bethesda, MD).
16. Cell culture incubator, 37°C , 5% CO_2 .
17. Vacuum pump for cell washes.

3.3. Equipment, Software, and Accessories.

1. LSM 510 (Carl Zeiss) or LSM 710 (Carl Zeiss) equipped with a 63x 1.4 NA Apochromat oil-immersion objective lens and a 488-nm excitation line (Ar laser or solid-state diode laser); LSM 510/710 image acquisition/analysis software or ImageJ (NIH image analysis freeware) to process time-lapse and z-stack fluorescence images; microscope-mounted environmental chamber.
2. 3- or 5-laser Beckton-Dickinson (BD Biosciences, San Jose, CA) bench-top flow cytometer equipped with a multiwall plate sample cube; 12x75 mm polystyrene flow cytometry tubes (BD Biosciences, San Jose, CA); FlowJo flow cytometry data analysis package (TreeStar, Ashland, OR).
3. High-speed, line-scanning Zeiss 5 Live confocal microscope equipped with a 63x 1.4 NA oil-immersion objective lens and a 488-nm 100-milliwatt solid-state diode laser; microscope-mounted environmental chamber; Zeiss LSM Image Examiner software; MatLab or IDL-based programming routines for analysis of real-time QD trajectory data.
4. Imaging medium: phenol red-free DMEM supplemented with 1% BSA.

3.4. Methods

For the purpose of this chapter, it is assumed that the NTT of interest is expressed in HEK293 cells; however, the general principles and protocols described below remain valid for any expression system being used.

3.4.1. Ensemble Microscopy Protocol

1. HEK293 cells are cultured in DMEM supplemented with 10% FBS, 2 mM L-glutamine, 100 units/mL penicillin, and 100 mg/mL streptomycin and maintained at 37°C with 5% CO₂. For ensemble imaging, cells are plated in poly-D-lysine-treated (1 hour at at 37°C) eight-well Lab-Tek chambered coverglass at a density of $1 \times 10^5 - 1 \times 10^6$ cells and cultured for 24 hours prior to imaging.
2. Prior to labeling, wash the cells gently three times with warm phenol red-free culture medium.
3. Incubate cells with a biotinylated ligand (0.1-1 μM) in phenol red-free DMEM for 5-20 min at 37°C. In the meantime, prepare a SavQD605 labeling by diluting SavQD605 stock solution in warm imaging buffer to reach a desired concentration of (0.5-2 nM) and incubate it in a 37°C water bath for 10 min.
4. Wash the cells three times with warm phenol red-free DMEM.
5. Incubate the cells with SavQD605 solution for 5 min at 37°C and wash at least three times with warm imaging buffer.
6. Immediately post-labeling, place the chambered coverglass on the microscope with the mounted environmental chamber.
7. Acquire fluorescent images at 37°C. Example data are shown in Figure 3.2.

3.4.2. Flow Cytometry Protocol

1. Cells are plated in a poly-D-lysine-treated (1 hour at at 37°C) 24-well/96-well culture plate at a density of $1-5 \times 10^5$ cells/mL 48 hours prior to the flow cytometry assay.

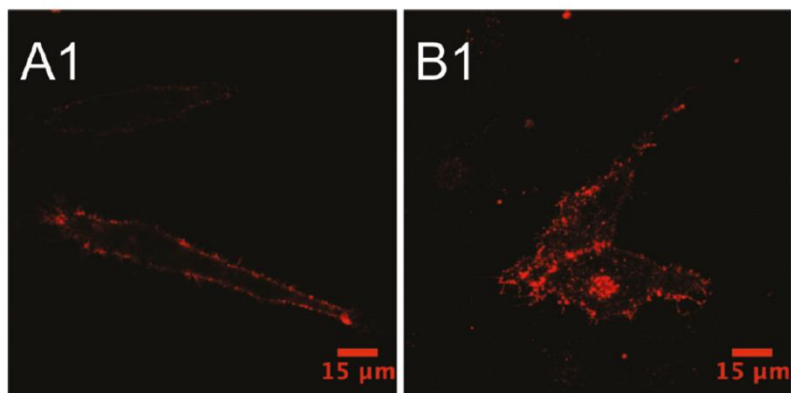


Figure 3.2. Labeling of dopamine transporter (DAT) with ligand-conjugated QDs in live cells. (left) streptavidin-conjugated QDs were used to label DATs previously exposed to a biotinylated, PEGylated cocaine analog. (A1) QD labeling of membrane DATs in a live HeLa cell. (B1) QD-bound DATs underwent acute redistribution from the plasma membrane to intracellular compartments as a result of protein kinase C (PKC) activation. Reprinted with permission from Ref 20. Copyright 2011 American Chemical Society.

2. Prior to labeling QD conjugate labeling, wash the cells three times with warm DMEM and incubate with a drug for 10-30 min in complete culture medium at 37°C and 5% CO₂. Parallel control wells are incubated with either drug-free complete culture medium (positive control) or in the presence of a high affinity transporter inhibitor (negative control).
3. Wash the cells three times with warm phenol red-free DMEM and incubate with biotinylated ligand (0.1-1 μM)/drug mixture for 10 min at 37°C in warm phenol red-free DMEM.
4. Wash the cells three times with ice-cold imaging buffer and incubate with previously prepared SavQD605 labeling solution in ice-cold imaging buffer.
5. Wash the cells gently three times with the ice-cold imaging buffer and add Cell Stripper solution. Incubate for 5-10 minutes at 37°C.
6. Analyze cell QD fluorescence using a flow cytometer.

7. Data are typically collected from >10,000 cells per sample, with median fluorescence intensity as one of the recorded fluorescent signal parameters.

8. By utilizing median fluorescence intensity (MFI) parameter obtained from control cell populations, it is possible to compute the percentage of DAT molecules unavailable for binding (PI, percent inhibition) according to the equation below:

$$PI = \frac{MFI_{pos} - MFI_{treated}}{MFI_{pos} - MFI_{neg}} \times 100\% \quad [2]$$

where MFI_{pos} is MFI of a positive control (QD-ligand-labeled cells), MFI_{neg} is MFI of a negative control (QD only-labeled cells), and $MFI_{treated}$ is MFI of a cell population incubated with a certain DAT modulator dose and subsequently labeled with ligand-conjugated QDs.²² Example data are shown in Figure 3.3.

3.4.3. Single-Molecule Microscopy Protocol

1. Cells are plated in poly-D-lysine-treated (1 hour at at 37°C) eight-well Lab-Tek chambered coverglass at a density of $1-5 \times 10^4$ cells and cultured for 24 hours prior to imaging.
2. Prior to labeling, wash the cells gently three times with warm phenol red-free culture medium.
3. Incubate cells with a biotinylated ligand (1-100 nM) in phenol red-free DMEM for 5-20 min at 37°C. In the meantime, prepare a SavQD605 labeling by diluting SavQD605 stock solution in warm imaging buffer to reach a desired concentration of (0.05-0.5 nM) and incubate it in a 37°C water bath for 10 min.
4. Wash the cells three times with warm phenol red-free DMEM.

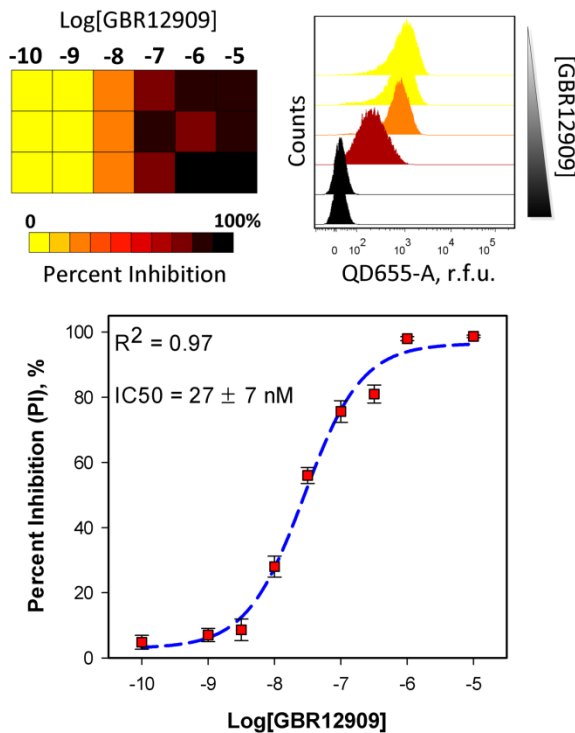


Figure 3.3. Flow cytometry-based screening of the inhibitory activity of GBR12909, a high-affinity DAT antagonist, using antagonist-conjugated QDs. DAT-expressing HEK cells were treated with five- or ten-fold dilutions of GBR12909. Percent inhibition at increasing doses of GBR12909 is represented as a heat map (top left) and representative histogram plots of the effects of increasing GBR12909 doses (top right) on QD conjugate binding are shown. The heat map and IC₅₀ curve (bottom) were generated using median QD fluorescence intensity values. Reprinted with permission from Ref 23. Copyright 2012 Royal Chemical Society.

5. Incubate the cells with SavQD605 solution for 5 min at 37°C and wash thoroughly at least three times with warm imaging buffer to remove unbound QDs.
6. Immediately post-labeling, place the chambered coverglass on the microscope with the mounted environmental chamber.
7. Acquire time-lapse fluorescent images at 37°C immediately after the final wash step. Typically, the final wash step is carried in the immediate vicinity of the imaging system.

8. Live imaging should not exceed 30 min at 37°C for cell survival and is optimally carried out within the initial 10-15 minutes to limit turnover of QD-bound membrane NTT molecules.

9. Real-time, time-lapse image recording is obtained with an integration time of 25-100 milliseconds for at least 500 consecutive frames. Example series are shown in Figure 3.4.

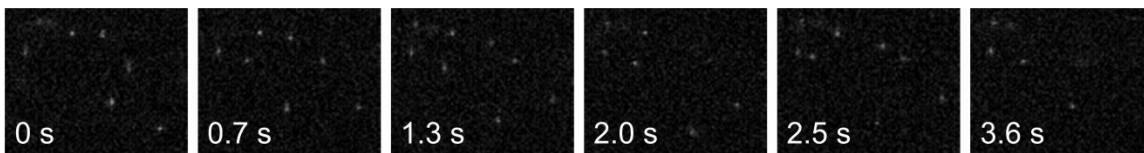


Figure 3.4. Time-lapse image series depicting movement of cell surface QD-bound transporters.

10. Real-time trajectory data is subsequently obtained from the recorded time-lapse image series and analyzed using custom programs written in Matlab or IDL programming software. Tracking analysis sequence is illustrated in Figure 3.5.

3.5 Troubleshooting and Notes

1. Optimal plating density and cell health are critical to keep weakly adherent cells, such as HEK293, from detaching off the Lab-Tek chambered coverglass throughout the protocol. Treatment of the chambered coverglass with poly-D-lysine solution is a necessary step to ensure the cells remain adhered to the glass bottom through the extensive series of incubation and wash steps. Also, it is of utmost importance that one carefully examines cell morphology and overall cell health prior to acquiring fluorescence data.

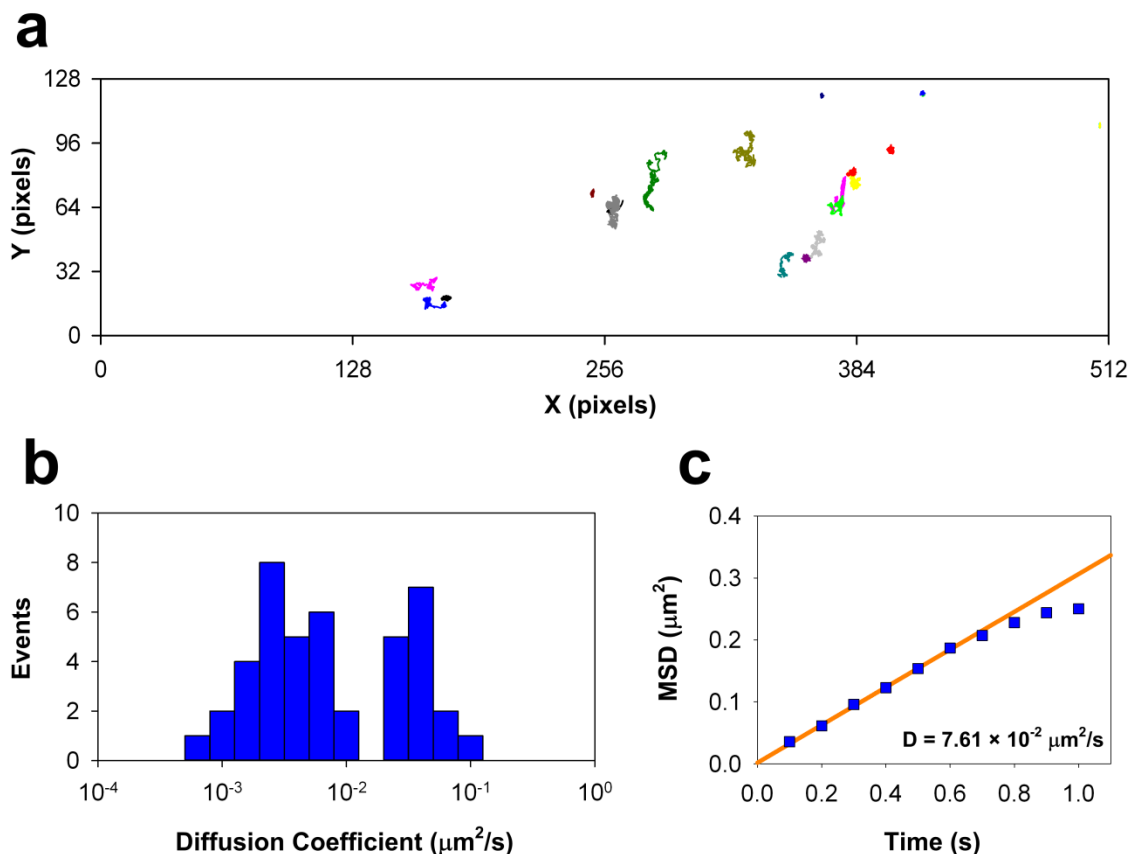


Figure 3.5. Schematic illustrating trajectory data analysis in a typical single-QD tracking experiment. (a) Example of QD-DAT trajectories on the surface of transfected HEK293 cells. Scale: 1 pixel = 200 nm. (b) A histogram showing diffusion coefficients determined for the trajectories in a. (c) Averaged mean square displacement (MSD)-time plot of QD trajectories. Ensemble diffusion coefficient is estimated via the linear fit of 2-5 MSD-time plot data points.

2. One of the most important variables for a successful experiment is adequate quality and quantity of washings after drug, biotinylated ligand, and QD incubation. One must wash extensively after each separate step to remove excess, unbound probes, as they have the potential to interfere with subsequent recognition events and ultimately affect the specificity of QD labeling. Additionally, it is imperative that one always prepares fresh working solutions the day of the experiment.

3. The most critical determinant of experimental success is the specificity of biotinylated ligand binding. One must find optimal ligand concentration and incubation time to maximize specific binding. In our experience, 0.1-1 μM and 5-20 min ranges for ligand dose and incubation time respectively are typically a good starting point. In all cases, one must run parallel control samples to ensure labeling specificity. The control samples usually are to (1) apply the same labeling conditions to parental cells not expressing the transporter of interest, (2) include a high-affinity inhibitor to block the specific binding site during the labeling protocol, and (3) label transporter-expressing cells with only the QD probes to assess the degree of nonspecific QD binding and the effectiveness of wash steps.

4. Another important aspect of assuring labeling specificity is the addition of a common blocking agent, such as BSA, to the QD solution and the imaging buffer. QD nonspecific binding varies significantly among cell types, and one must take great care to optimize the blocking conditions (Figure 2.6). Common blocking reagents are BSA, FBS, horse serum, gelatin, and nonfat dry milk.

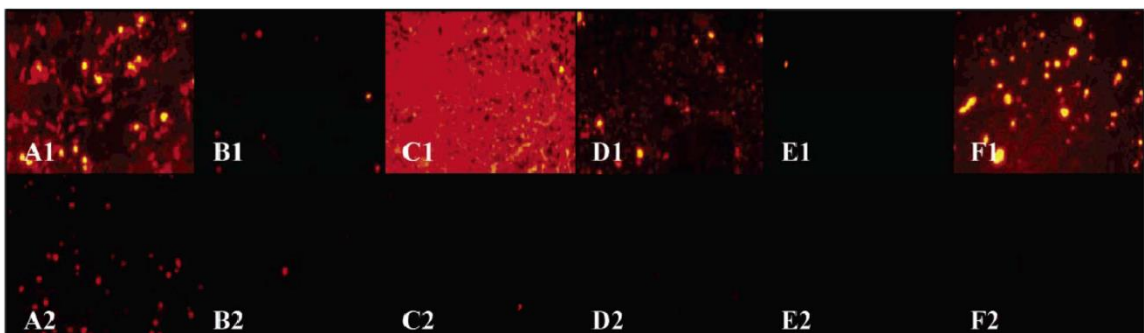


Figure 3.6. Comparison of nonspecific cell surface binding of 50 nM AMP™ Dots (A1-F1) and PEGylated AMP™ Dots (A2-F2). Nonspecific binding was found to be dependent upon the cell type, and conjugation of methoxy-terminated PEG2000 to the surface of AMP™ Dots resulted in significant reduction of nonspecific cellular binding. Figure reproduced with permission from Ref 40. Copyright 2005 American Chemical Society.

5. As QD-bound NTTs are subject to dynamic protein turnover, fluorescence data acquisition must be conducted immediately after the final wash step, especially in the case of single-molecule experiments. This helps prevent transporter endocytosis and allows adequate visualization of membrane-restricted signaling events.

6. An important consideration is controlling the valency of the binding. This is a particularly critical parameter in single-molecule experiments, as multivalent QD labeling leads to protein cross-linking that may inadvertently trigger downstream signal transduction cascades. To this end, there are two common solutions. One involves preincubation of SavQDs with the biotinylated ligand at ~1:1 ratio in a borate buffer (pH ~8.5) for 0.5-24 hours at room temperature with constant stirring; the other involves a two-step labeling protocol as described above and the use of ~equimolar doses of biotinylated ligand and SavQDs. In the case of endogenous expression systems, this requirement can be relaxed, as the low surface density of transporters is the primary determinant of monovalent labeling.

7. QD density must be adjusted accordingly to ensure maximum signal-to-noise ratio in ensemble imaging and permit observation of 10-20 individual QDs on the cell surface in a single-molecule experiment. This is achieved via titrating the QD concentration while keeping the concentration of biotinylated ligand constant.

8. Table 3.3 provides a set of troubleshooting instructions for a typical single-molecule experiment.^{38,39}

Table 3.3. Troubleshooting a single-QD imaging experiment.

Problem	Cause	Solution
Low or excessive QD label density	Inappropriate biotinylated ligand concentration	Optimize ligand concentrations for labeling
	Poor or excessive transporter expression	Check whether the transporter is delivered to the surface. Optimize protein expression level
	QD aggregation	Prepare fresh QD dilution and store for no longer than a few hours
	Poor ligand affinity	Check ligand affinity via transport uptake assay
Nonspecific labeling	Excessive ligand or QD concentration	Reduce and optimize ligand and QD concentrations
Excessive QD blinking	Excessive excitation duration or intensity	Minimize excitation intensity, use longer wavelengths, and reduce the excitation duration

3.6. References

- (1) Torres, G. E.; Gainetdinov, R. R.; Caron, M. G., Plasma membrane monoamine transporters: structure, regulation and function. *Nat Rev Neurosci* 2003, 4 (1), 13-25.
- (2) González, M. I.; Robinson, M. B., Neurotransmitter transporters: why dance with so many partners? *Current Opinion in Pharmacology* 2004, 4 (1), 30-35.
- (3) Sager, J. J.; Torres, G. E., Proteins Interacting with Monoamine Transporters: Current State and Future Challenges. *Biochemistry* 2011, 50 (34), 7295-7310.
- (4) Fei, H.; Grygoruk, A.; Brooks, E. S.; Chen, A.; Krantz, D. E., Trafficking of Vesicular Neurotransmitter Transporters. *Traffic* 2008, 9 (9), 1425-1436.
- (5) Ramamoorthy, S.; Shippenberg, T. S.; Jayanthi, L. D., Regulation of monoamine transporters: Role of transporter phosphorylation. *Pharmacology & Therapeutics* 2011, 129 (2), 220-238.
- (6) Haraguchi, T., Live cell imaging: approaches for studying protein dynamics in living cells. *Cell Struct Funct* 2002, 27 (5), 333-4.
- (7) Sako, Y.; Yanagida, T., Single-molecule visualization in cell biology. *Nat Rev Mol Cell Biol* 2003, Suppl, SS1-5.
- (8) Resch-Genger, U.; Grabolle, M.; Cavaliere-Jaricot, S.; Nitschke, R.; Nann, T., Quantum dots versus organic dyes as fluorescent labels. *Nat Meth* 2008, 5 (9), 763-775.
- (9) Lippincott-Schwartz, J.; Patterson, G. H., Development and Use of Fluorescent Protein Markers in Living Cells. *Science* 2003, 300 (5616), 87-91

- (10) Zhang, J.; Campbell, R. E.; Ting, A. Y.; Tsien, R. Y., Creating new fluorescent probes for cell biology. *Nat Rev Mol Cell Biol* 2002, 3 (12), 906-918.
- (11) Alivisatos, A. P.; Gu, W.; Larabell, C., Quantum dots as cellular probes. *Annu Rev Biomed Eng* 2005, 7, 55-76.
- (12) Bruchez, M., Jr.; Moronne, M.; Gin, P.; Weiss, S.; Alivisatos, A. P., Semiconductor Nanocrystals as Fluorescent Biological Labels. *Science* 1998, 281 (5385), 2013-2016
- (13) Chan, W. C.; nbsp; W; Nie, S., Quantum Dot Bioconjugates for Ultrasensitive Nonisotopic Detection. *Science* 1998, 281 (5385), 2016-2018.
- (14) Rosenthal, S. J.; Chang, J. C.; Kovtun, O.; McBride, J. R.; Tomlinson, I. D., Biocompatible Quantum Dots for Biological Applications. *Chemistry & Biology* 2011, 18 (1), 10-24
- (15) Chang, J. C.; Kovtun, O.; Blakely, R. D.; Rosenthal, S. J., Labeling of neuronal receptors and transporters with quantum dots. *Wiley Interdisciplinary Reviews: Nanomedicine and Nanobiotechnology* 2012, 4 (6), 605-619.
- (16) Rosenthal, S. J.; Tomlinson, I.; Adkins, E. M.; Schroeter, S.; Adams, S.; Swafford, L.; McBride, J.; Wang, Y.; DeFelice, L. J.; Blakely, R. D., Targeting Cell Surface Receptors with Ligand-Conjugated Nanocrystals. *Journal of the American Chemical Society* 2002, 124 (17), 4586-4594.
- (17) Tomlinson, I. D.; Mason, J. N.; Blakely, R. D.; Rosenthal, S. J., Inhibitors of the serotonin transporter protein (SERT): The design and synthesis of biotinylated derivatives of 3-(1,2,3,6-tetrahydro-pyridin-4-yl)-1H-indoles. High-affinity serotonergic ligands for conjugation with quantum dots. *Bioorganic & Medicinal Chemistry Letters* 2005, 15 (23), 5307-5310.
- (18) Tomlinson, I. D.; Mason, J. N.; Blakely, R. D.; Rosenthal, S. J., High affinity inhibitors of the dopamine transporter (DAT): Novel biotinylated ligands for conjugation to quantum dots. *Bioorganic & Medicinal Chemistry Letters* 2006, 16 (17), 4664-4667.
- (19) Tomlinson, I. D.; Chang, J.; Iwamoto, H.; Felice, L. J. D.; Blakely, R. D.; Rosenthal, S. J., Targeting the human serotonin transporter (hSERT) with quantum dots. *SPIE: 2008; Vol. 6866, p 68660X.*
- (20) Kovtun, O.; Tomlinson, I. D.; Sakrikar, D. S.; Chang, J. C.; Blakely, R. D.; Rosenthal, S. J., Visualization of the Cocaine-Sensitive Dopamine Transporter with Ligand-Conjugated Quantum Dots. *ACS Chemical Neuroscience* 2011, null-null.
- (21) Tomlinson, I. D.; Iwamoto, H.; Blakely, R. D.; Rosenthal, S. J., Biotin tethered homotryptamine derivatives: High affinity probes of the human serotonin transporter (hSERT). *Bioorganic & Medicinal Chemistry Letters* 2011, 21 (6), 1678-1682.
- (22) Kovtun, O.; Ross, E. J.; Tomlinson, I. D.; Rosenthal, S. J., A flow cytometry-based dopamine transporter binding assay using antagonist-conjugated quantum dots. *Chemical Communications* 2012, 48 (44), 5428-5430.
- (23) Chang, J. C.; Tomlinson, I. D.; Warnement, M. R.; Ustione, A.; Carneiro, A. M. D.; Piston, D. W.; Blakely, R. D.; Rosenthal, S. J., Single Molecule Analysis of Serotonin Transporter Regulation Using Antagonist-Conjugated Quantum Dots Reveals Restricted, p38 MAPK-Dependent Mobilization Underlying Uptake Activation. *The Journal of Neuroscience* 2012, 32 (26), 8919-8929.
- (24) Fjorback, A. W.; Pla, P.; Müller, H. K.; Wiborg, O.; Saudou, F.; Nyengaard, J. R., Serotonin transporter oligomerization documented in RN46A cells and neurons by

- sensitized acceptor emission FRET and fluorescence lifetime imaging microscopy. *Biochemical and Biophysical Research Communications* 2009, 380 (4), 724-728.
- (25) Schmid, J. A.; Scholze, P.; Kudlacek, O.; Freissmuth, M.; Singer, E. A.; Sitte, H. H., Oligomerization of the Human Serotonin Transporter and of the Rat GABA Transporter 1 Visualized by Fluorescence Resonance Energy Transfer Microscopy in Living Cells. *Journal of Biological Chemistry* 2001, 276 (6), 3805-3810.
- (26) Furman, C. A.; Chen, R.; Guptaroy, B.; Zhang, M.; Holz, R. W.; Gnegy, M., Dopamine and Amphetamine Rapidly Increase Dopamine Transporter Trafficking to the Surface: Live-Cell Imaging Using Total Internal Reflection Fluorescence Microscopy. *The Journal of Neuroscience* 2009, 29 (10), 3328-3336.
- (27) Egaña, L. A.; Cuevas, R. A.; Baust, T. B.; Parra, L. A.; Leak, R. K.; Hochendoner, S.; Peña, K.; Quiroz, M.; Hong, W. C.; Dorostkar, M. M.; Janz, R.; Sitte, H. H.; Torres, G. E., Physical and Functional Interaction between the Dopamine Transporter and the Synaptic Vesicle Protein Synaptogyrin-3. *The Journal of Neuroscience* 2009, 29 (14), 4592-4604.
- (28) Grånäs, C.; Ferrer, J.; Loland, C. J.; Javitch, J. A.; Gether, U., N-terminal Truncation of the Dopamine Transporter Abolishes Phorbol Ester- and Substance P Receptor-stimulated Phosphorylation without Impairing Transporter Internalization. *Journal of Biological Chemistry* 2003, 278 (7), 4990-5000.
- (29) Sorkina, T.; Richards, T. L.; Rao, A.; Zahniser, N. R.; Sorkin, A., Negative Regulation of Dopamine Transporter Endocytosis by Membrane-Proximal N-Terminal Residues. *The Journal of Neuroscience* 2009, 29 (5), 1361-1374.
- (30) Rao, A.; Richards, T. L.; Simmons, D.; Zahniser, N. R.; Sorkin, A., Epitope-tagged dopamine transporter knock-in mice reveal rapid endocytic trafficking and filopodia targeting of the transporter in dopaminergic axons. *The FASEB Journal* 2012, 26 (5), 1921-1933.
- (31) Rao, A.; Simmons, D.; Sorkin, A., Differential subcellular distribution of endosomal compartments and the dopamine transporter in dopaminergic neurons. *Molecular and Cellular Neuroscience* 2011, 46 (1), 148-158.
- (32) Hadrich, D.; Berthold, F.; Steckhan, E.; Bönisch, H., Synthesis and Characterization of Fluorescent Ligands for the Norepinephrine Transporter: Potential Neuroblastoma Imaging Agents. *Journal of Medicinal Chemistry* 1999, 42 (16), 3101-3108.
- (33) Cha, J. H.; Zou, M.-F.; Adkins, E. M.; Rasmussen, S. G. F.; Loland, C. J.; Schoenenberger, B.; Gether, U.; Newman, A. H., Rhodamine-Labeled 2 β -Carbomethoxy-3 β -(3,4-dichlorophenyl)tropane Analogues as High-Affinity Fluorescent Probes for the Dopamine Transporter. *Journal of Medicinal Chemistry* 2005, 48 (24), 7513-7516.
- (34) Eriksen, J.; Rasmussen, S. G. F.; Rasmussen, T. N.; Vaegter, C. B.; Cha, J. H.; Zou, M.-F.; Newman, A. H.; Gether, U., Visualization of Dopamine Transporter Trafficking in Live Neurons by Use of Fluorescent Cocaine Analogs. *The Journal of Neuroscience* 2009, 29 (21), 6794-6808.
- (35) Zhang, P.; Jørgensen, T. N.; Loland, C. J.; Newman, A. H., A rhodamine-labeled citalopram analogue as a high-affinity fluorescent probe for the serotonin transporter. *Bioorganic & Medicinal Chemistry Letters* 2013, 23 (1), 323-326.
- (36) Li, M.; Lester, H. A., Early Fluorescence Signals Detect Transitions at Mammalian Serotonin Transporters. *Biophysical Journal* 2002, 83 (1), 206-218.

- (37) Zhao, Y.; Terry, D.; Shi, L.; Weinstein, H.; Blanchard, S. C.; Javitch, J. A., Single-molecule dynamics of gating in a neurotransmitter transporter homologue. *Nature* 2010, 465 (7295), 188-193.
- (38) Bannai, H.; Levi, S.; Schweizer, C.; Dahan, M.; Triller, A., Imaging the lateral diffusion of membrane molecules with quantum dots. *Nat. Protocols* 2007, 1 (6), 2628-2634.

CHAPTER IV

VISUALIZATION OF THE COCAINE-SENSITIVE DOPAMINE TRANSPORTER WITH LIGAND-CONJUGATED QUANTUM DOTS

4.1. Introduction

Dopamine (DA) is a modulatory neurotransmitter in the central nervous system (Figure 4.1).¹⁻³ The dopaminergic system modulates a variety of physiological functions and behavioral responses including attention, arousal, cognition, reward, and motor activity.³ Impaired DA signaling has been linked to a number of neurodegenerative and psychiatric disorders such as attention deficit/hyperactivity disorder (ADHD), bipolar disorder, major depression, Tourette's syndrome, Parkinson's disease, and schizophrenia.⁴⁻⁸ The synaptic DA concentration dictates that postsynaptic DA signal transduction and is determined by the activity of the presynaptic D₂ dopamine autoreceptor, which modulates DA release, and the dopamine transporter (DAT)^{1,9}, which clears DA to achieve DA inactivation and recycling¹⁰. DAT (*SLC6A3*) is a member of a family of Na⁺-coupled solute transporters whose substrates include neurotransmitters, nutrients, osmolytes, and amino acids (Figure 3.1). Several reports have demonstrated that experimental DAT deficiency results in pronounced changes in dopaminergic tone and locomotor hyperactivity.¹⁰⁻¹² In addition, DAT is the primary target for widely used psychostimulants, such as amphetamine and cocaine, which acutely modify the synaptic DA concentration. Cocaine is a competitive DAT inhibitor and attenuates DA clearance by occupying the DAT native substrate binding site, whereas

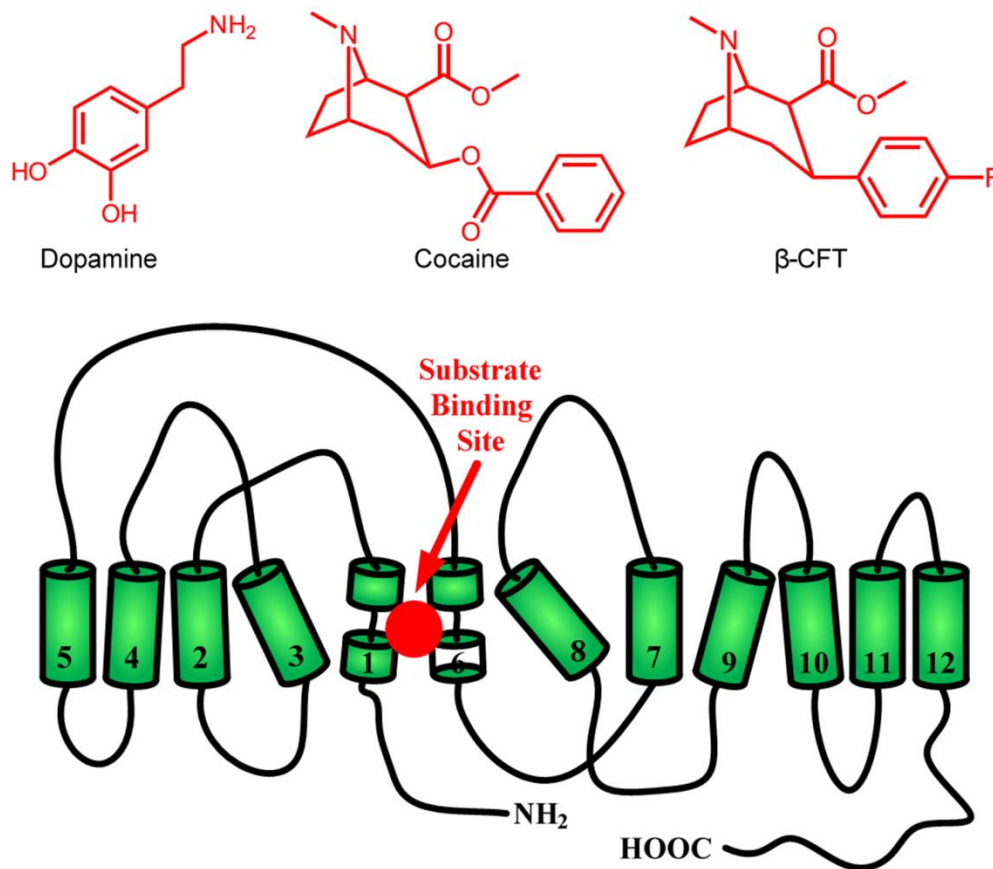


Figure 4.1. Structures of DAT and its relevant substrates. A two-dimensional topology of DAT based on the leucine transporter (LeuT) is shown with 12 transmembrane segments, intracellularly oriented N- and C-termini, and substrate binding site. Structures of dopamine, cocaine, and cocaine analog β -CFT are shown as well. The binding site for dopamine, cocaine, and cocaine analogs has been suggested to overlap and is buried deep between transmembrane segments 1, 3, 6, and 8. Adapted from ref. 39.

amphetamine promotes DAT-mediated DA efflux that results in the increased DA synaptic concentration.¹³ DAT activity has also been demonstrated to be a subject of acute, dynamic regulation by several post-translational mechanisms, such as constitutive endocytosis, protein kinase C (PKC)-dependent internalization, protein-protein interactions, and substrate-induced changes in surface expression level.^{13,14} The spatial organization and temporal

control of these mechanisms remains largely unknown and may be critically important in setting risk for disorders linked to compromised DA signaling.

The investigation of DAT regulation has thus far trailed similar efforts directed at membrane receptors and channels due a number of important challenges. First, it has been notoriously difficult to obtain neuronal cultures due to the relatively low number of DAT-expressing neurons.¹⁵ Therefore, much knowledge regarding DAT regulation has come from studies on heterologous expression systems. Second, the lack of an efficient antibody against an extracellular epitope does not allow direct localization and visualization of DAT molecules in living cells without prior chemical processing (fixation and permeabilization).¹⁶ Third, the use of popular fusion tags, such as green fluorescent protein (GFP) and hemagglutinin (HA), requires genetic perturbation of DAT and thus does not allow direct visualization of endogenous DAT. Fourth, traditional autoradiographic, biochemical, and optimal techniques to monitor DAT expression, function, cellular distribution suffer from suboptimal spatial and temporal resolution and are limited to providing ensemble-averaged information.^{17,18} Recently, a series of dye-conjugated fluorescent cocaine analogs has been developed and successfully used to directly visualize DAT in living cells for the first time. Cha, Eriksen and colleagues used an organic dye-conjugated 2 β -carbomethoxy-3 β -(3,4-dichlorophenyl)tropane (RTI 111) ligand to visualize changes in DAT cellular movement in response to different stimuli via laser confocal microscopy.¹⁶

In our group, we have focused on developing new DAT-specific ligands for conjugation with nanometer-sized semiconductor nanocrystals, known as quantum dots (QD). QDs offer several distinct advantages over conventional fluorophores and permit visualization of membrane-associated proteins with high accuracy and temporal resolution, with reported values as low as 10 nm with 10 ms integration time.¹⁹⁻²³ Specifically, their

excellent brightness and superior resistance to photodegradation enable noninvasive imaging of complex biological processes with high signal-to-noise ratio (SNR) over time scales from milliseconds to hours. Also, their broad absorption spectra and size-dependent, narrow, symmetric emission spectra considerably simplify multiplexed molecular imaging experiments. We have previously reported the synthesis of GBR12909- and GBR12935-based DAT-specific ligands for conjugation with QDs.^{24,25} In this effort, we sought to improve the design of the DAT ligand by incorporating a phenyltropane-based dopamine reuptake inhibitor parent compound (β -CFT, WIN 35,428) into the structure. β -CFT is a structural analog of cocaine and is 3-10x more potent than cocaine and is characterized by excellent structural stability.^{26,27} Our choice of the parent compound is also validated by multiple instances of the use of radiolabeled β -CFT to map DAT distribution in the animal and human brain.²⁸⁻³¹

Here, we present a relatively simple and rapid approach for QD-based direct visualization of DAT in living cells that uses a DAT-specific, biotinylated 2- β -carbomethoxy-3- β -(4-fluorophenyl)tropane (IDT444) in conjunction with SavQDs. We demonstrate the specificity of DAT QD labeling and the ability to detect DAT-expressing mammalian cells at a combination of low nanomolar concentrations of IDT444 and picomolar concentrations of QDs. To determine whether we could use our QD-based approach to capture DAT trafficking, we visualized acute, protein kinase C (PKC)-dependent internalization of DAT-QD complexes in response to phorbol ester treatment. Finally, we show the advantages of QD photophysical properties in time-lapse image series acquisition over extended periods of time.

4.2. Results and Discussion

4.2.1. Cocaine analog synthesis

To develop a DAT-specific probe, a biotinylated cocaine analog IDT444 (**6**) was synthesized (Figure 4.2 A). The IDT444 ligand is composed of four distinct parts: (i) a high-affinity cocaine analog, 2- β -carbomethoxy-3- β -(4-fluorophenyl)tropane (β -CFT or WIN 35,428), first reported by Clark *et al.*, (ii) a short alkyl spacer, (iii) a PEG chain (average MW 5000), (iv) and a biotin terminus (Figure 4.2 B).²⁶ β -CFT was chosen as the parent drug due to its high affinity for DAT, excellent structural stability, and pharmacological properties closely resembling those of cocaine.^{26,27} The hydrophobic alkyl linker was incorporated into the IDT444 ligand by attaching it to the nitrogen atom on the tropane ring. The tropane nitrogen was chosen as the attachment point based on previous studies, which showed that bulky groups attached to the tropane N-position had no significant effect on the phenyl tropane pharmacological properties and structural stability.²⁷⁻³² The short alkyl spacer was attached to the tropane nitrogen to increase flexibility and allow enhanced access to the binding site. The PEG chain was used to ensure the IDT444 ligand is soluble in aqueous buffers and possibly reduce any potential nonspecific interactions with the cellular membrane.³³ The biotin handle at the end of the PEG chain served as a binding site for SavQDs. Detailed synthetic steps are described in Supplementary Information available free of charge at <http://pubs.acs.org/doi/abs/10.1021/cn200032r>.

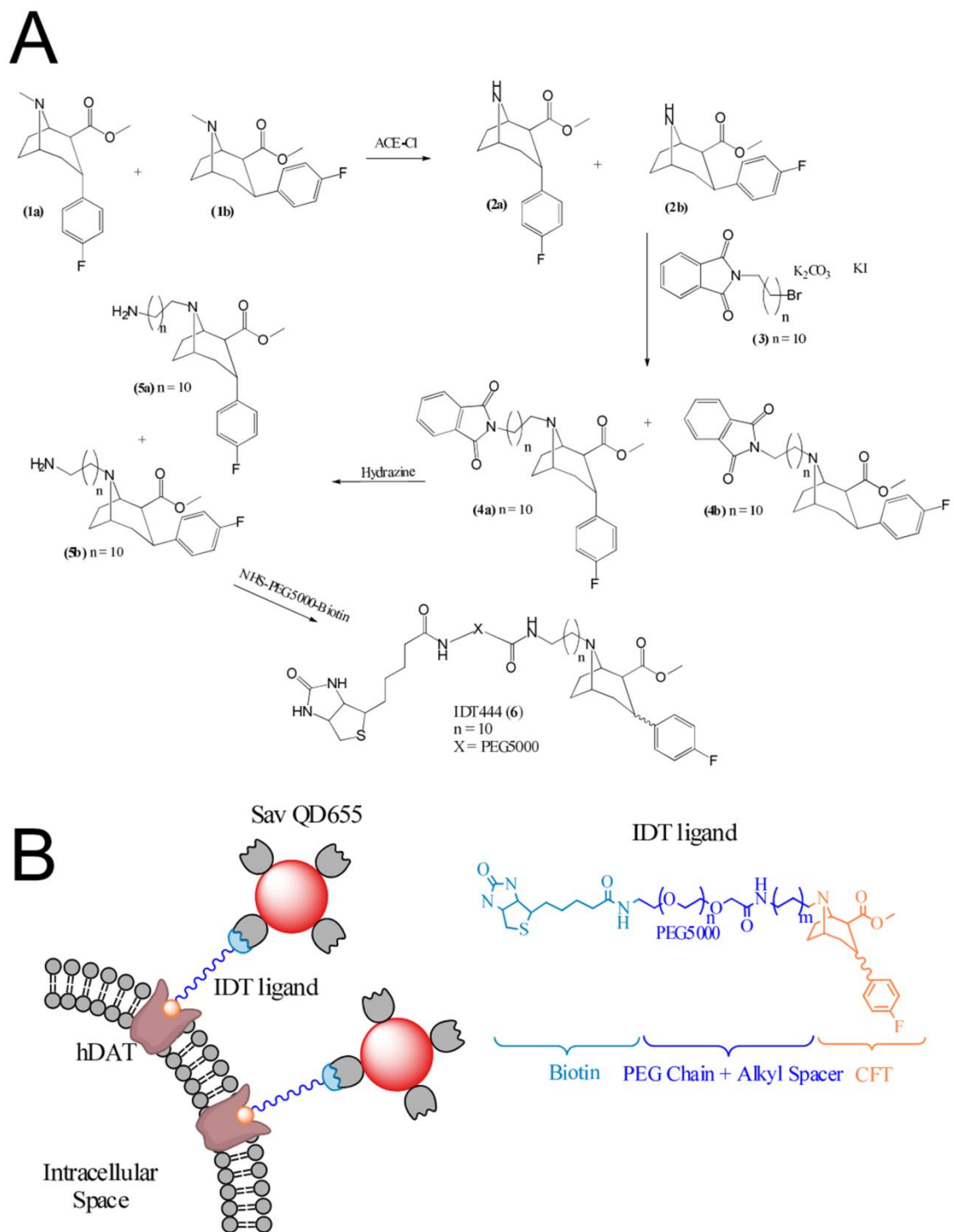


Figure 4.2. (A) The synthetic route used to prepare IDT444⁶. **(B).** Schematic representation of the two-step DAT labeling approach using IDT ligand and SavQDs.

4.2.2. DAT Visualization in Flp-In-293 Cells in Suspension

The HEK Flp-In-293 cell line was used as a model stable expression system to investigate the interactions of our QD-based fluorescent probes with DAT. The Flp-In-293 cells contain a Flp Recombination Target (FRT) site introduced into their genome (Invitrogen) that permits insertion of different DNAs into a common genomic locus in different cell lines. To achieve DAT expression, a plasmid vector containing the FRT site linked to the hygromycin resistance gene and the DAT cDNA was integrated into the genome via Flp recombinase-mediated DNA recombination at the FRT site. DAT-expressing Flp-In-293 cells were selected in the presence of 100 $\mu\text{g}/\text{mL}$ hygromycin B.

DAT-Flp-In-293 cells were subjected to a two-step solution-based QD labeling protocol. Flp-In-293 cells were incubated with the IDT444 ligand and subsequently labeled with SavQDs in solution to prevent the loss of cells due to detachment from the plate surface, reduce nonspecific QD interactions with the culture vessel, and enhance specific recognition of the biotinylated ligand. These cells were incubated with 100 nM IDT444 in PBS solution for 5 min at 37°C, lifted off the culture plate by gentle pipetting, centrifuged, and resuspended in 1 nM SavQD PBS solution for 5 min at 4°C. After several wash steps to rinse away the unbound ligands and conjugates, specific DAT QD labeling was demonstrated by confocal microscopy and flow cytometry, which were used as complementary techniques to quantify DAT QD labeling. Representative flow cytometry histograms and confocal images of the specific labeling of DAT expressed in hDAT-Flp-In-293 cells are shown in Figure 4.3. DAT-Flp-In-293 cells pretreated with 1 μM GBR12909, a high-affinity DAT antagonist, and DAT-Flp-In-293 cells incubated with 1 nM SavQDs only were used as control cell populations.^{34,35} Compared to the control samples, the prominent

increase of the median fluorescence intensity (MFI) as assessed by flow cytometry (Figure 4.3, A3) and the presence of membrane-associated uniform fluorescent halos on the

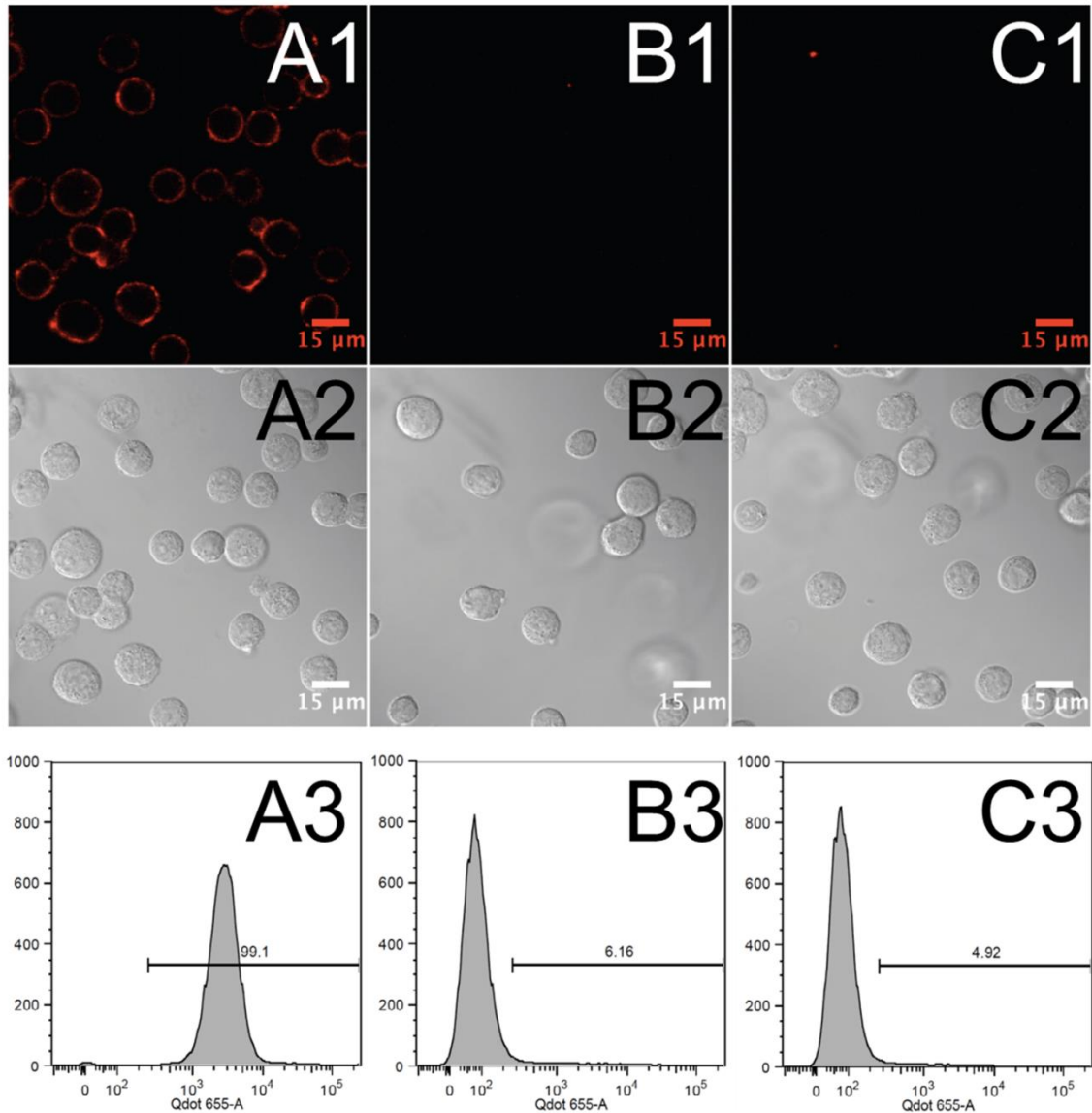


Figure 4.3. Specific SavQD-IDT444 labeling of DAT stably expressed in Flp-In-293 cells. Representative flow cytometry histograms and confocal images are shown for DAT-expressing cells (A1-A3), DAT-expressing cells pretreated with 1 μM GBR12909 (B1-B3), and DAT-expressing cells incubated with SavQD only (C1-C3). All samples were incubated with 100 nM solution of IDT444 in PBS for 5 min at 37°C and subsequently exposed to 1 nM SavQD in PBS for 5 min at 4°C.

acquired confocal images (Figure 4.3, A1-A2) indicated successful, specific hDAT QD labeling. GBR12909 effectively blocked the interaction of SavQD-IDT444 conjugates with hDAT (Figure 4.3, B1-B3), and the cell population exposed to SavQDs only (Figure 4.3, C1-C3) had similarly low percentage of labeled cells as observed for the preblocked cell population, indicating minimal ligand nonspecific binding. The images and flow cytometry histograms shown in Figure 4.3 are representative of at least 5 independent experiments.

4.2.3. IDT444 and SavQD Dose Response

Next, we investigated the sensitivity of flow cytometric detection of DAT-Flp-In-293 cells using our QD-based approach. In the first series of dose-response experiments, the SavQD concentration was kept constant at 1 nM, and IDT444 concentration was varied over several orders of magnitude (10 pM – 1 μ M). The cell populations were subjected to the two-step labeling protocol described above and analyzed by flow cytometry. Parallel DAT-Flp-In-293 cells preblocked with 1 μ M GBR12909 were used as a control to assess ligand nonspecific binding at different IDT444 concentrations. The IDT444 concentration-response curves are shown for both cell populations in Figure 4.4 A. Each data point represents the averaged MFI from three independent experiments. Robust standard deviation (rSD) was calculated from the MFI and the robust coefficient of variation (rCV) of the fluorescence intensity distribution (See SI). We observed statistically significant difference in MFI of labeled and control DAT-Flp-In-293 at the IDT444 concentration of 1 nM ($p < 0.05$). Also, it is apparent from the control population MFI curve that the increase of IDT444 concentration over several orders of magnitude does not result in significant ligand-mediated nonspecific binding. This suggests that DAT detection in Flp-In-293 cells is

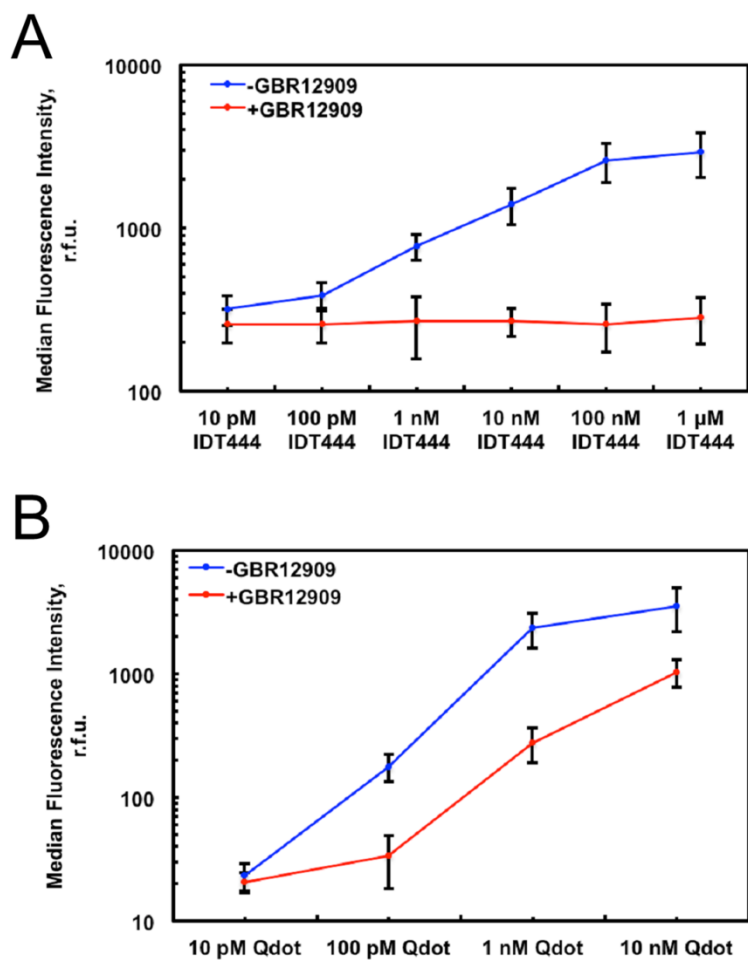


Figure 4.4. IDT444 (A) and SavQD (B) dose response curves. Individual data points represent averaged MFI from three independent experiments. Robust standard deviation (rSD) was calculated from the MFI and the robust coefficient of variation (rCV) of the fluorescence intensity distribution (See SI).

ligand-specific and dose-dependent. In the second series of dose-response experiments, IDT444 concentration was kept constant at 100 nM, and SavQD concentration was varied over several orders of magnitude (10 pM - 10 nM). Parallel DAT-Flp-In-293 cells preblocked with 1 μM GBR12909 were used as a control to assess QD nonspecific binding at different concentrations. We observed statistically significant difference in MFI of labeled and control

DAT-Flp-In-293 at SavQD concentration as low as 100 pM ($p < 0.05$, Figure 4.4 B). It should be noted that the MFI of the control population increased significantly with the increasing SavQD dose. This indicates that one must carefully optimize the concentration of QDs to be used in our approach, since the SNR will be dependent on the QD surface chemistry as well as cell type.³³ Here, we determined that we could successfully detect Flp-In-293 cells stably expressing DAT at a combination of low nanomolar concentrations of IDT444 and picomolar concentrations of SavQDs.

4.2.4. DAT Visualization in HeLa Cells *in situ*

After we successfully demonstrated specific QD labeling of DAT in stably transfected Flp-In-293 cells in suspension, we attempted to visualize Flp-In-293 cells in 8-well chamber slides *in situ*. This proved to be a very challenging task since Flp-In-293 cells are weakly adherent and detach easily during gentle washes between labeling steps even in collagen- and fibronectin-coated chamber slides. Therefore we chose a relatively strongly adherent HeLa cell line to determine whether we could use our approach to label living DAT-expressing cells *in situ*. HeLa cells were transiently transfected with a pcDNA3 vector containing the human DAT cDNA in 8-well chamber slides. Parallel HeLa cells were transfected with an empty (sham) pcDNA3 vector and served as a negative control to evaluate nonspecific cell labeling. Just prior to confocal imaging, DAT-transfected HeLa cells were incubated with 100 nM IDT444, washed 3x with warm imaging buffer, incubated with 1 nM SavQD, washed 3x with warm imaging buffer, and QD-labeled HeLa cells were subsequently visualized (Figure 4.5, A1-A2). Confocal images clearly demonstrate uniform plasma membrane labeling of DAT-transfected cells. No fluorescence staining was observed

for DAT-transfected HeLa cells preincubated with 1 μM GBR12909 (Figure 4.5, B1-B2) and sham-transfected HeLa cells (Figure 4.5, C1-C2), indicating a low level of nonspecific labeling. These data demonstrate that our QD-based approach can be used to specifically label DAT in living cells *in situ* with high SNR.

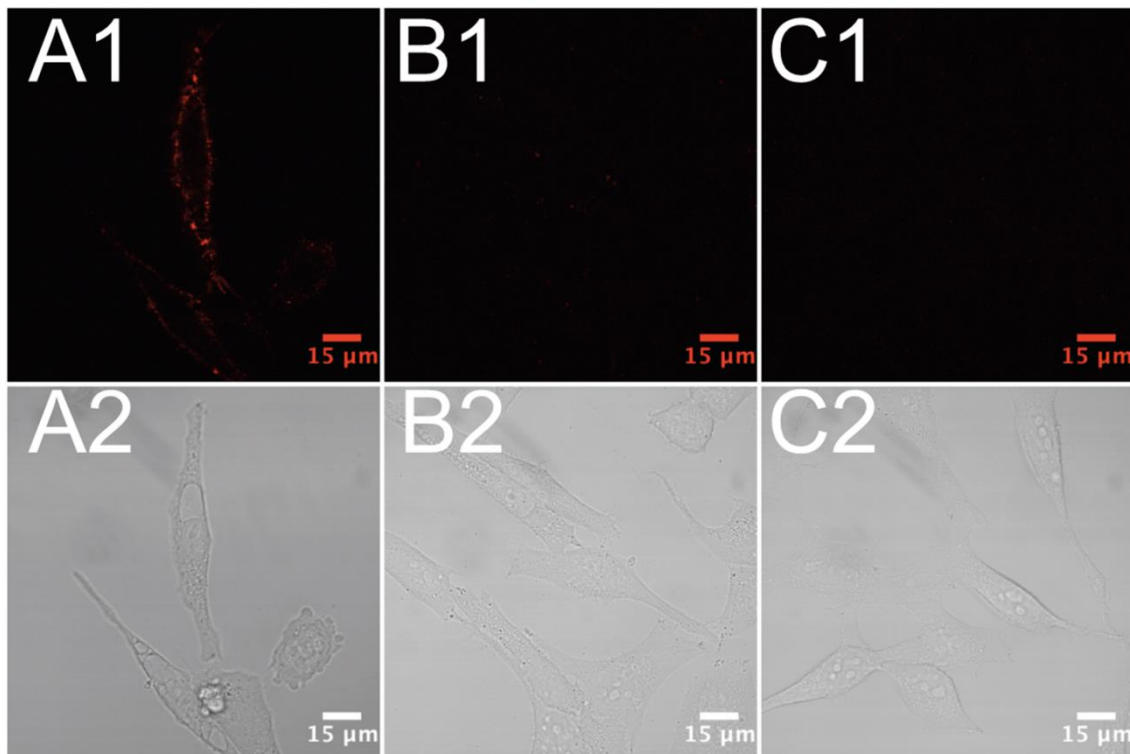


Figure 4.5. Specific SavQD-IDT444 labeling of DAT stably expressed in living HeLa cells *in situ*. Representative confocal images are shown for DAT-pcDNA3 transiently transfected HeLa cells (**A1-A2**), DAT-pcDNA3 transiently transfected cells pretreated with 1 μM GBR12909 (**B1-B2**), and Sham-pcDNA3 transiently transfected cells (**C1-C2**). Fluorescent (Top) and overlay (Bottom) images are shown. All samples were incubated with 100 nM solution of IDT444 in the imaging buffer for 5 min at 37°C and subsequently exposed to 1 nM SavQD in the imaging buffer for 2-3 min at 37°C. Images are representative of at least 5 independent experiments.

4.2.5. Visualization of PKC-Dependent DAT Internalization

It has been demonstrated that PKC activation by phorbol esters, such as phorbol 12-myristate 13-acetate (PMA), results in acute down-regulation of DAT surface expression

levels in several heterologous cell lines.³⁶⁻³⁸ To investigate whether we could use our IDT444-SavQD conjugates to visualize acute DAT internalization, we incubated transiently transfected HeLa cells with 100 nM IDT444 for 5 min at 37°C, washed the cells 3x with warm imaging medium, incubated the cells with 1 nM SavQD for 2-3 min 37°C, and washed the cells 3x with warm imaging medium. QD-labeled HeLa cells were then incubated for 30 min at 37°C in the presence or absence of 1 μM PMA. While we did not observe any apparent change in the distribution of membrane DAT-QD complexes in HeLa cells incubated in the presence of vehicle (DMSO) only (Figure 4.6, A,C), PMA treatment led to

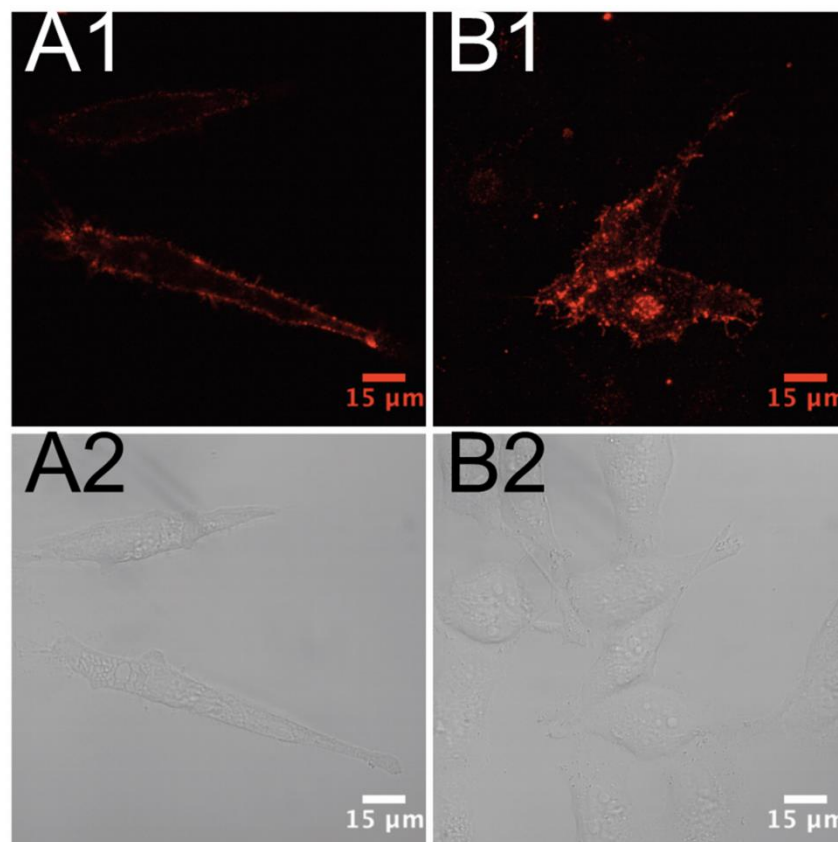


Figure 4.6. Visualization of DAT internalization in HeLa cells transiently expressing DAT using IDT444-SavQD conjugates. PMA promotes internalization of the DAT-QD complex in live HeLa cells transiently transfected with DAT-pcDNA3. The cells were incubated with 100 nM solution of IDT444 in the imaging buffer for 5 min at 37°C and subsequently exposed to 1 nM SavQD in the

imaging buffer for 2-3 min at 37°C before incubation in the absence (A1-A2) or presence of 1 μ M PMA (B1-B2) for 30 min at 37°C. Images are representative of at least 3 independent experiments.

the appearance of punctate intracellular fluorescence, a clear sign of acute, PKC-dependent DAT-QD complex internalization consistent with the previous reports (Figure 4.6, B,D). This experiment demonstrates the applicability and utility of our QD-based labeling approach in the investigation of DAT regulation in living cells.

4.2.6. Quantum Dot Photostability

To demonstrate that our QD-based labeling approach can be used as a tool to visualize DAT over extended periods of time, we compared SavQDs to a standard organic dye FITC. Individual 8-bit images (512 x 512 pixels, 1 Airy unit) were acquired every 30 seconds for 10 min at a scan speed of 51.20 μ sec/pixel, with laser intensity set to 20% (Figure 4.7, A-C). Fluorescence intensity of QD or FITC DAT membrane labeling in Flp-In-293 cells was quantified, normalized, and plotted as a function of acquisition time (Figure 4.7 D). Each data point represents average integrated membrane fluorescence intensity for 6 cells from two independent experiments. In the case of FITC, bleaching occurs within 300 s ($I_{norm} < 0.2$), whereas the intensity of QD labeling undergoes minimal decrease within 600 s. The photobleaching issue becomes important when one is monitoring biological processes for longer periods of time at high temporal resolution. Excellent photostability of QDs makes our QD-based labeling approach an excellent candidate for monitoring changes in DAT surface expression level and cellular localization for prolonged periods of time at temporal resolution higher than that allowed by the use of traditional fluorophores.

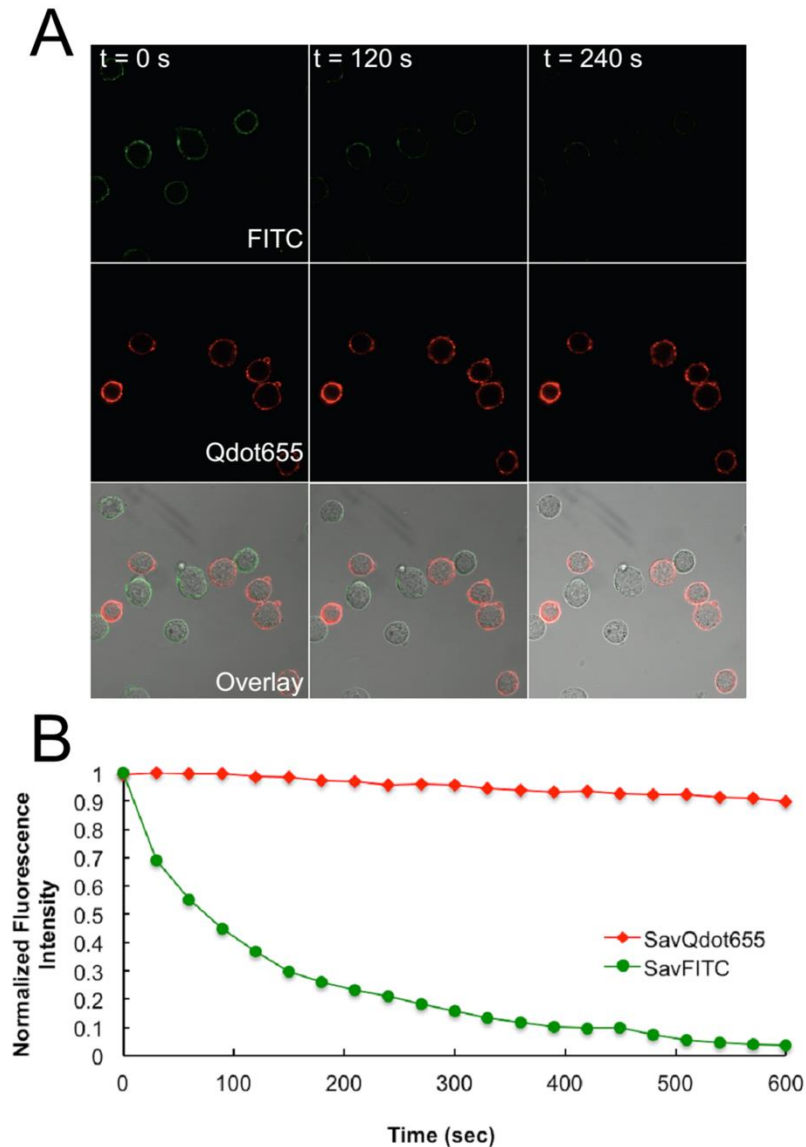


Figure 4.7. Photostability comparison between QD655 and FITC. (A) Top row: DAT-Flp-In-293 cells labeled with IDT444 and SavFITC. Bottom row: DAT-Flp-In-293 cells labeled with IDT444 and SavQD655. The time-lapse image series were acquired on the Zeiss LSM 510 inverted confocal microscope with the 488-nm excitation laser, a 650-nm long pass filter (QD) or a 505-550-nm band pass filter (FITC), and Zeiss Plan-Apo oil immersion objective (63X, NA 1.40). Images (512x512 pixels, 1 Airy unit) were acquired every 30 seconds for 10 min at a scan speed of 51.20 $\mu\text{sec}/\text{pixel}$, with laser intensity set to 20%. Images at 0, 120, and 240 s are shown. (B) Quantitative analysis of changes in intensities of SavQD655 and SavFITC. Membrane-associated intensity was quantified for each frame by integrating fluorescence intensity over a manually drawn region encompassing the membrane area, with DIC images serving as a reference point (Metamorph). Intensity values were normalized with respect to the highest intensity value obtained (I/I_0 , where $I_0 = I_{\text{max}}$).

4.3. Conclusion

To summarize, our goal for the current effort was to develop a DAT-specific ligand and demonstrate specific labeling of cell surface DAT using QD-based detection. The biotinylated derivative of the β -CFT cocaine analog, IDT444, was prepared by attaching the biotin-PEG-alkyl group to the tropane nitrogen. The ability to visualize mammalian cells stably expressing DAT with SavQD-IDT444 conjugates was clearly demonstrated by flow cytometry and confocal microscopy for Flp-In-293 cells in suspension and HeLa cells *in situ*. We determined that DAT-expressing cells could be detected at a combination of low nanomolar concentrations of IDT444 and picomolar concentrations of SavQDs, as assessed by flow cytometry. The relatively high sensitivity of our approach in combination with short sample preparation time renders IDT444 useful in a quantum dot-based fluorescent assay to monitor DAT expression, function, cellular distribution, and regulation. Specifically, we demonstrated the applicability and utility of our approach in the visualization of acute, PKC-dependent DAT internalization. Due to its sensitivity and flexibility, the quantum dot-based fluorescent assay platform we describe can potentially replace conventional biochemical and radiolabeled isotope-based approaches to study the distribution and regulation of DAT proteins. If issues related to blood-brain barrier penetration of QDs can be overcome, it is not unreasonable to consider whether our approach might not also be of diagnostic utility for perturbations of *in vivo* DAT levels in addiction, neuropsychiatric or neurodegenerative disorders. Finally, our QD-based approach should allow appropriation of the unique photophysical properties of QDs to achieve time-lapse imaging of DAT molecules in living cells for prolonged periods of time combined with improved temporal resolution, providing new opportunities to elucidate the molecular mechanisms supporting DAT regulation.

4.4. References

- (1) Giros, B.; Caron, M. G., Molecular characterization of the dopamine transporter. *Trends Pharmacol Sci* 1993, 14 (2), 43-9.
- (2) Darvas, M.; Palmiter, R. D., Restricting dopaminergic signaling to either dorsolateral or medial striatum facilitates cognition. *J Neurosci* 2010, 30 (3), 1158-65.
- (3) Bannon, M. J., Dopamine. *Nature Encyclopedia of Life Sciences*, Nature Publishing Group. Retrieved May 6, 2010 from www.els.net. 2004.
- (4) Swanson, J. M.; Flodman, P.; Kennedy, J.; Spence, M. A.; Moyzis, R.; Schuck, S.; Murias, M.; Moriarity, J.; Barr, C.; Smith, M.; Posner, M., Dopamine genes and ADHD. *Neurosci Biobehav Rev* 2000, 24 (1), 21-5.
- (5) Greenwood, T. A.; Alexander, M.; Keck, P. E.; McElroy, S.; Sadovnick, A. D.; Remick, R. A.; Kelsoe, J. R., Evidence for linkage disequilibrium between the dopamine transporter and bipolar disorder. *Am J Med Genet* 2001, 105 (2), 145-51.
- (6) Tremblay, L. K.; Naranjo, C. A.; Graham, S. J.; Herrmann, N.; Mayberg, H. S.; Hevenor, S.; Busto, U. E., Functional neuroanatomical substrates of altered reward processing in major depressive disorder revealed by a dopaminergic probe. *Arch Gen Psychiatry* 2005, 62 (11), 1228-36.
- (7) Sulzer, D., Multiple hit hypotheses for dopamine neuron loss in Parkinson's disease. *Trends in Neurosciences* 2007, 30 (5), 244-250.
- (8) Swerdlow, N. R.; Koob, G. F., Dopamine, schizophrenia, mania, and depression: Toward a unified hypothesis of cortico-striatopallido-thalamic function. *Behavioral and Brain Sciences* 1987, 10 (02), 197-208.
- (9) Usiello, A.; Baik, J.-H.; Rouge-Pont, F.; Picetti, R.; Dierich, A.; LeMeur, M.; Piazza, P. V.; Borrelli, E., Distinct functions of the two isoforms of dopamine D2 receptors. *Nature* 2000, 408 (6809), 199-203.
- (10) Giros, B.; Jaber, M.; Jones, S. R.; Wightman, R. M.; Caron, M. G., Hyperlocomotion and indifference to cocaine and amphetamine in mice lacking the dopamine transporter. *Nature* 1996, 379 (6566), 606-12.
- (11) Raul, R. G.; Sara, R. J.; Marc, G. C., Functional hyperdopaminergia in dopamine transporter knock-out mice. *Biological psychiatry* 1999, 46 (3), 303-311.
- (12) Ralph, R. J.; Paulus, M. P.; Fumagalli, F.; Caron, M. G.; Geyer, M. A., Prepulse Inhibition Deficits and Perseverative Motor Patterns in Dopamine Transporter Knock-Out Mice: Differential Effects of D1 and D2 Receptor Antagonists. *Journal of Neuroscience* 2001, 21 (1), 305-313.
- (13) Schmitt, K. C.; Reith, M. E. A. *Annals of the New York Academy of Sciences* 2010, 1187, 316-340.
- (14) Eriksen, J.; Jorgensen, T. N.; Gether, U., Regulation of dopamine transporter function by protein-protein interactions: new discoveries and methodological challenges. *J Neurochem* 2010, 113 (1), 27-41.
- (15) Furman, C. A.; Chen, R.; Guptaroy, B.; Zhang, M.; Holz, R. W.; Gnegy, M., Dopamine and amphetamine rapidly increase dopamine transporter trafficking to the surface: live-cell imaging using total internal reflection fluorescence microscopy. *J Neurosci* 2009, 29 (10), 3328-36.
- (16) Eriksen, J.; Rasmussen, S. G.; Rasmussen, T. N.; Vaegter, C. B.; Cha, J. H.; Zou, M. F.; Newman, A. H.; Gether, U., Visualization of dopamine transporter trafficking in

- live neurons by use of fluorescent cocaine analogs. *J Neurosci* 2009, 29 (21), 6794-808.
- (17) Haraguchi, T., Live cell imaging: approaches for studying protein dynamics in living cells. *Cell Struct Funct* 2002, 27 (5), 333-4.
- (18) Adkins, E. M.; Samuvel, D. J.; Fog, J. U.; Eriksen, J.; Jayanthi, L.D.; Vaegter, C.B.; Ramamoorthy, S.; Gether, U., Membrane Mobility and Microdomain Association of the Dopamine Transporter Studied with Fluorescence Correlation Spectroscopy and Fluorescence Recovery after Photobleaching. *Biochemistry* 2007, 46 (37), 10484-10497.
- (19) Bruchez, M., Jr.; Moronne, M.; Gin, P.; Weiss, S.; Alivisatos, A. P., Semiconductor Nanocrystals as Fluorescent Biological Labels. *Science* 1998, 281 (5385), 2013-2016.
- (20) Chan, W. C. W.; Nie, S., Quantum Dot Bioconjugates for Ultrasensitive Nonisotopic Detection. *Science* 1998, 281 (5385), 2016-2018.
- (21) Pinaud, F.; Clarke, S.; Sittner, A.; Dahan, M., Probing cellular events, one quantum dot at a time. *Nat Meth* 2010, 7 (4), 275-285.
- (22) Alivisatos, A. P., Semiconductor Clusters, Nanocrystals, and Quantum Dots. *Science* 1996, 271 (5251), 933-937.
- (23) Rosenthal, S. J.; Tomlinson, I.; Adkins, E. M.; Schroeter, S.; Adams, S.; Swafford, L.; McBride, J.; Wang, Y.; DeFelice, L. J.; Blakely, R. D., Targeting Cell Surface Receptors with Ligand-Conjugated Nanocrystals. *Journal of the American Chemical Society* 2002, 124 (17), 4586-4594.
- (24) Tomlinson, I. D.; Mason, J.; Burton, J. N.; Blakely, R.; Rosenthal, S. J., The design and synthesis of novel derivatives of the dopamine uptake inhibitors GBR 12909 and GBR 12935. High-affinity dopaminergic ligands for conjugation with highly fluorescent cadmium selenide/zinc sulfide core/shell nanocrystals. *Tetrahedron* 2003, 59 (40), 8035-8047.
- (25) Tomlinson, I. D., J. N. Mason, et al. High affinity inhibitors of the dopamine transporter (DAT): Novel biotinylated ligands for conjugation to quantum dots. *Bioorganic & Medicinal Chemistry Letters* 2006, 16 (17), 4664-4667.
- (26) Clarke, R. L.; Daum, S. J.; Gambino, A. J.; Aceto, M. D.; Pearl, J.; Levitt, M.; Cumiskey, W. R.; Bogado, E. F., Compounds affecting the central nervous system. 4. 3 Beta-phenyltropane-2-carboxylic esters and analogs. *J Med Chem* 1973, 16 (11), 1260-7.
- (27) Carroll, F. I.; Lewin, A. H.; Boja, J. W.; Kuhar, M. J., Cocaine receptor: biochemical characterization and structure-activity relationships of cocaine analogues at the dopamine transporter. *J Med Chem* 1992, 35 (6), 969-81.
- (28) Meltzer, P. C.; Blundell, P.; Zona, T.; Yang, L.; Huang, H.; Bonab, A. A.; Livni, E.; Fischman, A.; Madras, B. K., A Second-Generation ^{99m}Techetium Single Photon Emission Computed Tomography Agent That Provides in Vivo Images of the Dopamine Transporter in Primate Brain. *Journal of Medicinal Chemistry* 2003, 46 (16), 3483-3496.
- (29) Davis, M. R., J. R. Votaw, et al. Initial Human PET Imaging Studies with the Dopamine Transporter Ligand 18F-FECNT. *The Journal of Nuclear Medicine* 2003, 44 (6), 855-861.
- (30) J. Rinne, H. Ruottinen, J. Bergman, M. Haaparanta, P. Sonninen, and O. Solin. Usefulness of a dopamine transporter PET ligand [18F]β-CFT in assessing disability in Parkinson's disease. *Journal of Neurology, Neurosurgery, Psychiatry* 1999, 67 (6), 737-741.

- (31) Harada, N., Ohba, H., Fukumoto, D., Kakiuchi, T., Tsukada, H. Potential of [(18)F]beta-CFT-FE (2beta-carbomethoxy-3beta-(4-fluorophenyl)-8-(2-[(18)F]fluoroethyl)nortropane) as a dopamine transporter ligand: A PET study in the conscious monkey brain. *Synapse* 2004, 54 (1), 37-45.
- (32) Tomlinson, I. D.; Gies, A. P.; Gresch, P. J.; Dillard, J.; Orndorff, R. L.; Sanders-Bush, E.; Hercules, D. M.; Rosenthal, S. J., Universal polyethylene glycol linkers for attaching receptor ligands to quantum dots. *Bioorganic & Medicinal Chemistry Letters* 2006, 16 (24), 6262-6266.
- (33) Bentzen, E. L.; Tomlinson, I. D.; Mason, J.; Gresch, P.; Warnement, M. R.; Wright, D.; Sanders-Bush, E.; Blakely, R.; Rosenthal, S. J., Surface modification to reduce nonspecific binding of quantum dots in live cell assays. *Bioconjug Chem* 2005, 16 (6), 1488-94.
- (34) Hösl, E.; Hösl, L., Autoradiographic studies on the uptake of 3H-dopamine by neurons and astrocytes in explant and primary cultures of rat CNS: effects of uptake inhibitors. *International Journal of Developmental Neuroscience* 1997, 15 (1), 45-53.
- (35) Inazu, M.; Kubota, N.; Takeda, H.; Zhang, J.; Kiuchi, Y.; Oguchi, K.; Matsumiya, T., Pharmacological characterization of dopamine transport in cultured rat astrocytes. *Life Sciences* 1999, 64 (24), 2239-2245.
- (36) Blakely, R. D., Bauman, A. L. Biogenic amine transporters: regulation in flux. *Current Opinion in Neurobiology* 2000, 10, 328 –336.
- (37) Daniels, G. M., Amara, S. G. Regulated trafficking of the human dopamine transporter. Clathrin-mediated internalization and lysosomal degradation in response to phorbol esters. *Journal of Biological Chemistry* 1999, 274, 35794–35801.
- (38) Melikian, H. E., Buckley, K. M. Membrane trafficking regulates the activity of the human dopamine transporter. *Journal of Neuroscience* 1999, 19, 7699 –7710.
- (39) Kurian, M. A.; Zhen, J.; Cheng, S.-Y.; Li, Y.; Mordekar, S. R.; Jardine, P.; Morgan, N. V.; Meyer, E.; Tee, L.; Pasha, S.; Wassmer, E.; Heales, S. J. R.; Gissen, P.; Reith, M. E. A.; Maher, E. R. Homozygous loss-of-function mutations in the gene encoding the dopamine transporter are associated with infantile parkinsonism-dystonia. *The Journal of Clinical Investigation* 2009, 119 (6), 1595-1603.

CHAPTER V

A FLOW CYTOMETRY-BASED DOPAMINE TRANSPORTER BINDING ASSAY USING ANTAGONIST-CONJUGATED QUANTUM DOTS

5.1. Introduction

Bioanalytical and pharmacological approaches aimed at either interrogation of cell surface protein activity, distribution, and regulation, or screening for small-molecule modulators of the protein function have benefited greatly from the integration of fluorescence-based methods.¹⁻³ Fluorescence-based approaches greatly complement information attained via gold standard radioisotope-based assays, in part due to breakthrough advances in sensitivity and versatility of available instrumentation and elimination of concerns arising from handling and disposal of radioactive materials. Moreover, it has now become possible to perform real-time kinetic measurements using viable cells in a multi-well plate format.^{4,6}

Flow cytometry has emerged as one of the dominant fluorescence-based techniques, as it enables a quantitative, high-content measurement of ligand-protein and protein-protein interactions in single cells; in fact, high-content flow cytometry is now an integral part of the Molecular Libraries Initiative (MLI) of the National Institutes of Health (NIH) Roadmap.^{1,7-12} In addition, flow cytometry offers truly unique multiplexing capabilities that allow simultaneous monitoring of up to seventeen fluorescent parameters in addition to discriminating mixtures of cells based on two physical parameters.^{10,12} As a result, flow cytometry may be used to determine both pathway and cell-type selectivity of drug candidates in a routine screen.

There are several classes of fluorophores available for fluorescence-based measurements, including genetically encoded fluorescent proteins, traditional organic fluorophores, and inorganic nanomaterials.¹³ Quantum dots (QDs), nanometer-sized semiconductor nanocrystals, are a particularly attractive class of fluorescent reporters due to superior photostability, excellent brightness, broad absorption spectra, and narrow emission spectra.¹⁴⁻¹⁷ The latter two are particularly useful since instrumental requirements for multiplexing are considerably simplified as a result.

Since 2000, the Rosenthal group has been successfully preparing novel antagonist-conjugated QD probes that allow interrogation of neurotransmitter transporter protein function, with one ultimate goal being the development of fluorescence-based assays to aid in the discovery of more effective antidepressants and antipsychotic drugs.¹⁸⁻²⁵ Recently, we reported the synthesis of a dopamine transporter (DAT)-specific probe that was used in conjunction with streptavidin-conjugated QDs (SavQDs) to visualize membrane DATs in live cells.²⁵ Our labeling approach utilized a biotinylated, pegylated, high-affinity DAT antagonist β -CFT (2- β -carbomethoxy-3- β -(4-fluorophenyl)tropane (IDT444). Previously, radioactive forms of β -CFT have been used in discovery of novel DAT antagonists and mapping of the distribution of DAT in the mammalian brain.²⁶⁻³⁰ DAT is of particular interest to us as it is a major target for the psychostimulants cocaine and amphetamine. Moreover, alterations in human DAT structure and/or function have been associated with schizophrenia, bipolar disorder, Parkinson's disease, and attention deficit hyperactivity disorder (ADHD). As a consequence, novel DAT activity modulators represent a promising category of therapeutics.³⁵⁻³⁹

Here, we describe a flow cytometry-based assay that utilizes DAT antagonist-conjugated QDs to assay DAT activity and regulation in live cells in a multi-well plate

format. The quality and performance of the assay were initially evaluated using negative and positive control data. To test the versatility of the QD-based assay, two sets of experiments using known DAT modulators were performed. The QD-based platform described here offers a useful alternative to conventional techniques utilized to study protein function, as it is readily adaptable to a system of interest and may be amenable to high-throughput screening (HTS) of novel small-molecule DAT modulators.

5.2. Results and Discussion

Temporal stability of a binding interaction between a fluorescent probe and its target protein is an important parameter in the development of a fluorescence-based affinity screening assay. Thus, we first sought to determine the reversibility of DAT QD labeling. DAT-expressing Flp-In-HEK-293 cells were sequentially labeled with IDT444 and SavQDs, washed several times with warm imaging buffer, and subsequently incubated for at least 30 min at 37°C/5% CO₂ in presence of varying doses of the high-affinity DAT antagonist GBR12909.^{29,30} The degree of QD conjugate dissociation was assessed with confocal microscopy (data not shown here). Dissociation was not apparent even in presence of a large excess of GBR12909 (50 μM). Parallel flow cytometry analysis confirmed that QD-IDT444 off-rate is very slow, with no statistically significant QD fluorescence loss observed after 30 min of incubation. It was therefore established that the fluorescence readout could be reliably used to determine the amount of surface DATs available for binding, as an alternative to radioligand- or antibody-based conventional techniques.

Next, we sought to establish a flow cytometry-based protocol that would allow multi-well plate screening of both adherent and suspension cell cultures using our ligand-conjugated QDs. The platform is depicted in Figure 5.1. Adherent DAT-expressing cells are

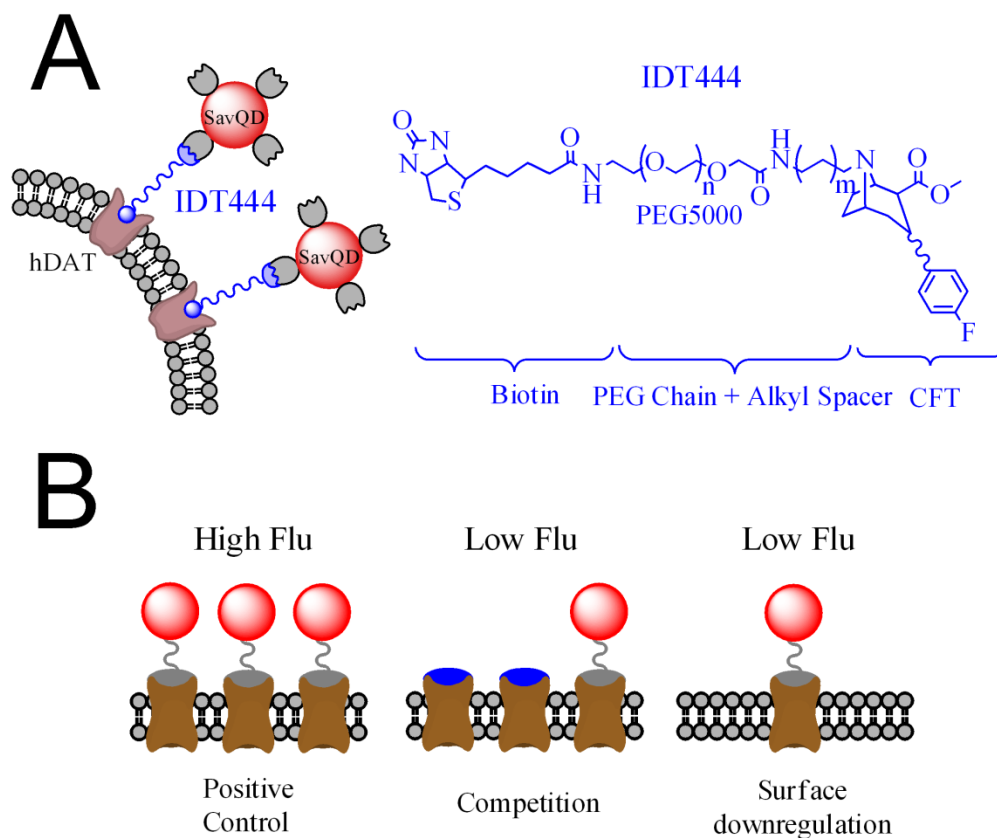


Figure 5.1. Schematic of a QD-based assay that uses antagonist-conjugated QDs to determine inhibitory activity of DAT modulators. IDT444 structure and DAT labeling schematic are shown in (A). Expected effects of competition and surface downregulation of DAT on QDIDT444 binding and the single-cell fluorescence intensity measured are demonstrated in (B).

(i) exposed to an antagonist candidate, (ii) incubated with 100 nM IDT444/inhibitor mixture for 10 min, (iii) washed several times with KRH buffer and incubated with 1 nM QD/1% BSA (bovine serum albumin) mixture, (iv) nonenzymatically dissociated, and (v) assayed by flow cytometry. With the use of a multichannel pipette, a 24-, 48-, or 96-well plate could be

ready for flow cytometry analysis within an hour. To test the robustness of this platform, a Z' statistical factor was determined using only the control data as follows:

$$Z' = 1 - \frac{(3\sigma_{C+} + 3\sigma_{C-})}{|\mu_{C+} - \mu_{C-}|} \quad [3]$$

The Z' -factor takes into account the signal-to-noise ratio and s.d. of control samples and is commonly utilized for quality assessment in assay development. Values of $Z' \geq 0.5$ are considered excellent.³¹ The Z' -factor of our QD-based assay was determined to be 0.73, indicating robust assay performance.

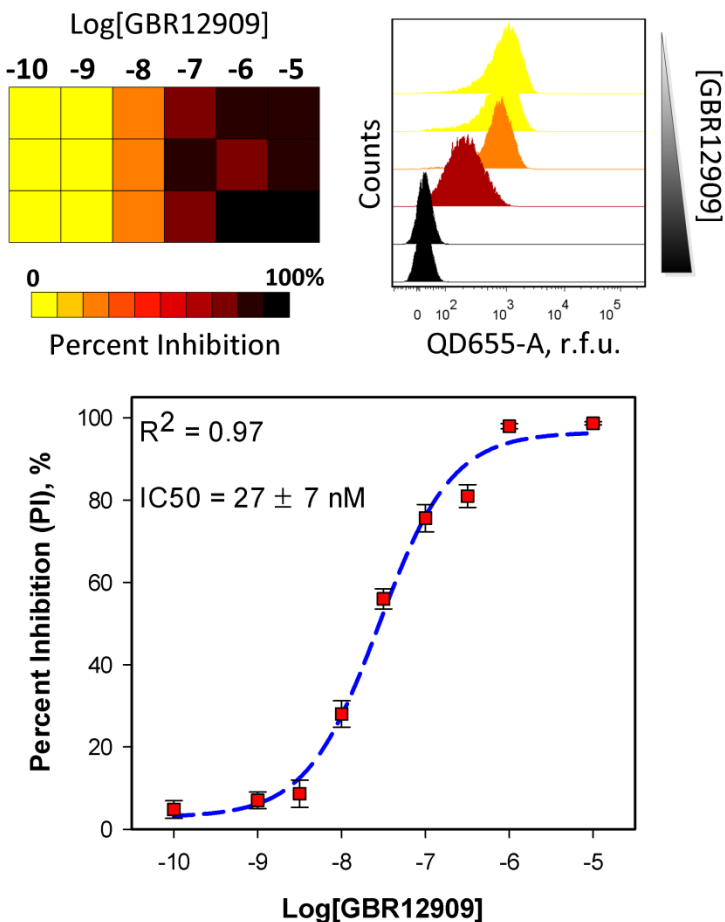


Figure 5.2. Flow cytometry-based screening of the inhibitory activity of **GBR12909**, a high-affinity DAT antagonist, using antagonist-conjugated QDs. DAT-expressing HEK cells were treated with five- or ten-fold dilutions of GBR12909. Percent inhibition at increasing doses of GBR12909 is represented as a heat map (top left) and representative

histogram plots of the effects of increasing GBR12909 doses (top right) on QD conjugate binding are shown. The heat map and IC₅₀ curve (bottom) were generated using median QD fluorescence intensity values.

Once the assay quality was determined, two sets of experiments using known DAT modulators were performed to evaluate its versatility. In the first set of experiments, adherent DAT-expressing HEK cells were exposed to varying GBR12909 antagonist doses. The median fluorescence intensity (MFI) was used to estimate percent inhibition (PI) of QD conjugate binding according to the equation below:

$$PI = \frac{MFI_{pos} - MFI_{treated}}{MFI_{pos} - MFI_{neg}} \times 100\% \quad [4]$$

where MFI_{pos} is MFI of a positive control (QD-IDT444-labeled cells), MFI_{neg} is MFI of a negative control (QD-labeled cells), and MFI_{treated} is MFI of a cell population incubated with a certain DAT modulator dose and subsequently labeled with IDT444 and SavQDs. Obtained PI data were pooled from three independent experiments with triplicate samples to generate a dose-response curve (Figure 5.2). The half-maximal inhibitory concentration (IC₅₀) of GBR12909 was determined to be 27 ± 7 nM, which is in excellent agreement with values obtained using conventional techniques. Typical IC₅₀ values reported for inhibition of [³H]DA transport are in the 1-50 nM range for GBR12909.^{32,33} In the second set of experiments, DAT-expressing cells were exposed to varying concentrations of phorbol-12-myristate-13-acetate (PMA), a potent protein kinase C activator that leads to acute surface DAT downregulation.²⁵ A dose-response curve generated from three independent experiments with triplicate samples is shown in Figure 5.3. As expected, surface DAT downregulation reached saturation at μM PMA doses, and a total of ~50% surface DAT was lost after a 20-minute incubation period. The IC₅₀ value was determined to be 20 ± 11 nM and was found to be in excellent agreement with the previously reported data.³⁴ Together,

these experiments demonstrated that our QD-based platform could be used to accurately predict inhibitory activity of both direct and indirect DAT modulators.

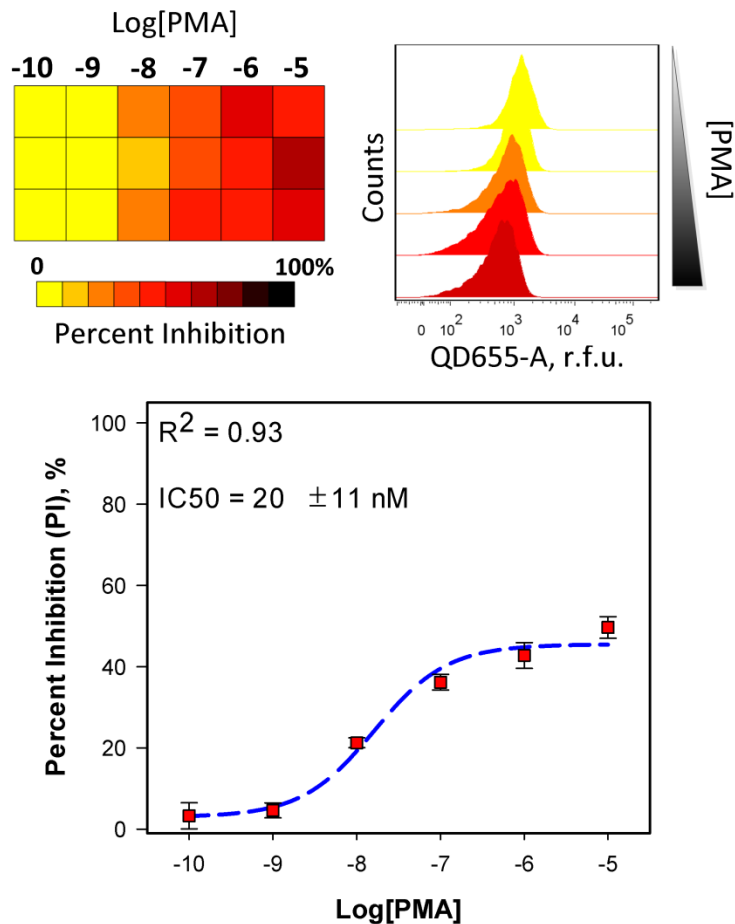


Figure 5.3. Flow cytometry-based screening of the inhibitory activity of PMA using antagonist-conjugated QDs. DAT-expressing HEK cells were treated with five- or ten-fold dilutions of PMA. Percent surface DAT downregulation at increasing doses of PMA is represented as a heat map (top left) and representative histogram plots of the effects of increasing PMA doses (top right) on QD conjugate binding are shown. The heat map and IC₅₀ curve (bottom) were generated using median QD fluorescence intensity values.

5.3. Summary

Development of fluorescence-based binding assays that target cell surface proteins with unresolved crystal structures and ineffective antibodies against the extracellular epitope

is particularly challenging. Here, we presented a platform that addresses these issues and does not require genetic perturbation, chemical processing (fixation/permeabilization), or special handling as in the case of radioactive materials. The QD-based flow cytometric assay was used to accurately measure inhibitory action of known DAT modulators. The Z' -factor, a statistical measure of assay quality and performance, was calculated to be 0.73, with the “excellent” rating for Z' -factor values above 0.5. The modular design of our antagonist-conjugated QD probes makes the platform described here readily adaptable to any cell surface protein system of interest. Furthermore, our QD-based assay may also be of potential value to HTS of small-molecule modulators of DAT function, as it can be easily miniaturized to 384-well plates. In addition, broad absorption and narrow emission spectra of QDs will allow monitoring of several targets or cellular responses and may therefore establish pathway and cell-type selectivity of DAT modulators in a high-content screen.

5.4. References

- (1) Eccleston, J. F.; Hutchinson, J. P.; Jameson, D. M. (2005). Fluorescence-Based Assays. In *Progress in Medicinal Chemistry*, Vol. 43, King, F. D.; Lawton, G., Eds.; Elsevier B. V.: New York; pp. 19-48.
- (2) Lang, P.; Yeow, K.; Nichols, A.; Scheer, A. (2006). *Nat Rev Drug Discov.* 5 (4), 343-356.
- (3) Pepperkok, R.; Ellenberg, J., High-throughput fluorescence microscopy for systems biology. (2006). *Nat Rev Mol Cell Biol.* 7 (9), 690-696.
- (4) Pargellis, C.; Tong, L.; Churchill, L.; Cirillo, P. F.; Gilmore, T.; Graham, A. G.; Grob, P. M.; Hickey, E. R.; Moss, N.; Pav, S.; Regan, J. (2002). Inhibition of p38 MAP kinase by utilizing a novel allosteric binding site. *Nat Struct Mol Biol.* 9 (4), 268-272.
- (5) Bevilacqua, P. C.; Kierzek, R.; Johnson, K. A.; Turner, D. H. (1992). Dynamics of ribozyme binding of substrate revealed by fluorescence-detected stopped-flow methods. *Science.* 258 (5086), 1355-1358.
- (6) Chang, J. C.; Tomlinson, I. D.; Warnement, M. R.; Iwamoto, H.; DeFelice, L. J.; Blakely, R. D.; Rosenthal, S. J. (2011). A Fluorescence Displacement Assay for Antidepressant Drug Discovery Based on Ligand-Conjugated Quantum Dots. *Journal of the American Chemical Society.* 133 (44), 17528-17531.

- (7) Barlogie, B.; Raber, M. N.; Schumann, J.; Johnson, T. S.; Drewinko, B.; Swartzendruber, D. E.; Göhde, W.; Andreeff, M.; Freireich, E. J. (1983). Flow Cytometry in Clinical Cancer Research. *Cancer Research*. 43 (9), 3982-3997.
- (8) Benoist, C.; Hacoen, N. (2011). Flow Cytometry, Amped Up. *Science*. 332 (6030), 677-678.
- (9) Davey, H. M.; Kell, D. B. (1996). Flow cytometry and cell sorting of heterogeneous microbial populations: the importance of single-cell analyses. *Microbiological Reviews*. 60 (4), 641-696.
- (10) Chattopadhyay, P. K.; Price, D. A.; Harper, T. F.; Betts, M. R.; Yu, J.; Gostick, E.; Perfetto, S. P.; Goepfert, P.; Koup, R. A.; De Rosa, S. C.; Bruchez, M. P.; Roederer, M. (2006). Quantum dot semiconductor nanocrystals for immunophenotyping by polychromatic flow cytometry. *Nat Med*. 12 (8), 972-977.
- (11) Krutzik, P. O.; Nolan, G. P. (2006). Fluorescent cell barcoding in flow cytometry allows high-throughput drug screening and signaling profiling. *Nat Meth*. 3 (5), 361-368.
- (12) Krutzik, P. O.; Crane, J. M.; Clutter, M. R.; Nolan, G. P. (2008). High-content single-cell drug screening with phosphospecific flow cytometry. *Nat Chem Biol*. 4 (2), 132-142.
- (13) Kovtun, O.; Rosenthal, S. J. (2011). Biological Applications of Photoluminescent Semiconductor Quantum Dots. In *Handbook of Luminescent Semiconductor Materials*, 1st Ed., Bergman, L.; McHale, J. L., Eds.; Taylor and Francis Group: New York, pp. 411-439.
- (14) Bruchez, M., Jr.; Moronne, M.; Gin, P.; Weiss, S.; Alivisatos, A. P. (1998). *Science*, 281, 2013-2016.
- (15) Chan, W. C. W.; Nie, S. (1998). *Science*, 281, 2016-2018.
- (16) Medintz, I. L., H. T. Uyeda, et al. (2005). *Nat. Mater*. 4, 435-446.
- (17) Rosenthal, S. J.; Chang, J. C.; Kovtun, O.; McBride, J. R.; Tomlinson, I. D. (2011). Biocompatible Quantum Dots for Biological Applications. *Chemistry & Biology*, 18 (1), 10-24.
- (18) Rosenthal, S. J.; Tomlinson, I.; Adkins, E. M.; Schroeter, S.; Adams, S.; Swafford, L.; McBride, J.; Wang, Y.; DeFelice, L. J.; Blakely, R. D. (2002). *JACS*, 124 (17), 4586-4594.
- (19) Gussin, H. I. n. A.; Tomlinson, I. D.; Little, D. M.; Warnement, M. R.; Qian, H.; Rosenthal, S. J.; Pepperberg, D. R. (2006). *JACS*, 128 (49), 15701-15713.
- (20) Tomlinson, I.; Grey, J.; Rosenthal, S. (2002a). *Molecules*. 7 (11), 777-790.
- (21) Tomlinson, I. D.; Kippeny, T.; Swafford, L.; Siddiqui, N. H.; Rosenthal, S. J. (2002b). *Journal of Chemical Research (Synopsis)*, 203-204.
- (22) Tomlinson, I. D.; Mason, J.; Burton, J. N.; Blakely, R.; Rosenthal, S. J. (2003). *Tetrahedron*. 59 (40), 8035-8047.
- (23) Tomlinson, I. D.; Mason, J. N.; Blakely, R. D.; Rosenthal, S. J. (2005). *Bioorganic & Medicinal Chemistry Letters*. 15 (23), 5307-5310.
- (24) Tomlinson, I. D.; Iwamoto, H.; Blakely, R. D.; Rosenthal, S. J. (2011). Biotin tethered homotryptamine derivatives: High affinity probes of the human serotonin transporter (hSERT). *Bioorganic & Medicinal Chemistry Letters*. 21 (6), 1678-1682.
- (25) Kovtun, O.; Tomlinson, I. D.; Sakrikar, D. S.; Chang, J. C.; Blakely, R. D.; Rosenthal, S. J. (2011). Visualization of the Cocaine-Sensitive Dopamine Transporter with Ligand-Conjugated Quantum Dots. *ACS Chemical Neuroscience*. 2 (7), 370-378.

- (26) Laakso, A.; Bergman, J.; Haaparanta, M.; Vilkkumäki, H.; Solin, O.; Hietala, J. (1998). [18F]CFT ([18F]WIN 35,428), a radioligand to study the dopamine transporter with PET: Characterization in human subjects. *Synapse*. 28 (3), 244-250.
- (27) Rinne, J. O.; Sahlberg, N.; Ruottinen, H.; Nägren, K.; Lehtikoinen, P. (1998). Striatal uptake of the dopamine reuptake ligand [11C]β-CFT is reduced in Alzheimer's disease assessed by positron emission tomography. *Neurology*. 50 (1), 152-156.
- (28) Wiener, H. L.; Reith, M. E. A. (1992). Determination of radioligand specific activity using competition binding assays. *Analytical Biochemistry*. 207 (1), 58-62.
- (29) Hösl, E.; Hösl, L. (1997). *International Journal of Developmental Neuroscience*. 15 (1), 45-53.
- (30) Inazu, M.; Kubota, N.; Takeda, H.; Zhang, J.; Kiuchi, Y.; Oguchi, K.; Matsumiya, T. (1999). *Life Sciences*. 64 (24), 2239-2245.
- (31) Zhang, J.-H.; Chung, T. D. Y.; Oldenburg, K. R. (1999). A Simple Statistical Parameter for Use in Evaluation and Validation of High Throughput Screening Assays. *Journal of Biomolecular Screening* 1999, 4 (2), 67-73.
- (32) Peter H, A. (1989). The dopamine uptake inhibitor GBR 12909: selectivity and molecular mechanism of action. *European Journal of Pharmacology* 1989, 166 (3), 493-504.
- (33) Heikkilä, R. E.; Manzino, L. (1984). Behavioral properties of GBR 12909, GBR 13069 and GBR 13098: Specific inhibitors of dopamine uptake. *European Journal of Pharmacology*. 103 (3-4), 241-248.
- (34) Zhu, S.-J.; Kavanaugh, M. P.; Sonders, M. S.; Amara, S. G.; Zahniser, N. R. (1997). Activation of Protein Kinase C Inhibits Uptake, Currents and Binding Associated with the Human Dopamine Transporter Expressed in *Xenopus* Oocytes. *Journal of Pharmacology and Experimental Therapeutics*. 282 (3), 1358-1365.
- (35) Swanson, J. M.; Flodman, P.; Kennedy, J.; Spence, M. A.; Moyzis, R.; Schuck, S.; Murias, M.; Morikawa, J.; Barr, C.; Smith, M.; Posner, M. (2000). Dopamine genes and ADHD. *Neurosci Biobehav Rev*. 24 (1), 21-5.
- (36) Greenwood, T. A.; Alexander, M.; Keck, P. E.; McElroy, S.; Sadovnick, A. D.; Remick, R. A.; Kelsoe, J. R. (2001). Evidence for linkage disequilibrium between the dopamine transporter and bipolar disorder. *Am J Med Genet*. 105 (2), 145-51.
- (37) Sulzer, D. (2007). Multiple hit hypotheses for dopamine neuron loss in Parkinson's disease. *Trends in Neurosciences*. 30 (5), 244-250.
- (38) Giros, B.; Jaber, M.; Jones, S. R.; Wightman, R. M.; Caron, M. G. (1996). Hyperlocomotion and indifference to cocaine and amphetamine in mice lacking the dopamine transporter. *Nature*. 379 (6566), 606-12.
- (39) Schmitt, K. C.; Reith, M. E. A. (2010). *Annals of the New York Academy of Science*. 1187, 316-340.

CHAPTER VI

SINGLE QUANTUM DOT TRACKING OF DOPAMINE TRANSPORTER PLASMA MEMBRANE DYNAMICS: A LINK BETWEEN TRAFFICKING AND ATTENTION DEFICIT/HYPERACTIVITY DISORDER

6.1. Introduction

The high-affinity dopamine (DA) transporter protein (DAT) plays a critical role in maintaining coordinated, dopamine-mediated signaling in the central nervous system (CNS).¹⁻⁶ DAT controls the intensity and duration of dopamine signals by reducing the extracellular concentrations of the neurotransmitter through re-uptake into presynaptic nerve terminals (Figure 6.1 A). Dysfunction and/or polymorphisms in DAT have been linked to a variety of brain disorders, including schizophrenia, bipolar disorder, dystonia, Parkinson's disease, and attention-deficit/hyperactivity disorder.³⁻¹⁰ In addition, DAT is a major target for the widely abused psychostimulants, amphetamine and cocaine (Figure 6.1A).⁶ DAT has been shown to be tightly regulated through multiple mechanisms including phosphorylation, protein-protein interactions and membrane trafficking, mechanisms that can be influenced by psychoactive drugs.¹¹⁻²³ Over the past decade, several reports have demonstrated that populations of cell surface DAT molecules are associated with distinct, cholesterol-enriched membrane microdomains, termed "lipid rafts" and can also display cholesterol-dependent lateral diffusion and/or functional states.^{18,20,24-27} DAT surface dynamics appear to depend both on localization with membrane microdomains and interactions with intracellular protein networks which appear to be critical for proper spatiotemporal regulation of DAT function.^{11,13-15} Despite the clear clinical importance of

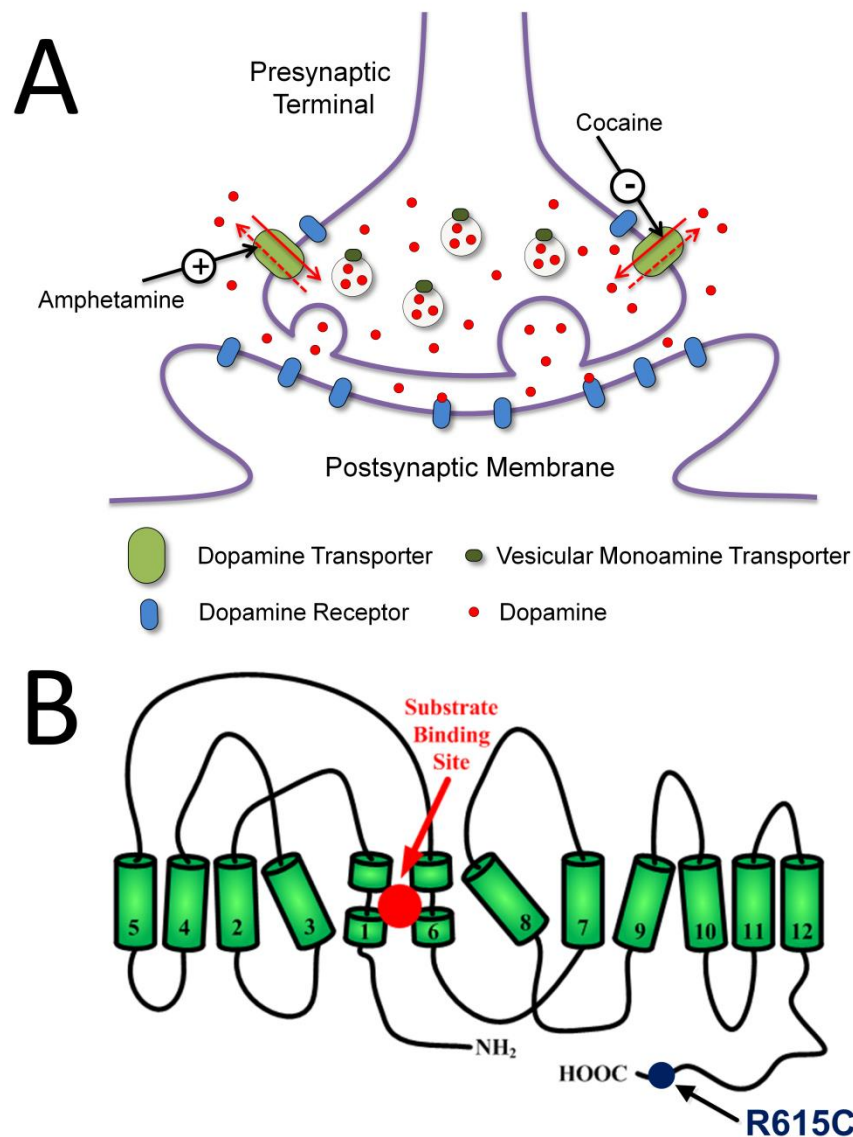


Figure 6.1. Dopaminergic synapse and dopamine transporter two-dimensional topology. (A) A diagram depicting signal transduction in the dopaminergic synapse. Dopamine is transported within synaptic vesicles and is released by a presynaptic neuron into the synaptic cleft, where it can bind to dopamine receptors on postsynaptic terminals. Normally, dopamine is recycled back into the presynaptic terminal by the dopamine transporter. Cocaine acts as a dopamine transporter antagonist, blocking dopamine reuptake and thereby increasing dopamine synaptic concentration. Amphetamine, on the other hand, depletes synaptic vesicles of dopamine and induces dopamine reverse transport through the dopamine transporter. Amphetamine also binds reversibly to dopamine transporter, slowing dopamine reuptake. (B) A two-dimensional topology of DAT based on the leucine transporter (LeuT) is shown with 12 transmembrane segments, intracellularly oriented N- and C-termini, and substrate binding site. The location of the R615C substitution in a highly conserved region of the transporter's C-terminus is shown. (Adapted from Ref. 38 Copyright 2011 American Chemical Society)

understanding DAT modulation, a dearth of information exists to indicate whether or how such regulatory mechanisms may be impacted in brain disorders. To a significant degree, inspection of these mechanisms has been limited by a reliance on the ensemble-averaging approaches available with conventional biochemical and optical techniques.

Biomolecule detection using quantum dots (QDs), nanometer-sized semiconductor crystals, addresses the limitations associated with population-based optical and biochemical techniques, as QDs offer several key advantages over traditional fluorophores: (i) broad absorption spectra and narrow, Gaussian-like emission spectra (25-40 nm at full-width half-maximum of the emission peak), (ii) high quantum yields and large molar extinction coefficients, (iii) superior resistance to photobleaching, and (iv) versatility of surface functionalization.²⁸⁻³⁰ Moreover, the use of QDs considerably simplifies the technical requirements for a highly sensitive, single molecule tracking experiments where observation of single QD-labeled targets can be achieved with ~5-10 nm accuracy over time periods that range from milliseconds to minutes.^{31,32} The primary focus of our group has been the development of ligand-conjugated QD probes that enable a specific targeting of neuronal membrane proteins, such as the serotonin (5-HT) transporter (SERT), DAT and the norepinephrine (NE) transporter (NET), as well as the γ -aminobutyric acid (GABA) receptor.³³⁻⁴¹ Since many membrane proteins lack surface-epitope antibodies suitable for dynamic tracking of single molecules, the cornerstone of our probe development has been the QD coupling of high-affinity, small-molecule antagonists that can provide for pseudo-irreversible probe binding and the analysis of surface trafficking properties.³⁹⁻⁴¹ Our approach enables both highly sensitive population detection of transporters and receptors as well as single QD analysis of target protein diffusion dynamics. In the most recent effort, Chang et al. used antagonist-conjugated QD probes in conjunction with high-speed, line-scanning

laser confocal microscopy to reveal a connection between receptor-mediated signaling-pathways that alter SERT activity and the membrane dynamics of SERT proteins on the surface of serotonergic cells.⁴¹

Here we adapted our recently reported, DAT-specific probe IDT444 to establish dynamic imaging of single DAT-QD complexes on the surface of living cells.^{38,40} The biotinylated, PEGylated cocaine analog IDT444 provides for labeling of surface DAT molecules via streptavidin-conjugated QD (SavQD) coupling to DAT-bound ligand, and has been shown to bind to DAT with high affinity and excellent specificity.³⁸ In this study, we extend our efforts to visualize single QD-labeled DAT complexes in living cells, providing for a characterization of their membrane dynamics and their sensitivity to membrane cholesterol extraction, drug impact, and ADHD-derived coding variation. Our studies support a significant confinement of membrane DAT molecules to GM-1 ganglioside enriched membrane microdomains that can be perturbed by disease-associated DAT coding variation.

6.2. Results and Discussion

6.2.1. Tracking Single DAT-QD Complexes

To overcome the limitations of ensemble-averaging and poor spatiotemporal resolution of the currently existing arsenal of DAT probes, we developed a high-affinity, biotin-labeled and DAT-specific cocaine analog IDT444 that permits pseudo-irreversible binding to SavQDs, while retaining high-affinity interactions with DAT.^{38,40} The flexible PEG-based linker of IDT444 also reduces potential steric hindrance of QDs with the cell

surface in addition to enhancing water solubility of the ligand.⁵¹ With this probe strategy, we demonstrated previously that QD-IDT444 conjugates successfully detected plasma membrane-localized DATs in both transiently and stably-transfected expression systems. Importantly, DAT-bound QD-IDT444 conjugates displayed a very slow off-rate (>1 hr), allowing for prolonged visualization of surface DAT molecules.⁴⁰ In the current study, we implemented our two-step QD labeling strategy to establish, for the first time, the dynamic imaging of membrane DATs in live cells with single QDs. The two-step labeling approach employed to detect membrane DATs is illustrated in Figure 6.2A. A representative confocal fluorescence image in Figure 6.2B depicts individual DAT-QD complexes on the cell surface. Nonspecific QD binding could be virtually eliminated by the inclusion of at least 1% w/w bovine serum albumin (BSA) in the QD imaging buffer. We monitored the movement of QD-labeled DATs in Flp-In 293 cell membranes using time-lapse image acquisition at a scan speed of 10 Hz over 1 min.⁴¹ It should be noted that only cell surface-bound QDs in a focal plane at the membrane-glass interface were detected. To minimize the effects of endocytosis, QD labeling was carried as the last experimental step, and QD-labeled cells were imaged immediately post-labeling. Also, data acquisition was achieved within 10 minutes of the final wash step. Fluorescence intermittency, an intrinsic property of single nanocrystals, was used as a criterion to assure analysis of single QD events (Figure 6.2C).⁴²⁻⁴⁵ An example of a DAT-QD trajectory is shown in blue in Figure 6.2D, with blinking/off intervals shown in red. To successfully interpolate the position of QDs between frames during which they blinked, IDL-based single tracking algorithms were employed (See Methods).

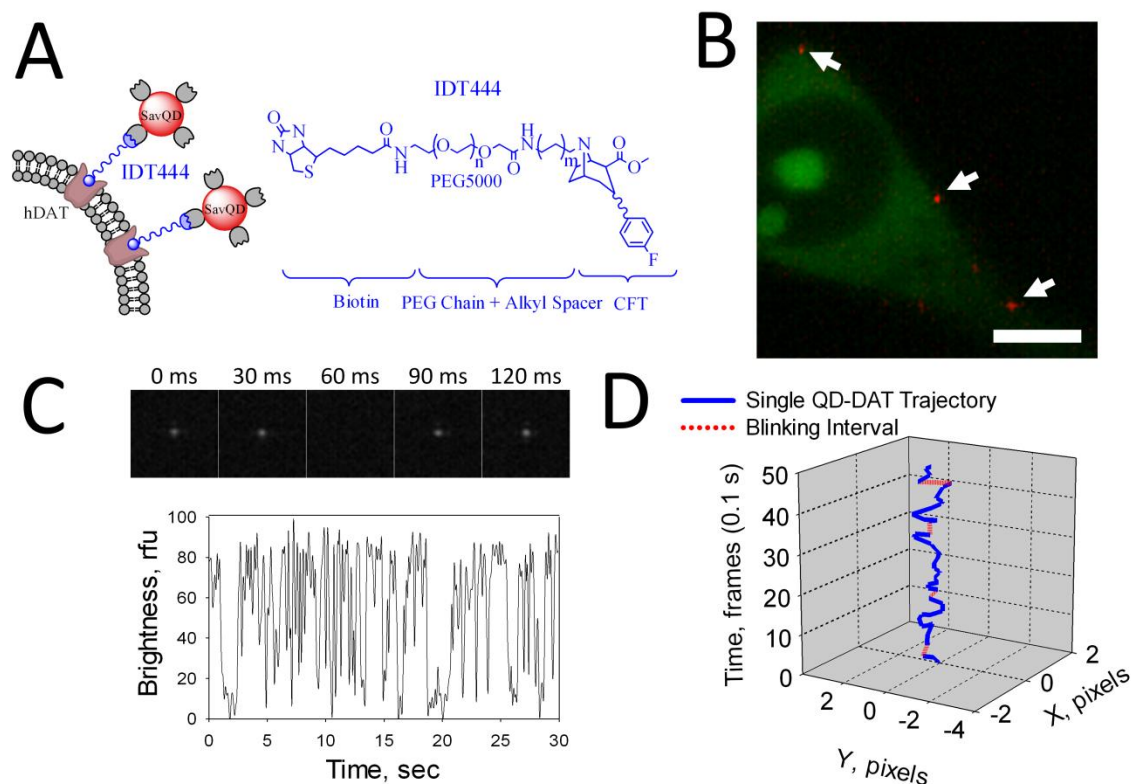


Figure 6.2. Time-lapse imaging of DAT in the plasma membrane of stably-transfected Flp-In 293 cells. (A) Schematic of the QD labeling protocol. DAT-specific IDT444 cocaine analog accesses the high-affinity binding site of DAT. Its biotin terminus facilitates subsequent DAT recognition with SavQDs. (B) Fluorescence micrograph showing characteristic surface QD labeling of DATs. Intracellular green fluorescence is characteristic of DAT-mediated IDT307 transport and was used as a cell position and focal plane gauge. Bar: 5 μm . (C) A representative time-lapse image series of a single SavQD immobilized (spun-cast) on a glass coverslip and a corresponding emission spectrum trace. Emission spectra of single nanocrystals exhibit fluorescence intermittency, a criterion used to distinguish single QDs from aggregation artifacts. (D) An example trajectory of single DAT-QD complex undergoing diffusion in the plasma membrane.

6.2.2. DAT-QD Membrane Dynamics Reveals Confined Behavior

Initially, we examined the differences in cell surface diffusive motion of individual, nonspecifically adsorbed carboxyl-terminated AMPTM QDs (Figure 6.3 A, Left) in parallel with DAT-bound QDs in stably-transfected Flp-In 293 cells (Figure 6.3 A, Middle-Right). Although limited in abundance, AMPTM QDs nonspecifically bound to the cell membrane

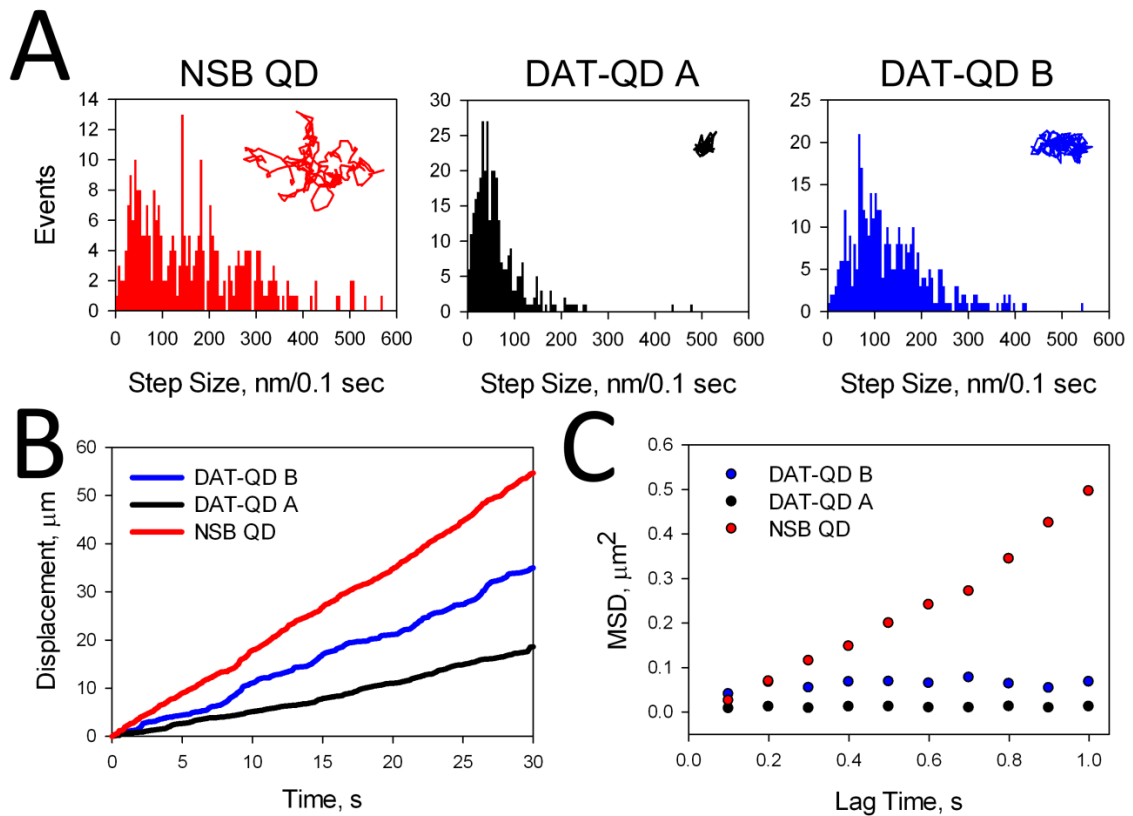


Figure 6.3. Single-quantum dot tracking of AMP[™] QDs nonspecifically bound to the membrane of Flp-In 293 cells and SavQDs specifically bound to membrane DATs expressed in Flp-In 293 cells. (A) Single particle real-time trajectories of DAT-bound or nonspecifically bound QDs are shown as inset zoom-ins, and instantaneous velocity distributions are displayed for the corresponding trajectories. (B) Trajectories from (A) are depicted as a displacement from the initial position (x_0, y_0) over time; trajectories appear continuous, increasing linearly with time. (C) Averaged MSD as a function of time for a single AMP[™] QD and single DAT-QD complexes. MSD (t) plot for a single AMP[™] QD reflects linear increase over time, indicative of simple, Brownian-like diffusion, whereas MSD (t) plots for single DAT-QDs are characterized by pronounced negative curvature at increasing lag time, indicative of confined diffusion.

can be used as a background control in particle tracking studies.^{46,47} As expected, membrane dynamics of single AMP[™] QDs was characterized by a continuous, Brownian-like lateral diffusion with no apparent transient confinement. Analysis of the instantaneous velocity of a single AMP[™] QD revealed a broad, multimodal distribution of step sizes, with a mean

instantaneous velocity of $1.8 \pm 0.2 \mu\text{m/s}$. In contrast, real-time trajectory data of single DAT-QD complexes was characterized by much more limited lateral movement. Thus, mean instantaneous velocity of single DAT-QDs was considerably slower than that of nonspecifically bound AMPTM QDs with a mean instantaneous velocity of $0.65 \pm 0.02 \mu\text{m/s}$ and $1.27 \pm 0.03 \mu\text{m/s}$ (Figure 6.3 A Middle and Right respectively). Although the visual inspection of single DAT-QD trajectories indicated restricted lateral diffusion, their motion was uniform and did not contain discrete stop-and-go features on the subsecond timescale (Figure 6.3 B), suggesting stable confinement over the time-scale of our measurements versus “in and out” microdomain dynamics. To more accurately analyze the diffusion pattern of single DAT-QD complexes, we performed the mean square displacement (MSD) analysis.⁴⁸ Individual mean-square displacement (MSD) as a function of time plots for single DAT-QD complexes were characterized by pronounced negative curvature at increasing lag times, consistent with persistent membrane confinement of DAT proteins (Figure 6.3 C). In contrast, MSD of single AMP QDs increased linearly with time, reflecting a Brownian-like motion pattern devoid of membrane confinement.

6.2.3. DAT-QD Lateral Diffusion is Highly Restricted in Two Heterologous Expression Systems

To test whether the choice of a heterologous expression system, or the mode of expression (transient versus stable transfection), alters membrane DAT mobility, we analyzed at least 200 individual real-time trajectories of DAT-QD complexes from transiently-transfected HeLa cells (human epithelial cervical carcinoma cells) as well as stably-transfected Flp-In 293 cells (human embryonic kidney cells). Sample trajectories are

shown in Figure 6.4 A. To assess mean population instantaneous velocity, distributions of single step displacements (>10,000 steps for each data set) were fit to a truncated form (Cauchy distribution) of the Lévy probability distribution function:

$$f(x) = \left[b \cdot \left(1 + \frac{x-x_0}{a} \right)^2 \right]^{-1} \quad [5]$$

where x_0 is the best-fit instantaneous displacement, a and b are fit coefficients, and the goodness of fit is defined by the R^2 values, with R^2 being greater than 0.95 for all data sets.^{47,49} Unimodality of step size distributions was apparent, and the mean instantaneous velocity was determined to be nearly identical for single DAT-QDs in the two cell lines, with values of $0.48 \pm 0.01 \mu\text{m/s}$ and $0.51 \pm 0.01 \mu\text{m/s}$ in HeLa cells and Flp-In 293 cells, respectively (Figure 6.4 B). Ensemble MSD versus time plots featured pronounced negative curvature at increasing lag times, a reliable indicator of restricted diffusive behavior of single DAT-QD complexes (Figure 5.4 C). To determine the dimensions of the confinement zone, ensemble MSD plots were fit according to the method previously described by Daumas *et al.*:

$$\text{MSD}(t) = 2L^2 \left(1 - e^{-\frac{t}{\tau}} \right) + 4D_M t \quad [6]$$

where L is the size of the confining domain, τ is the relaxation/equilibration time on short timescales, D_M is the long-term macroscopic diffusion coefficient, and the goodness of fit is defined by the R^2 value, with R^2 greater than 0.98 for all data sets.⁵⁰ The average size of a putative membrane subdomains restricting lateral diffusion of DAT was determined to be $150 \pm 43 \text{ nm}$ and $170 \pm 32 \text{ nm}$ in HeLa cells and Flp-In 293 cells, respectively (Figure 6.4 D).

Previous reports have proposed that lateral diffusion of membrane proteins is constrained by transient confinement zones (TCZs), such as cholesterol-rich lipid rafts or

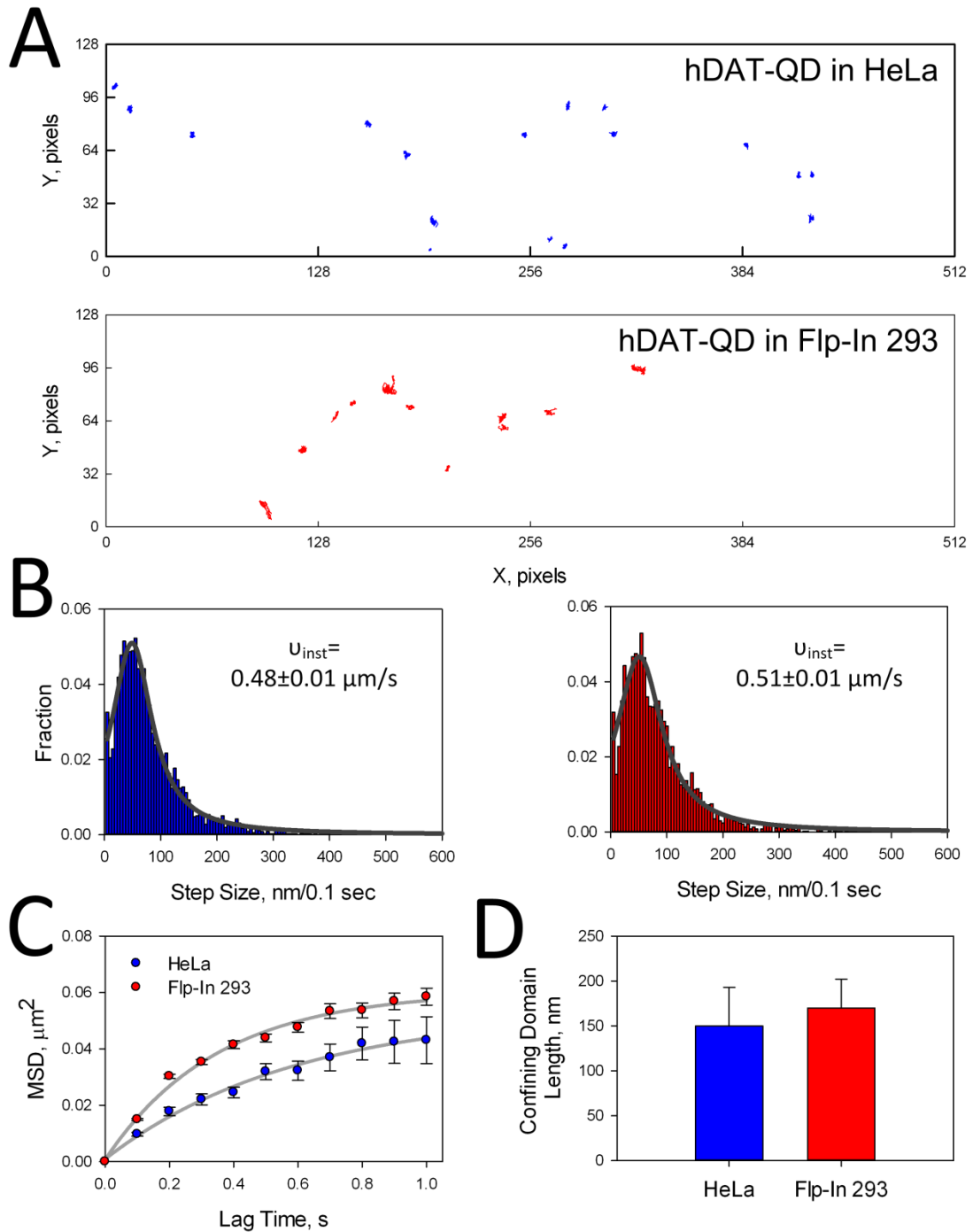


Figure 6.4. Instantaneous velocity and diffusion behavior of single DAT-QD complexes in HeLa and Flp-In 293 cells. (A) Example trajectories. Scale: 1 pixel = 200 nm. (B) Comparison of instantaneous velocity distributions of single DAT-QD complexes in HeLa and Flp-In 293 under basal conditions. Each histogram comprises at least 10,000 individual displacement steps. (C) Plots of MSD as a function of time. Each plot is based on at least 200 individual trajectories acquired during at least three independent experiments.

(D) Comparison of the confining domain length (L , nm) restricting the diffusion of single DAT-QDs in HeLa and Flp-In 293 cells. Domain size is represented as mean \pm SEM.

cytoskeletal corrals.⁵¹⁻⁵³ Recently, we demonstrated that the DAT homolog SERT, labeled in serotonergic RN46A cells with ligand-conjugated QDs, associates with cholesterol- and GM1 ganglioside-rich membrane microdomains where confined lateral diffusion is evident under basal conditions.⁴¹ Our analyses of surface trafficking of membrane DAT molecules are in agreement with these observations and could be demonstrated in multiple transfected cell models. Biochemical studies of the past decade have provided evidence that (i) DAT is associated and immobilized with cholesterol-rich membrane fractions in transfected cells and (ii) that cholesterol modulates DAT activity as well as cocaine binding to DAT.^{20,24} In parallel, multiple lines of evidence suggest that plasma membrane is compartmentalized into many small subdomains, ranging from 20 nm to 2 μ m in diameter, in which membrane protein molecules are confined on the time scale of 1-30 s.^{47,51-53} In a recent effort, Chang *et al.* demonstrated that QD-labeled ganglioside GM-1, a principal constituent of lipid rafts, slowly diffuses within membrane confinement zones (\sim 200 nm) with the dwelling time greater than 10 s.⁴⁷ Our estimate of the diameters of the membrane subdomains restricting DAT-QD diffusion (150-170 nm) agree closely with such values, indicating persistent confinement of DAT molecules on the millisecond-second timescale.

To determine whether our SERT observations extend to heterologously-expressed DAT proteins, we performed single QD tracking of endogenous GM-1 ganglioside in the plasma membrane of HeLa and Flp-In 293 cells to examine the correlation between GM-1 resident microdomains and DAT diffusion patterns. As seen in RN46A cells, we found GM1-QD movement to be highly restricted in both cell lines, matching dynamic behavior

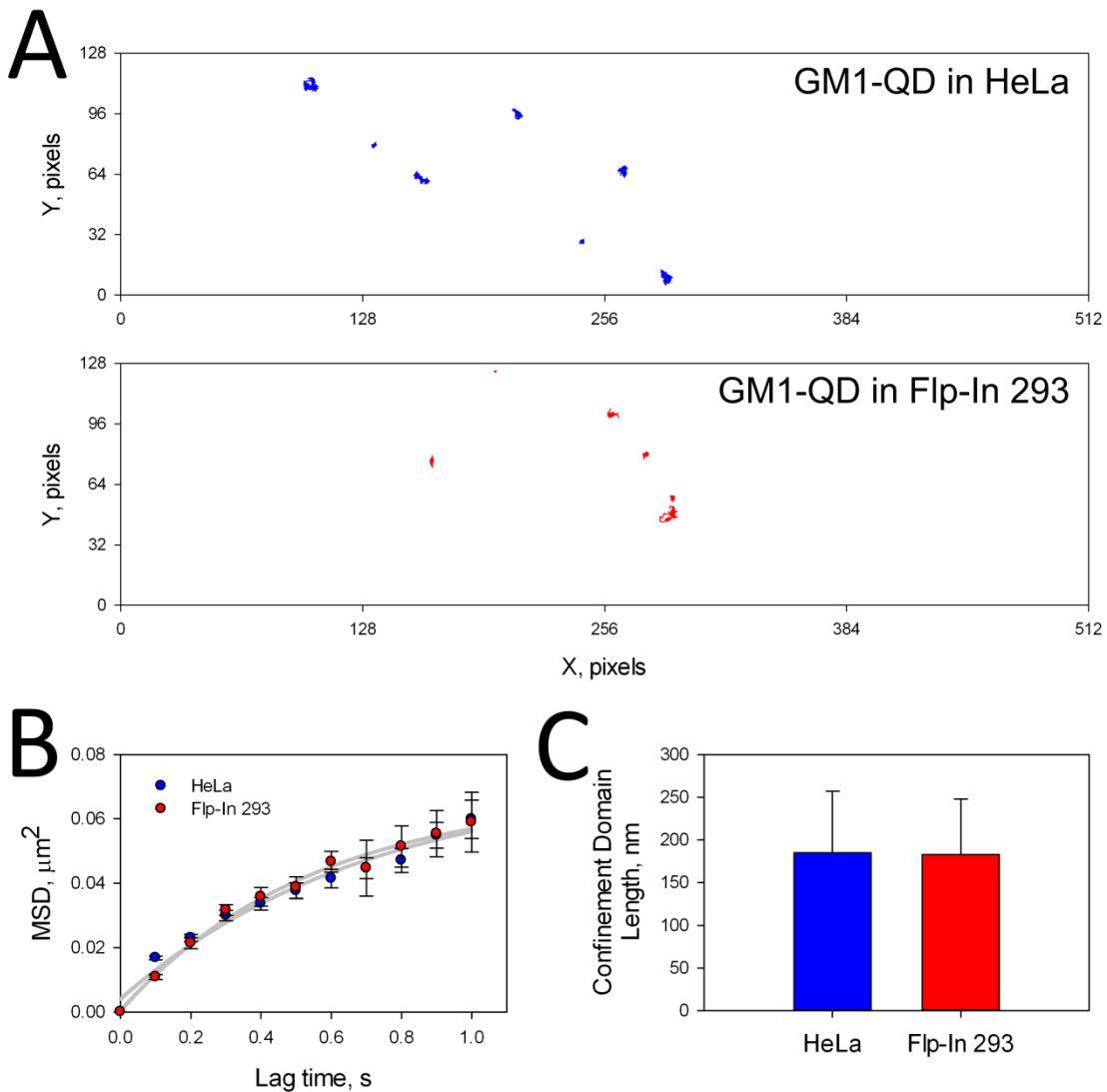


Figure 6.5. Diffusion behavior of single ganglioside GM1-QD complexes in HeLa and Flp-In 293 cells. (A) Example trajectories. Scale: 1 pixel = 200 nm. (B) Plots of MSD as a function of time. Each plot is based on at least 100 individual trajectories acquired during at least three independent experiments. (C) Comparison of the confining domain length (L , nm) restricting the diffusion of single GM1-QDs in HeLa and Flp-In 293 cells. Domain size is represented as mean \pm SEM.

of DAT expressed in these cells (Figure 6.5A). Consistent with these findings, MSD analysis revealed significantly lower mobility than expected for free diffusion of GM1 (Figure 6.5B), with mobility essentially identical to that of DAT-QD complexes in these cells. To extract

the size of confining domain, ensemble MSD plots were fit according to the method described above (Figure 6.5C). The diameters of the confining microdomain were calculated to be 185 ± 72 nm and 183 ± 65 nm in HeLa cells and Flp-In 293 cells, respectively, in excellent agreement with the size of confinement zones restricting DAT-QD mobility. The biological implications of DAT confinement at the nanoscale, particularly when confined to membrane microdomains known to support the accretion of regulatory proteins are manifold, as membrane compartmentalization appears to be an evolved strategy to facilitate and co-localize biomolecular interactions that can be targeted by intracellular signal transduction mechanisms.⁵¹ In the future, we should be able to extend our approach to a multicolor, multitarget screening platform (e.g., one color of QD labeling a raft component and another color of QD bound to the transporter) to provide an effective method of dissecting regulated dynamic interactions in real time.

6.2.4. Attention Deficit/Hyperactivity Disorder-Derived DAT Coding Variation Produces Altered Transporter Mobility

Recently, in a screen for genetic changes in DAT in ADHD subjects, we identified and characterized the rare human DAT (hDAT) coding variant, R615C.²⁷ DAT 615R is located in a highly conserved region of the transporter's C-terminus that has been previously implicated in DAT trafficking regulation (Figure 6.1B).^{21,54,55} The DAT 615C substitution results in a loss of DAT trafficking sensitivity to both protein kinase C activation as well as amphetamine treatments. In the same report, we also demonstrated that the DAT 615C mutant is hyperphosphorylated and displays altered associations with flotillin- and GM1 ganglioside-enriched membrane microdomains in stably-transfected Flp-In 293 cells. We

sought to test the hypothesis that these behaviors may be supported by disrupted lateral diffusion. Example time series of Flp-In 293 cells expressing DAT 615R (wildtype) or 615C (mutant) labeled with QDs are shown in Supplemental Video 1 and Supplemental Video 2, respectively (Supplementary Materials are freely available at <http://www.acs.org>) . Visual inspection indicated that the majority of QD-DATs in both populations remained largely confined over a 1 min time interval. Examples of QD trajectories are shown in Figure 6.6A. Several trajectories of QDs immobilized on a glass coverslip are shown for comparison (Figure 6.6A, Bottom Row). The obtained trajectories were analyzed, and the combined MSD versus time plots for all measured trajectories of QD-DAT615R, QD-DAT-615C, and immobilized QDs are shown in Figure 6.6B. All MSD plots showed a characteristic negative curvature, indicating confined DAT diffusion in the membrane of Flp-In 293 cells. Figure 6.6C compares the distributions of diffusion coefficients ($D_{1,3}$) derived from individual MSD versus time plots. The median diffusion coefficient of QD-DAT 615R (wildtype) was $0.016 \mu\text{m}^2/\text{s}$ ($1.6 \times 10^{-10} \text{ cm}^2/\text{s}$), in the range found for other membrane proteins,³² whereas QD-tagged DAT 615C mutants exhibited significantly faster diffusion, with the median diffusion coefficient of $0.024 \mu\text{m}^2/\text{s}$ ($2.4 \times 10^{-10} \text{ cm}^2/\text{s}$) (Table 6.1, $p < 0.001$, one-way ANOVA with a Dunn's *post hoc* test). We then compared the median area explored at 1 second by DAT in the plasma membrane and confirmed that the explored area is significantly larger for the 615C variant (Figure 6.6D; $p < 0.001$, one-way ANOVA with a Dunn's *post hoc* test). Figure 6.6E shows 5 sec displacement vector maps for all QD-DAT 615R and QD-DAT 615C trajectories, with initial QD positions located at the origin. Again, QD-DAT 615C complexes exhibited greater mobility than their QD-DAT 615R counterparts, as indicated by a more scattered distribution and a significantly larger 5-sec radial displacement ($p < 0.001$, one-way ANOVA with a Dunn's *post hoc* test). Thus, in agreement with our hypothesis, we

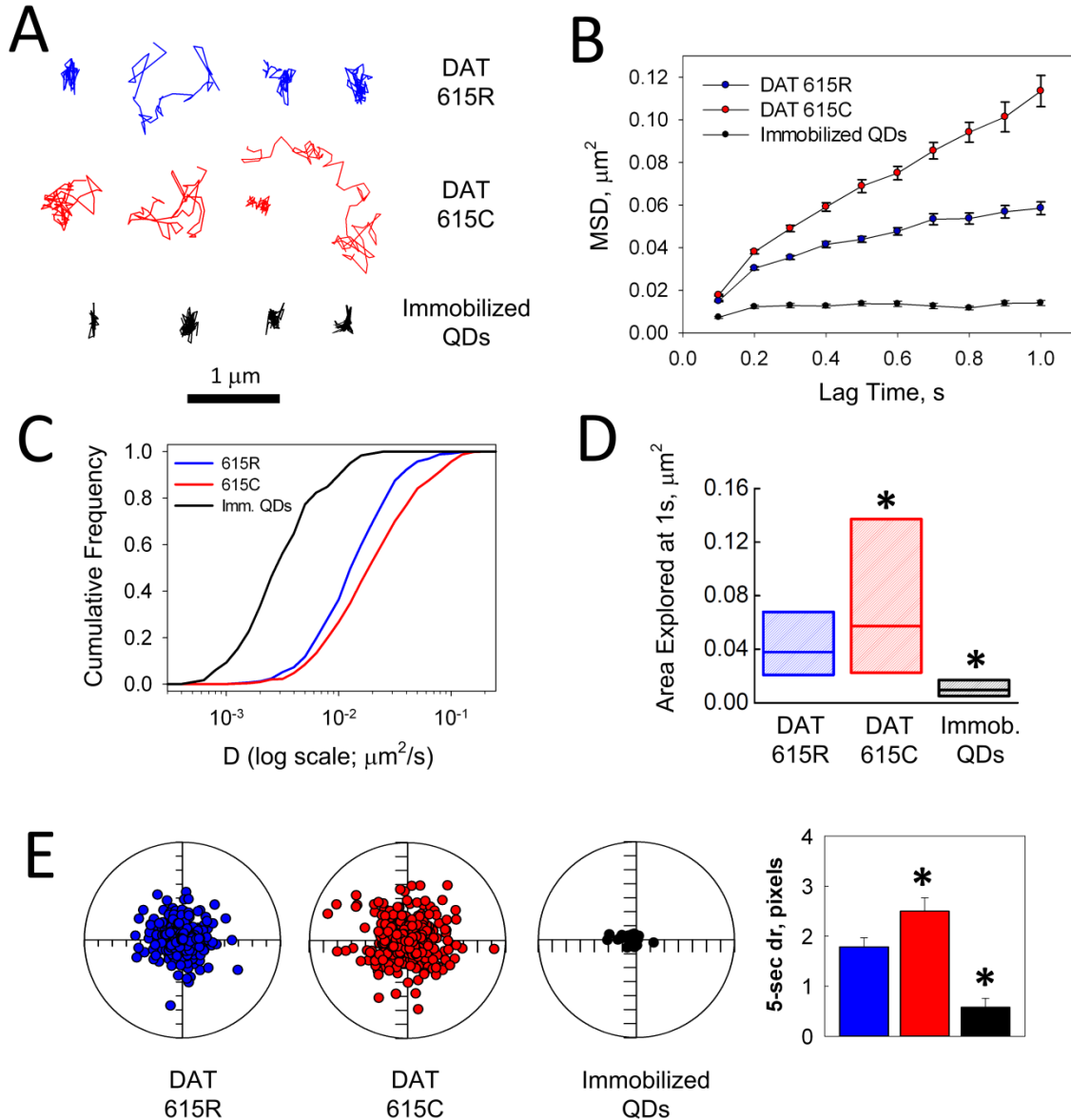


Figure 6.6. Single-quantum dot tracking of the wildtype DAT 615R variant and the attention deficit/hyperactivity-derived DAT 615C variant in Flp-In 293 cells. (A) Example trajectories of single DAT 615R-QD and DAT 615C-QD complexes ($n \geq 500$ trajectories from at least 20 cells over the course of at least three independent experiments). Trajectories of immobilized QDs on a coverglass (Bottom Row) are shown for comparison. (B) Ensemble mean square displacement versus time plots for QD-labeled DAT 615R and DAT 615C in Flp-In 293 cells as well as QDs spun-cast on a coverslip. Error bars indicate S.D. (C) Cumulative probability plots depicting diffusion rate distributions (one-way ANOVA with Dunn's *post hoc* test on raw diffusion coefficient values: DAT 615R vs DAT 615C, *** $P < 0.001$; DAT615R vs Immobilized QDs on a coverslip, *** $P < 0.001$). (D) Explored areas at 1 s, shown as color box plot histograms. Median is represented as a line; color box represents the 25%-75% interquartile range (one-way ANOVA with Dunn's *post*

hoc test: DAT 615R vs DAT 615C, ***P<0.001; DAT615R vs Immobilized QDs on a coverslip, ***P<0.001). (E) Two-dimensional polar plots of 5 sec radial displacements (d_{5s}) of single QD-DAT 615R, QD-DAT 615C, and immobilized QDs normalized to their starting coordinates. Radius of a polar plot is 2.8 μm . Mean d_5 values were compared using one-way ANOVA with Dunn's *post hoc* test; ***P<0.001 with respect to QD-DAT 615R. Asterisks in D and E denote P<0.001 statistical significance level.

determined that DAT 615C membrane dynamics were characterized by a significantly faster diffusion rate, a larger explored membrane area at 1s, and a greater mobile fraction under basal conditions. Our data point are consistent with altered DAT 615C basal membrane dynamics as contributory to the functional dysregulation observed with the variant.²⁷ Our findings are also consistent with previous observations that cholesterol-rich membrane rafts play a major role in the capacity for DAT regulation, produced both by endogenous signaling pathways and by psychostimulants.^{18,20,24}

Table 6.1. Comparison of median diffusion coefficients and explored areas at 1 s of QD-labeled DAT 615R and DAT 615C variants under basal, methyl- β -cyclodextrin-treated, and amphetamine-treated conditions in Flp-In 293 cells.

DAT Coding Variant	Experimental Conditions	Trajectories Analyzed	Median D, $\mu\text{m}^2/\text{s}$	Median Explored Area at 1s, μm^2
615R	Basal	584	0.016	0.038
	+ M β CD	251	0.025	0.052
	+ AMPH	273	0.020	0.045
615C	Basal	550	0.024	0.057
	+ M β CD	265	0.023	0.054
	+ AMPH	259	0.027	0.060

6.2.5. DAT-615R and DAT-615C Surface Mobility is Differentially Regulated by Methyl- β -Cyclodextrin and Amphetamine

To examine the effects of membrane raft disruption on DAT lateral mobility, we utilized methyl- β -cyclodextrin, a commonly used, cholesterol-extracting agent. Previously, Adkins *et al.* were able to mobilize a fraction of the DAT molecules after membrane raft disruption with 10 mM methyl- β -cyclodextrin, as measured using ensemble-averaged fluorescence recovery after photobleaching (FRAP).²⁴ Furthermore, Sakrikar *et al.* proposed that the disrupted localization of the DAT 615C coding variant away from cholesterol-, GM1 ganglioside-, and flotillin-enriched membrane microdomains might be responsible for its insensitivity to amphetamine and protein kinase C activation.²⁷ To investigate this possibility at the single molecule level, we treated DAT 615R- and DAT 615C- expressing Flp-In 293 cells with 5 μ M methyl- β -cyclodextrin for 30 min, performed the two-step QD labeling protocol, and then acquired confocal time-lapse images. Wildtype DAT 615R mobility after membrane raft disruption was characterized by significantly greater diffusion coefficient than in untreated cells along with a larger explored area as compared to basal conditions (Table 1; Figure 6.7 A-C; $p < 0.001$, one-way ANOVA with a Dunn's *post hoc* test). Remarkably, methyl- β -cyclodextrin treatment failed to enhance the mobility of DAT 615C (Figure 6.7 A-C; $p > 0.05$, one-way ANOVA with a Dunn's *post hoc* test), supporting the hypothesis that the variant transporter's functional and regulatory disturbance arises from its mislocalization to a compartment where cholesterol content is not a determinant of the transporter's lateral mobility. Interestingly, as we previously demonstrated that DAT 615C exhibits constitutive endocytosis and recycling, as compared with the highly regulated intracellular trafficking of DAT 615R, our findings support the idea that membrane compartmentalization is critical for normal DAT regulation and that risk for DA-related

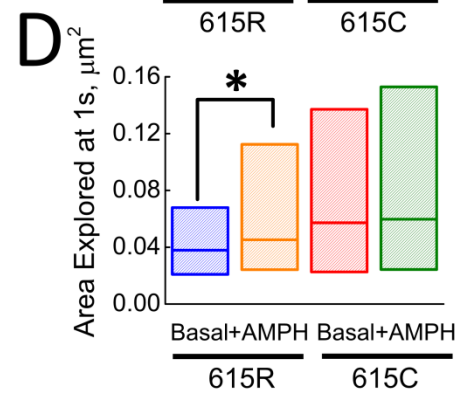
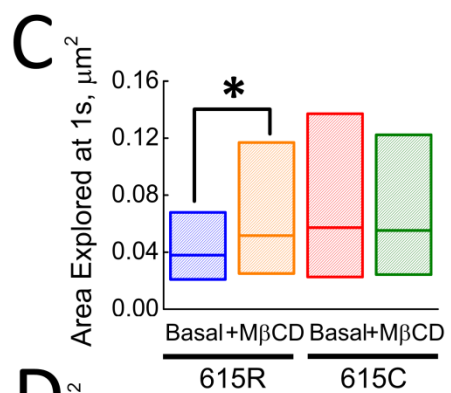
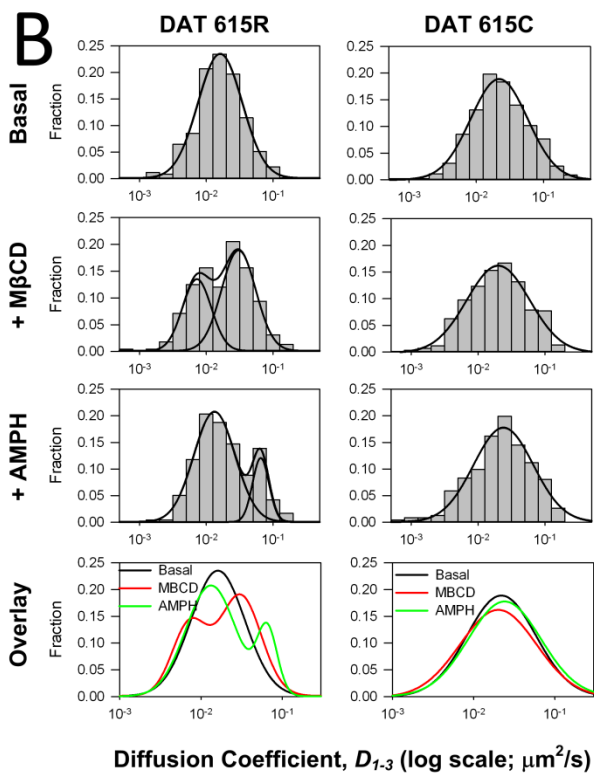
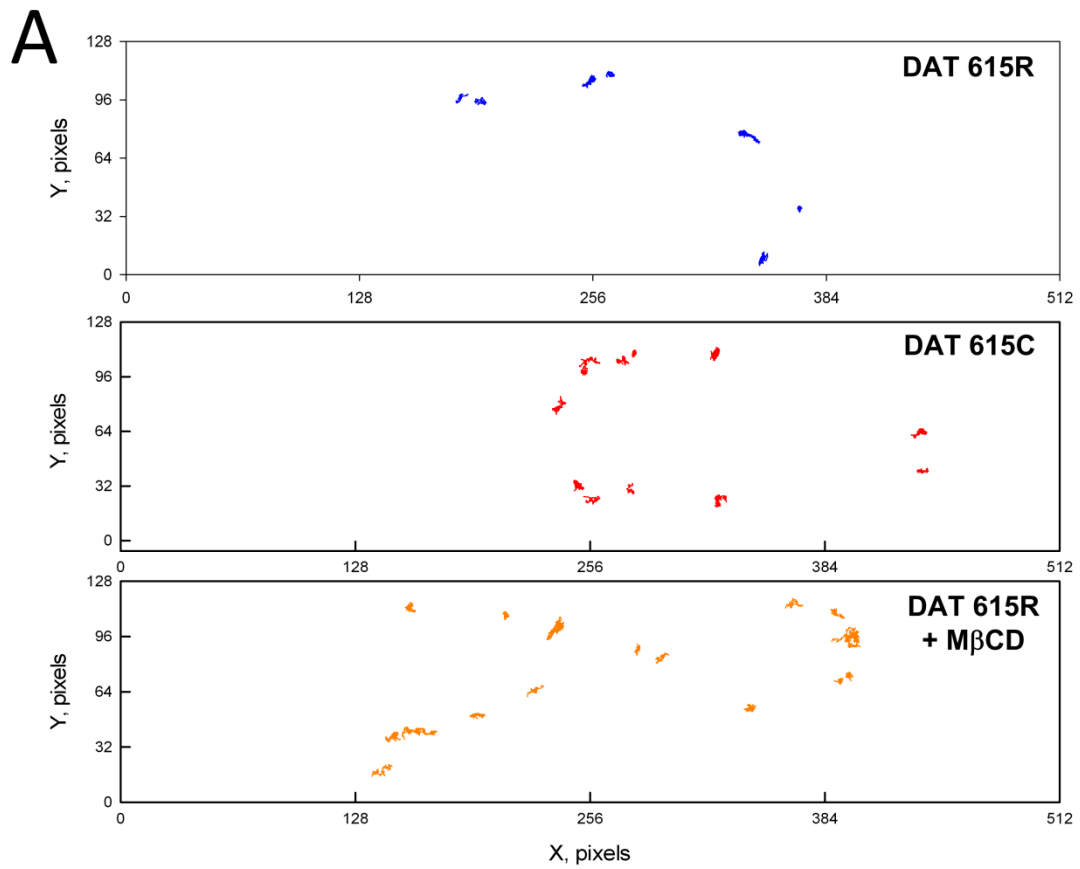


Figure 6.7. DAT 615R and DAT 615C membrane diffusion after M β CD-mediated cholesterol depletion and amphetamine treatment in Flp-In 293 cells. (A) Example trajectories. Scale: 1 pixel = 200 nm. (B) Comparison of diffusion coefficient distributions for single DAT 615R-QDs and DAT 615C-QDs under basal, methyl- β -cyclodextrin-treated, amphetamine-treated conditions (one-way ANOVA with Dunn's *post hoc* test on non-transformed data: DAT 615R basal vs DAT 615C basal, ***P<0.001; DAT 615R basal vs DAT 615R + methyl- β -cyclodextrin, ***P<0.001; DAT 615C basal vs DAT 615C + methyl- β -cyclodextrin, P=0.4; DAT 615R basal vs DAT 615R + amphetamine, ***P<0.001; DAT 615C basal vs DAT 615C + amphetamine, P=0.2). (C) Comparison of the distributions of explored areas (MSD at 1 s) by single DAT 615R-QDs and DAT 615C-QDs under basal and methyl- β -cyclodextrin-treated conditions (one-way ANOVA with Dunn's *post hoc* test on non-transformed values: DAT 615R basal vs DAT 615C basal, ***P<0.001; DAT 615R basal vs DAT 615R + methyl- β -cyclodextrin, ***P<0.001; DAT 615C basal vs DAT 615C + methyl- β -cyclodextrin, P=0.2). (D) Comparison of the distributions of explored areas (at 1 s) by single DAT 615R-QDs and DAT 615C-QDs under control and amphetamine-treated conditions (one-way ANOVA with Dunn's *post hoc* test: DAT 615R basal vs DAT 615C basal, ***P<0.001; DAT 615R basal vs DAT 615R + amphetamine, **P<0.01; DAT 615C basal vs DAT 615C + amphetamine, P=0.7). For each dataset, n \geq 250 single DAT-QD trajectories from at least three independent experiments. Asterisks in B and C denote P<0.001 and P<0.01 statistical significance levels respectively.

disorders, here modeled with a genetic variant linked to ADHD, may arise in some individuals as a result of DAT mis-targeting to these domains.

In our initial studies, we also demonstrated that the DAT 615C variant exhibits hyperphosphorylation and a marked insensitivity to amphetamine-induced trafficking.²⁷ Amphetamine treatments evoke both an acute translocation of DAT to the cell surface, seconds after exposure, or cause DAT internalization after minutes of amphetamine treatment.^{17,22,27} Our visualization methods, implemented over a millisecond to seconds time scale, should not be influenced by rapid membrane insertion events as QD labeling is restricted to proteins labeled at the cell surface. Thus, we treated DAT 615R- and DAT 615C-expressing Flp-In 293 cells with 10 μ M amphetamine for 30 min and then exposed cells to the two-step QD labeling protocol. Real-time trajectory analysis of single QD-labeled DAT movement revealed a significant increase in amphetamine-treated DAT 615R lateral

membrane mobility when compared to basal conditions (Table 6.1; Figure 5.7 B,D; $p < 0.001$, one-way ANOVA with a Dunn's *post hoc* test). In contrast, DAT 615C proteins are already as mobile as wildtype DAT 615R proteins treated with amphetamine and amphetamine treatments produce no further effect on DAT 615C lateral diffusion ($p > 0.05$, one-way ANOVA with a Dunn's *post hoc* test). Although not a focus of this study, we suspect that the failure of amphetamine to increase the diffusion rate of DAT 615C reflects an untethering of the variant transporter from critical protein associations that normally both localize the transporter to membrane microdomains and that place the transporter in a dephosphorylated state, awaiting regulatory phosphorylation as a result of amphetamine application. In relation to the site of the DAT 615C variant in the transporter's distal C-terminus, we recently provided evidence that single QD imaging of SERT surface mobility is supported by the transporters C-terminus.⁴¹ Rao et al., using ensemble-averaged fluorescence recovery after photobleaching, demonstrated increased AlexaFluor488-DAT lateral mobility in filopodia of postnatal DA neurons after 60 μM amphetamine treatment for 30 min.⁵⁶ These authors hypothesized that this increase in DAT mobility could be attributed to amphetamine-induced, calcium/calmodulin-dependent protein kinase II-mediated phosphorylation of the DAT N terminus and subsequent untethering of DAT molecules from interacting proteins/lipids. In support of this model, we demonstrated that DAT 615C is hyperphosphorylated on the transporter's N-terminus.^{16,27} Our single molecule imaging approach should provide a high resolution approach to exploration of how the structure and protein interactions of the DAT C-terminus influence the regulatory control of DAT exhibited by the transporter's C-terminus.

6.3. Summary and Conclusions

The goal of this study was to establish a generalizable strategy for evaluation of the plasma membrane dynamics of the cocaine- and amphetamine-sensitive DAT protein with the nanometer resolution required to monitor transporters localized to membrane subdomains. Our single QD-based imaging approach enabled us, for the first time, to detect the lateral mobility of individual DAT-QD complexes in living cells and to assess transporter responses to microdomain destabilization, a disease-associated mutation, and an addictive psychostimulant also used in the treatment of ADHD. Our data show that the movement of transporter molecules in the plasma membrane in several cell expression platforms to be highly restricted, with the confinement zone size in close agreement with the previously reported dimensions for lipid raft and cytoskeletal corrals and that detected for SERT in neuronal RN46A cells. Consistent with these measures, analysis of single GM1-QD real-time trajectory data revealed that the diffusion patterns of QD-bound DAT and GM1 ganglioside molecules are identical. Finally, real-time, single DAT-QD trajectory analysis revealed that plasma membrane dynamics of the ADHD-associated DAT R615C coding variant exhibits a significantly higher diffusion rate, a larger explored membrane area, and a greater mobile fraction under basal conditions. In response to cholesterol extraction and amphetamine stimulation, single DAT 615C molecules fail to exhibit altered mobility, likely a result of the transporter's mislocalization and consequent elevation in basal mobility. We hypothesize that the higher basal mobility of the mutant transporter reflects an untethering of the variant transporter from C-terminal directed or regulated protein associations that normally serve to localize the transporter to membrane microdomains. Identifying these proteins may offer additional clues to DA regulatory perturbations supporting ADHD risk.

6.4. Experimental Section

6.4.1. Materials

DMEM, FBS, Hygromycin B, AMPTM QDs and SavQDs (emission max at 655 nm) were from Life Technologies. Amphetamine, methyl- β -cyclodextrin, poly-D-lysine, and BSA were purchased from Sigma-Aldrich. Four-well chambered coverglass dishes were purchased from Lab-Tek. IDT307 and IDT444 were synthesized as previously described.

6.4.2. Cell culture, transfections, and stable cell line generation

Flp-In 293 cells were used to generate stable lines expressing either DAT 615R or DAT 615C following the manufacturer's protocol (Life Technologies). Flp-InTM 293 cell line is designed for rapid generation of stable cell lines that ensure high level expression of the protein of interest from a Flp-In expression vector. These cells contain a single stably integrated FRT site at a transcriptionally active genomic locus. Targeted integration of a Flp-In expression vector ensures high-level expression of the gene of interest. The Flp-In 293 host cell line (Invitrogen) was grown in complete medium (D-MEM with 2 mM L-glutamine, 10% FBS, 1% pen/strep) supplemented with 100 μ g/mL Hygromycin B in a 37 °C incubator with 5% CO₂. The wild-type or mutant human DAT (hDAT) cDNA cloned in the pcDNA5/FRT expression vector was transfected into Flp-In-293 cells using the Fugene 6 transfection reagent (Roche, NJ). After 48 h recovery, the cells were grown in medium with 100 μ g/mL hygromycin B added for several weeks to select for resistant cells where the cDNA construct had been recombined into the Flp-In site in the Flp-In-293 cells. HeLa cell line (ATCC #CCL-2) was grown in complete medium (D-MEM with 2 mM L-glutamine, 10% FBS, 1% penn/strep) in a 37°C incubator with 5% CO₂. For transient transfection

experiments, HeLa cells were grown in complete medium in absence of penn/strep. 24 hours after seeding HeLa cells, non-expressing (Sham) and DAT-expressing pcDNA3 vectors containing the SV40 origin and early promoter region for episomal replication were introduced into HeLa cells. Fugene HD (Roche, NJ) was used to facilitate transient transfection according to the manufacturer's recommendations. The cells were allowed 24 hours post-transfection for successful expression of DAT.

6.4.3. QD Labeling of DAT-expressing Flp-In 293 cells

DAT 615R- or DAT 615C-expressing cells were seeded in poly-D-lysine coated Lab-Tek slides and grown for 24 hours. QD labeling was implemented via a two-step protocol. Cells were washed twice with warm Krebs'-Ringer's-HEPES (KRH) (130 mM NaCl, 1.3 mM KCl, 2.2 mM CaCl₂, 1.2 mM MgSO₄, 1.2 mM KH₂PO₄, 10 mM HEPES, pH 7.4) buffer and incubated with a sub-saturating IDT444 concentration of 10 nM in KRH at 37°C and 5% CO₂. Following two washes with warm KRH, cells were then incubated with a 50 pM dose of SavQDs in warm phenol red-free DMEM/2% bovine serum albumin (imaging buffer), washed three times with warm imaging buffer, and used for time-lapse image series acquisition. To perform cholesterol depletion, methyl- β -cyclodextrin was added to Flp-In 293 cells to a final concentration of 5 μ M (30 min incubation at 37°C and 5% CO₂). Cells were then washed three times with warm KRH, subjected to the QD labeling protocol, and imaged. Amphetamine was administered in an analogous way, with a final effective dose of 10 μ M (20 min incubation at 37°C and 5% CO₂). Amphetamine-treated cells were washed three times with warm KRH, subjected to the QD labeling protocol, and imaged in presence of 10 μ M amphetamine.

6.4.4. Ganglioside GM1-QD Tracking

Ganglioside GM1 labeling and tracking was performed as previously described.⁴⁷ Briefly, cells were incubated with 50-200 nM biotinylated cholera toxin b subunit (CTxB, Sigma-Aldrich, St. Louis, MO) for 5 min prior to 5 min SavQD655 incubation at 37°C. Data acquisition was performed immediately after the final wash step to prevent endocytosis of GM1-QD complexes.

6.4.5. High-Speed Confocal Microscopy

For high speed line-scanning confocal microscopy, images were obtained on a Zeiss LSM 5 Live confocal system and viewed with a Zeiss 63×/1.4 NA oil immersion objective lens. Excitation was provided by a 488 nm 100-milliwatt diode laser. Imaging was performed at 37°C. QD fluorescence was collected using a long pass 650 filter. Single QD tracking was performed at a scan rate of 10 Hz for 1 min. Data were obtained within 10 minutes of the final wash step after QD labeling.

6.4.6. Data Analysis

Individual TIF images were extracted from sequence files and recompiled as 8-bit image stacks by using ImageJ (National Institutes of Health, Bethesda, MD). Image analysis and trajectory construction were performed using IDL software (Research Systems, Boulder, CO) with algorithms available as shareware at <http://www.physics.emory.edu/faculty/weeks/>. The localization accuracy of the central position of the QD in our imaging approach was estimated to be $\pm 10-15$ nm.⁴⁷ The uncertainty of the fitted coordinate was estimated ($\Delta\sigma$) via $\Delta\sigma \approx w/\text{SNR}$ (nm), where w (width) is approximately equal to the wide-field diffraction limit (which for visible light is

about 250 nm) and SNR is signal-to-noise ratio defined as $\text{SNR} = I_0 / (\sigma_{\text{bg}}^2 + \sigma_{I_0}^2)^{1/2}$, where I_0 is the maximum signal intensity above background, σ_{bg}^2 is the variance of the background intensity values, and $\sigma_{I_0}^2$ is the variance of the maximum signal intensity above the background. Intermittency of QD fluorescence was used to verify that single fluorophores were analyzed, and extracted trajectories were at least 5 s in length. Trajectories were considered continuous if a blinking QD was rediscovered within a 3-pixel radius and 10-frame window. For each trajectory, mean square displacement (MSD), $r^2(t)$, was computed as follows:

$$\langle r^2(n\delta t) \rangle = \frac{1}{N-n} \sum_{j=0}^{N-n-1} \{ [x(j\delta t + n\delta t) - x(j\delta t)]^2 + [y(j\delta t + n\delta t) - y(j\delta t)]^2 \}$$

$$(n = 0, 1, 2, \dots, N - 1) \quad [7]$$

where δt is the temporal resolution of the acquisition device, $(x(j\delta t), y(j\delta t))$ is the particle coordinate at $t = j\delta t$, and N is the number of total frames recorded for an individual particle. The median MSD (at $t = 1$ s) of the QD population represents the area explored within 1 s. Individual microscopic diffusion coefficient D was determined by fitting the first 1-3 points of the MSD versus time curves with the equation:

$$\langle r^2(t) \rangle_{1-3} = 4D_{1-3}t + \text{offset} \quad [8]$$

This fit is generally used because it determines D independently of the type of motion.^{57,58} The distribution of explored area (at $t = 1$ s) was represented as box plot histograms with median, 25% and 75% interquartiles, and the distribution of D_{1-3} -values for each experimental condition was displayed as either cumulative probability histograms or vertical bar histograms fitted to a unimodal or bimodal Gaussian function. The optimal bin size was evaluated using the Friedman-Diaconis rule. Statistical significance of differences in median

values was determined using the one-way ANOVA with Dunn's *post hoc* test on non-transformed values.

6.5. References

- (1) Giros, B.; Caron, M. G., Trends in Pharmacological Science 1993, 14 (2), 43-9.
- (2) Bannon, M. J., Dopamine. Nature Encyclopedia of Life Sciences, Nature Publishing Group. Retrieved May 6, 2010 from www.els.net. 2004.
- (3) Giros, B.; Jaber, M.; Jones, S. R.; Wightman, R. M.; Caron, M. G., Nature 1996, 379 (6566), 606-12.
- (4) Raul, R. G.; Sara, R. J.; Marc, G. C., Biological psychiatry 1999, 46 (3), 303-311.
- (5) Ralph, R. J.; Paulus, M. P.; Fumagalli, F.; Caron, M. G.; Geyer, M. A., Journal of Neuroscience 2001, 21 (1), 305-313.
- (6) Schmitt, K. C.; Reith, M. E. A. Annals of the New York Academy of Sciences 2010, 1187, 316-340.
- (7) Greenwood, T. A.; Alexander, M.; Keck, P. E.; McElroy, S.; Sadovnick, A. D.; Remick, R. A.; Kelsoe, J. R., Am J Med Genet 2001, 105 (2), 145-51.
- (8) Swanson, J. M.; Flodman, P.; Kennedy, J.; Spence, M. A.; Moyzis, R.; Schuck, S.; Murias, M.; Moriarity, J.; Barr, C.; Smith, M.; Posner, M., Neurosci Biobehav Rev 2000, 24 (1), 21-5.
- (9) Kirley, A.; Lowe, N.; Hawi, Z.; Mullins, C.; Daly, G.; Waldman, I.; McCarron, M.; O'Donnell, D.; Fitzgerald, M.; Gill, M., American Journal of Medical Genetics Part B: Neuropsychiatric Genetics 2003, 121B (1), 50-54.
- (10) Kurian, M. A.; Zhen, J.; Cheng, S.-Y.; Li, Y.; Mordekar, S. R.; Jardine, P.; Morgan, N. V.; Meyer, E.; Tee, L.; Pasha, S.; Wassmer, E.; Heales, S. J. R.; Gissen, P.; Reith, M. E. A.; Maher, E. R., The Journal of Clinical Investigation 2009, 119 (6), 1595-1603.
- (11) Eriksen, J.; Jorgensen, T. N.; Gether, U., J Neurochem 2010, 113 (1).
- (12) Cremona, M. L.; Matthies, H. J. G.; Pau, K.; Bowton, E.; Speed, N.; Lute, B. J.; Anderson, M.; Sen, N.; Robertson, S. D.; Vaughan, R. A.; Rothman, J. E.; Galli, A.; Javitch, J. A.; Yamamoto, A., Nat Neurosci 2011, 14 (4), 469-477.
- (13) Binda, F.; Dipace, C.; Bowton, E.; Robertson, S. D.; Lute, B. J.; Fog, J. U.; Zhang, M.; Sen, N.; Colbran, R. J.; Gnegy, M. E.; Gether, U.; Javitch, J. A.; Erreger, K.; Galli, A., Molecular Pharmacology 2008, 74 (4), 1101-1108.
- (14) Bjerggaard, C.; Fog, J. U.; Hastrup, H.; Madsen, K.; Loland, C. J.; Javitch, J. A.; Gether, U., The Journal of Neuroscience 2004, 24 (31), 7024-7036.
- (15) Boudanova, E.; Navaroli, D. M.; Stevens, Z.; Melikian, H. E., Molecular and Cellular Neuroscience 2008, 39 (2), 211-217.
- (16) Bowton, E.; Saunders, C.; Erreger, K.; Sakrikar, D.; Matthies, H. J.; Sen, N.; Jessen, T.; Colbran, R. J.; Caron, M. G.; Javitch, J. A.; Blakely, R. D.; Galli, A., The Journal of Neuroscience 2010, 30 (17), 6048-6057.
- (17) Fog, J. U.; Khoshbouei, H.; Holy, M.; Owens, W. A.; Vaegter, C. B.; Sen, N.; Nikandrova, Y.; Bowton, E.; McMahan, D. G.; Colbran, R. J.; Daws, L. C.; Sitte, H. H.; Javitch, J. A.; Galli, A.; Gether, U., Neuron 2006, 51 (4), 417-429.

- (18) Foster, J. D.; Adkins, S. D.; Lever, J. R.; Vaughan, R. A., *Journal of Neurochemistry* 2008, 105 (5), 1683-1699.
- (19) Foster, J. D.; Vaughan, R. A., *Journal of Biological Chemistry* 2011, 286 (7), 5175-5186.
- (20) Hong, W. C.; Amara, S. G., *Journal of Biological Chemistry* 2010, 285 (42), 32616-32626.
- (21) Navaroli, D. M.; Stevens, Z. H.; Uzelac, Z.; Gabriel, L.; King, M. J.; Lifshitz, L. M.; Sitte, H. H.; Melikian, H. E., *The Journal of Neuroscience* 2011, 31 (39), 13758-13770.
- (22) Saunders, C.; Ferrer, J. V.; Shi, L.; Chen, J.; Merrill, G.; Lamb, M. E.; Leeb-Lundberg, L. M. F.; Carvelli, L.; Javitch, J. A.; Galli, A., *Proceedings of the National Academy of Sciences* 2000, 97 (12), 6850-6855.
- (23) Torres, G. E.; Carneiro, A.; Seamans, K.; Fiorentini, C.; Sweeney, A.; Yao, W.-D.; Caron, M. G., *Journal of Biological Chemistry* 2003, 278 (4), 2731-2739.
- (24) Adkins, E. M.; Samuvel, D. J.; Fog, J. U.; Eriksen, J.; Jayanthi, L.D.; Vaegter, C.B.; Ramamoorthy, S.; Gether, U., *Biochemistry* 2007, 46 (37), 10484-10497.
- (25) Furman, C. A.; Chen, R.; Guptaroy, B.; Zhang, M.; Holz, R. W.; Gnegy, M., *J Neurosci* 2009, 29 (10), 3328-36.
- (26) Eriksen, J.; Rasmussen, S. G.; Rasmussen, T. N.; Vaegter, C. B.; Cha, J. H.; Zou, M. F.; Newman, A. H.; Gether, U., *J Neurosci* 2009, 29 (21), 6794-808.
- (27) Sakrikar, D.; Mazei-Robison, M. S.; Mergy, M. A.; Richtand, N. W.; Han, Q.; Hamilton, P. J.; Bowton, E.; Galli, A.; Veenstra-VanderWeele, J.; Gill, M.; Blakely, R. D., *The Journal of Neuroscience* 2012, 32 (16), 5385-5397.
- (28) Bruchez, M., Jr.; Moronne, M.; Gin, P.; Weiss, S.; Alivisatos, A. P., *Science* 1998, 281 (5385), 2013-2016.
- (29) Chan, W. C. W.; Nie, S., *Science* 1998, 281 (5385), 2016-2018.
- (30) Rosenthal, S. J., J. C. Chang, O. Kovtun, J. R. McBride, I. D. Tomlinson, *Chemistry & Biology* 2011, 18 (1), 10-24.
- (31) Dahan, M.; Lévi, S.; Luccardini, C.; Rostaing, P.; Riveau, B.; Triller, A., *Science* 2003, 302 (5644), 442-445.
- (32) Pinaud, F.; Clarke, S.; Sittner, A.; Dahan, M., *Nat Meth* 2010, 7 (4), 275-285.
- (33) Rosenthal, S. J.; Tomlinson, I.; Adkins, E. M.; Schroeter, S.; Adams, S.; Swafford, L.; McBride, J.; Wang, Y.; DeFelice, L. J.; Blakely, R. D., *Journal of the American Chemical Society* 2002, 124 (17), 4586-4594.
- (34) Tomlinson, I. D.; Mason, J.; Burton, J. N.; Blakely, R. D.; Rosenthal, S. J., *Tetrahedron* 2003, 59 (40), 8035-8047.
- (35) Tomlinson, I. D., J. N. Mason, Blakely, R. D.; Rosenthal, S. J., *Bioorganic & Medicinal Chemistry Letters* 2006, 16 (17), 4664-4667.
- (36) Tomlinson, I. D.; Mason, J. N.; Blakely, R. D.; Rosenthal, S. J., *Bioorganic & Medicinal Chemistry Letters* 2005, 15 (23), 5307-5310.
- (37) Tomlinson, I. D.; Iwamoto, H.; Blakely, R. D.; Rosenthal, S. J., *Bioorganic & Medicinal Chemistry Letters* 2011, 21 (6), 1678-1682.
- (38) Kovtun, O.; Tomlinson, I. D.; Sakrikar, D. S.; Chang, J. C.; Blakely, R. D.; Rosenthal, S. J., *ACS Chemical Neuroscience* 2011, 2 (7), 370-378.
- (39) Chang, J. C.; Tomlinson, I. D.; Warnement, M. R.; Iwamoto, H.; DeFelice, L. J.; Blakely, R. D.; Rosenthal, S. J., *Journal of the American Chemical Society* 2011, 133 (44), 17528-17531.

- (40) Kovtun, O.; Ross, E. J.; Tomlinson, I. D.; Rosenthal, S. J., *Chemical Communications* 2012, 48 (44), 5428-5430.
- (41) Chang, J. C.; Tomlinson, I. D.; Warnement, M. R.; Ustione, A.; Carneiro, A. M. D.; Piston, D. W.; Blakely, R. D.; Rosenthal, S. J., *Journal of Neuroscience* 2012, 32, 8919-29.
- (42) Nirmal, M.; Brus, L., *ChemInform* 1999, 30 (29).
- (43) Kuno, M.; Fromm, D. P.; Hamann, H. F.; Gallagher, A.; Nesbitt, D. J., *The Journal of Chemical Physics* 2000, 112 (7), 3117-3120.
- (44) Neuhauser, R. G.; Shimizu, K. T.; Woo, W. K.; Empedocles, S. A.; Bawendi, M. G., *Physical Review Letters* 2000, 85 (15), 3301-3304.
- (45) Frantsuzov, P.; Kuno, M.; Janko, B.; Marcus, R. A., *Nat Phys* 2008, 4 (5), 519-522.
- (46) Bentzen, E. L.; Tomlinson, I. D.; Mason, J.; Gresch, P.; Warnement, M. R.; Wright, D.; Sanders-Bush, E.; Blakely, R.; Rosenthal, S. J., *Bioconjugate Chemistry* 2005, 16 (6), 1488-1494.
- (47) Chang, J. C. and Rosenthal, S. J., *ACS Chemical Neuroscience* 2012, 3, 737-743.
- (48) Vrljic, M., Nishimura, S. Y., and Moerner, W. E., *Methods in Molecular Biology* 2007, 398, 193-219.
- (49) Martin, D. S., Forstner, M. B., and Kas, J. A., *Biophysical Journal* 2002, 83, 2109–2117.
- (50) Daumas, F., Destainville, N., Millot, C., Lopez, A., Dean, D., and Salome, L., *Biophysical Journal* 2003, 84, 356–366.
- (51) Lingwood, D., and Simons, K., *Science* 2010, 327, 46–50.
- (52) Simmons, K., and Toomre, D. *Nat. Rev. Mol. Cell Bio.* 2000, 1, 31-40.
- (53) Brown, D. A., and London, E. *Annu. Rev. Cell Dev. Biol.* 1998, 14, 111–36
- (54) Torres, G. E.; Yao, W.-D.; Mohn, A. R.; Quan, H.; Kim, K.-M.; Levey, A. I.; Staudinger, J.; Caron, M. G., *Neuron* 2001, 30 (1), 121-134.
- (55) Bjerggaard, C.; Fog, J. U.; Hastrup, H.; Madsen, K.; Loland, C. J.; Javitch, J. A.; Gether, U., *The Journal of Neuroscience* 2004, 24 (31), 7024-7036.
- (56) Rao, A.; Richards, T. L.; Simmons, D.; Zahniser, N. R.; Sorkin, A., *The FASEB Journal* 2012, 26(5), 1921-33.
- (57) Kusumi, A., Sako, Y., and Yamamoto, M., *Biophysical Journal* 1993, 65, 2021-2040.
- (58) Triller, A., and Choquet, D., *Neuron* 2008, 59, 359-374.

CHAPTER VII

SUMMARY AND FUTURE DIRECTIONS

In this research, I utilized a DAT-specific, biotinylated IDT444 cocaine analog, which accesses the high-affinity binding site of DAT and enables subsequent DAT recognition with streptavidin-conjugated QDs, to (i) to visualize membrane-bound DAT molecules in single live cells, (ii) to develop a fluorescence-based assay that is aimed at facilitating high-content screening for novel DAT modulators, (iii) to quantify single-molecule diffusive behavior of DAT in the plasma membrane of live cells, and (iv) to investigate the effects of the attention deficit/hyperactivity disorder-derived coding variation in DAT and pathway-specific pharmacological perturbations on DAT plasma membrane dynamics in heterologous model expression systems. In particular, my recent data suggest that dopamine transporter molecules are subject to complex, dynamic regulation in the plasma membrane that may be mediated by key protein-protein interactions and facilitated by the plasma membrane compartmentalization. Since all of the dynamic imaging data has thus far been acquired in heterologous cell cultures, it is logical that one of the immediate questions to be tackled is whether DAT dynamic properties in primary neuronal cultures are consistent with our current findings. Another promising research avenue to be explored is the use of multicolor QD tracking to confirm existing and identify novel dynamic interactions of DAT molecules with various membrane protein (protein kinases, dopamine receptor, integrin, synaptic scaffolding elements) and lipid (ganglioside GM1, phospholipids) molecules. To this end, it might be Furthermore, our results described in Chapter V of this dissertation pinpoint to a critical effect of the DAT C-terminus coding variation on DAT

plasma membrane dynamics as well as its functional state. However, it is still unclear how the rate of DAT plasma mobility and confinement regime are correlated with the transport rate of dopamine, the native substrate of DAT. As such, studies that monitor the rate of uptake of a fluorescent false neurotransmitter or a fluorescent transporter substrate (IDT 307) and assess DAT diffusive behavior in parallel are warranted. To perform such a study, a silent QD labeling strategy that minimally perturbs the substrate uptake by DAT must be designed. Additionally, it is of utmost importance to determine how other coding variations of the conserved amino acids in the DAT N- and C-termini affect DAT lateral diffusion and functionality.

To conclude, quantum dots are swiftly becoming an indispensable tool for molecular neurobiological research. In particular, quantum dot technology is experiencing a markedly increased use to establish molecular mechanisms of disease and at the same time to facilitate next-generation drug discovery. The varieties of commercially available quantum dots for the research community will continue to expand, and multifunctional nanoparticles will become readily available, such as the nanoparticles that can be used for dual imaging modalities. We believe that the future of quantum dots in biology is exceptionally bright.

APPENDIX A

QUANTUM DOT APPROACHES FOR TARGET-BASED DRUG SCREENING AND MULTIPLEXED ACTIVE BIOSENSING

A.1. Introduction

Since their introduction to the field of biology in the mid-1990s, luminescent semiconductor nanocrystals, colloquially known as quantum dots, have secured an important niche in the field of fluorescence detection and visualization of molecular targets at the nanoscale.^{1,2} Owing to their unique photophysical properties, QDs are now routinely employed as cellular and molecular fluorescent reporters of first choice.³⁻⁵ In addition to ensemble and single-molecule target detection, QD use has been successfully extended to such applications as single-particle tracking, intracellular drug delivery, fluorescence resonance energy transfer (FRET)-based sensing, and multimodal molecular/tissue imaging.³⁻²⁰ QD photophysical properties are dictated by the inorganic semiconductor materials comprising the nanometer-sized (2-10 nm) crystalline core. The QD core is composed of a few hundreds to thousands of atoms of semiconductor materials in group II-VI (e. g., CdS, CdSe, CdTe) and group III-V (e. g., InP, InAs).^{5,21} The core particle is typically passivated with a one- to two-layer thick shell of wider band-gap semiconductor material to improve QD stability and enhance their photoluminescence quantum yield by eliminating the surface defects at the core/shell interface.^{21,22} For instance, the shell of choice in the case of CdSe core particle is ZnS, leading to quantum yield enhancements up to 300%. QD optical properties, which are governed by quantum confinement effects, can be effectively tuned through varying core particle size, composition, and morphology. Compared to traditional fluorophores, QDs are characterized by unparalleled resistance to

photobleaching and excellent brightness, a product of high quantum yields (0.1-0.8 in visible region) and large molar absorption coefficients (10^5 - 10^6 M⁻¹cm⁻¹).^{23,24} Broad absorption spectra and narrow, symmetric emission spectra (30-70 nm) of QDs offer great flexibility in excitation wavelength selection and enable efficient multicolor experiments, wherein one can successfully resolve signals from up to twelve spectrally distinct QDs simultaneously.²⁵ Another important feature of QDs is their large surface area and surface functionalization versatility that allow orthogonal attachment of multiple target recognition and active biosensing elements to the central QD nanoscaffold.²⁶ As a result, such functionalized nanocrystals can actively sense multiple signal transduction cascades simultaneously and combine several functionalities into a multimodal nanoplatform. Although QDs have proven to be potent, passive fluorescent reporters in cellular and molecular labeling applications, their use in target-based drug discovery assays and active biosensing has only recently been actively researched. Here, we will briefly address the versatility of QD surface functionalization and then discuss recent advances in drug screening- and biosensing-oriented applications.

A.2. Quantum Dot Surface Functionalization

Core/shell nanocrystals (*e. g.*, CdSe/Zns) are typically synthesized in high-temperature, nonpolar, organic coordinating solvents to ensure best crystalline quality, size monodispersity, and optimal photoluminescence properties.²⁷⁻²⁹ Due to the hydrophobicity of native surfactants (trioctylphosphine oxide, TOPO; hexadecylamine, HDA), the as-prepared core/shell QDs do not possess intrinsic aqueous solubility and must be further functionalized to provide a hydrophilic interface that ensures optimal compatibility with biologically relevant environment. As such, QDs must be rendered water-soluble through

either the ligand cap exchange or heterofunctional polymer shell encapsulation. The ultimate goal of QD solubilization is to obtain a nanoscaffold that (i) possesses long-term stability in physiologically relevant pH and ionic strength ranges, (ii) contains reactivity handles necessary for further bioconjugation, (iii) and exhibits minimal nonspecific interactions with biological systems. In the ligand exchange approach, QD native surfactants are displaced with hetero-bifunctional ligands that possess a functional group with high affinity to the QD surface (e.g., thiols, amines, phosphines) on one end and a hydrophilic functional group to aid in water solubility. Thiolated carboxylic acids are routinely selected as the capping ligands due to their strong binding affinity to the surface QD semiconductor atoms (e.g., 3-mercaptopropionic acid, MPA; dihydrolipoic acid, DHLA).⁴ In addition, a poly(ethylene glycol) (PEG) spacer is routinely incorporated into the ligand structure and QD architecture to minimize nonspecific binding.³⁰ The disadvantage of the ligand exchange approach is a significant reduction in QD photoluminescence quantum yield and reduced long-term stability due to the gradual loss of capping ligands from the QD surface. To date, the best and most prevalent approach for rendering QD water-soluble and biocompatible while minimizing the loss of original photophysical properties is encapsulation in a heterofunctional, amphiphilic polymer shell. In this strategy, native QD surfactants are retained and facilitate the association of the QD surface with polymer side chains via hydrophobic interactions.³¹⁻³³ As a result, the original, ligand-capped QD scaffold and its photophysical properties are minimally perturbed.

Once QDs are rendered water-soluble, they must be functionalized with surface elements that enable specific recognition of cellular biological targets. The key criteria for a successful conjugation of a biologically active probe to the QD surface are (i) conjugate stability, (ii) retention of biological activity, and (iii) controlled, reproducible display of probes on the QD

surface. To this end, several conjugation methodologies have been developed and are primarily categorized as either covalent conjugation or noncovalent self-assembly. In a conventional covalent conjugation approach, a carboxyl, amine, or thiol group at the QD surface is coupled to a desired biomolecule (proteins, peptides, nucleic acids, small molecules) with the use of hetero-bifunctional crosslinkers, such as 1-ethyl-3-(3-dimethylaminopropyl) carbodiimide (EDC) and succinimidyl-4-(N-maleimidomethyl) cyclohexane-1-carboxylate (SMCC). Moreover, recent advances in bioorthogonal chemistry provide highly chemoselective and well-controlled alternatives to conventional covalent conjugation strategies, such as strain-promoted azide-alkyne cycloaddition, alkene-tetrazine ligation, and the Staudinger ligation.²⁶ Currently, noncovalent self-assembly strategies are arguably the most popular means of presenting a functional biomolecule on the QD surface due to improved control over conjugate valence, biological activity, and binding specificity. The most commonly used methodologies involve the use of a biotin-streptavidin noncovalent interaction and spontaneous self-assembly of polyhistidine tags on the QD surface via metal-affinity interactions.^{26, 34-36}

A.3. Quantum Dot-Based Pharmacological Assays

Minimal nonspecific interactions, relatively small QD size, high target specificity, and superior resistance to degradation allow QD-based ensemble and single-molecule detection of extra- and intracellular targets with unprecedented spatiotemporal resolution. Consequently, QD-based cellular imaging has emerged as an important tool to unravel the molecular details of biological processes. Recent efforts have focused on the application of QD technology to the drug discovery process (Table A.1). Superior photophysical features

Table A.1. Quantum dots in biosensing applications of pharmacological relevance.

Target Analyte	Qdot Surface Sensing Element	Detection Strategy	Reference
acetylcholine esterase (AChE) inhibitors	AChE	electrochemical sensing	69
	FITC and choline oxidase	ratiometric ($\text{flu}_{\text{FITC}}/\text{flu}_{\text{QDOT}}$) fluorescence detection	70
adenosine	Au NPs (quenchers) attached to the Qdot surface via aptamers	Qdot release and fluorescence in the presence of adenosine	71
ATP	ATP aptamer fragment	Qdot-luminol CRET	72
	DNA oligonucleotide	Qdot-Cy5 FRET	73
beta secretase inhibitor	Qdot-peptide-Au NP	Qdot-Au NP FRET	74
botulinum neurotoxin (BoNT)	Cy3-labeled BoNT light chain protease substrate peptide	Qdot-Cy3 FRET	75
Ca^{2+}	CalciumRuby indicator dye	Qdot-CalciumRuby FRET	76
caspase	caspase peptide substrate	Qdot-Cy3 or Qdot-mCherry FRET	77,78
chymotrypsin/trypsin	Cy3-, Cy5-, or Tb^{3+} -labeled trypsin/chymotrypsin peptide substrate	singleplex or multiplex FRET	65-67, 79
	Au NPs (quenchers) attached to the Qdot surface via cocaine aptamers	Qdot release and fluorescence in the presence of cocaine	71
cocaine	Cy5-labeled aptamer	single-molecule Qdot-Cy5 FRET	80
	Cy3-labelled peptide substrate	Qdot-Cy3 FRET	77
collagenase	Cy3-labelled peptide substrate	Qdot-Cy3 FRET	77
DNA/RNA polymerase	single stranded DNA	Qdot-dUTP FRET	79
DNase	double stranded DNA labeled with dUTP	Qdot-dUTP FRET/Qdot emission	79
dopamine	Ag_2Se Qdots	electrogenerated chemiluminescence	81
dopamine transporter inhibitor	biotinylated IDT444	Qdot fluorescence	45
glucose	CdS/FITC/avidin/glucose oxidase hybrid system	ratiometric ($\text{flu}_{\text{FITC}}/\text{flu}_{\text{QDOT}}$) fluorescence detection	70
HIV drug	Qdot conjugated to Rev sensing element RNA (RRE RNA)	single-molecule FRET	61
maltose	maltose-binding protein and dye-labeled cyclodextrin	Qdot-QSY9 FRET	57
		Qdot-Cy3-Cy3.5 two-step FRET	
NADH:ubiquinone oxidoreductase	ubiquinone	electrochemical switching of Qdot fluorescence	82
O_2	cytochrome c	redox modulation of Qdot emission	83
	Pt(II) octaethylporphine ketone (PtOEPK)	Qdot-PtOEPK FRET	84
serotonin transporter inhibitor	biotinylated IDT318	Qdot fluorescence	44
thrombin	substrate peptide	Qdot-Cy3 or Qdot-QXL520	77
κ -opioid receptor inhibitor	anti-hemagglutinin antibody	Qdot fluorescence	55

of QDs combined with the latest advances in the state-of-the-art high content, automated microscopy permit the development of high throughput screening (HTS) assays that enable high-resolution, real-time, dynamic analysis of live cells. As QDs considerably simplify the technical requirements for a cell-based drug-discovery process, the application of QD technology to facilitate automated drug screening is inevitable.

To date, several formats of QD-based platforms amenable to the drug-discovery process have been reported. Our work has focused on the development of target-based, QD fluorescence assays to facilitate the discovery of small-molecule modulators of the monoamine neurotransmitter transporters (MATs), a family of integral plasma membrane proteins that regulate extracellular concentrations of monoamine neurotransmitters and are sites of action for widely prescribed antidepressants and psychostimulant drugs.³⁷⁻⁴⁶ Our ultimate goal is the discovery of novel drugs that exhibit antidepressant-like properties and expand the arsenal of currently available therapeutics for combatting mental disorders. The cornerstone of our strategy lies in the use of antagonist-conjugated QD nanopobes, which specifically target the primary binding site of MATs, such as serotonin transporter (SERT) and dopamine transporter (DAT) (Figure A.1). In our initial SERT labeling effort, the QD probe architecture was based on a central CdSe/ZnS core/shell scaffold with thiolated, PEGylated serotonin molecules assembled on its surface via ligand exchange of the native TOPO surfactants.³⁷ These multivalent, serotonin-terminated QD probes were then used to detect plasma membrane SERTs in living human embryonic kidney (HEK) cells (Figure A.1). Furthermore, these probes were utilized for subsequent electrophysiological studies, wherein biologically active QD probes induced transporter currents in an antagonist-like manner. Over time, our labeling strategy has evolved to include the biotin-streptavidin noncovalent assembly and a target-specific organic ligand. The use of these components

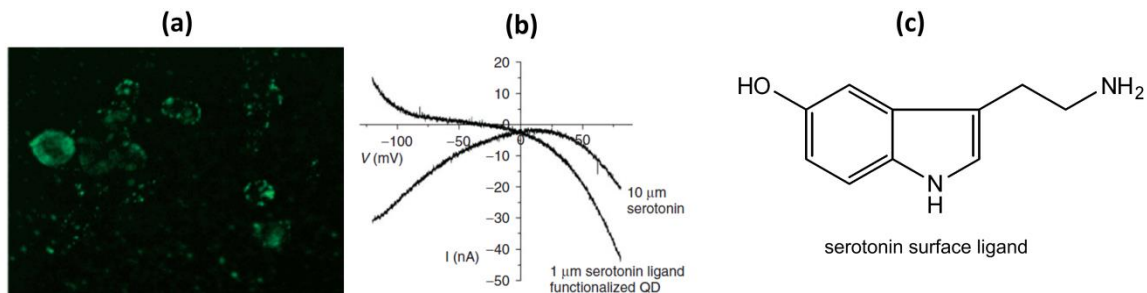


Figure A.1. Biologically active, serotonin-conjugated QDs for serotonin transporter (SERT) labeling in living HEK cells. (a) Fluorescence image of SERT-expressing in the membrane is indicated by characteristic green fluorescent halos. (b) Electrophysiological transporter currents induced by serotonin and biologically active, serotonin-conjugated QDs. Serotonin-functionalized QDs elicit an antagonist-like current, as opposed to serotonin itself. (c) Structure of the serotonin ligand used to functionalize QDs. Reprinted with permission from Ref 37. Copyright 2002 American Chemical Society.

considerably enhanced specificity and sensitivity of transporter recognition and resulted in much more streamlined and robust assay protocols. Currently, the organic ligand that serves as a bridge between the transporter protein and QD probe is composed of the following elements: (i) a high-affinity parent drug that enables recognition of specific binding sites within the transporter structure, (ii) a hydrophobic alkyl spacer which permits sufficient flexibility and provides a hydrophobic interface for a successful drug-binding pocket interaction, (iii) a PEG polymer that aids in aqueous solubility and abolishes possible nonspecific interactions with the plasma membrane, and (iv) a biotin moiety that allows subsequent QD recognition upon the transporter binding event (Figure A.2). The modular design of our tailored organic ligands results in an exceptional degree of control over modulating the free energy/temporal stability of the binding interaction as well as carefully selecting which specific binding site is targeted. Labeling of surface proteins with these probes is done via a two-step labeling protocol. The cells expressing a target protein are initially incubated with a biotinylated ligand, and then subsequently labeled with streptavidin-

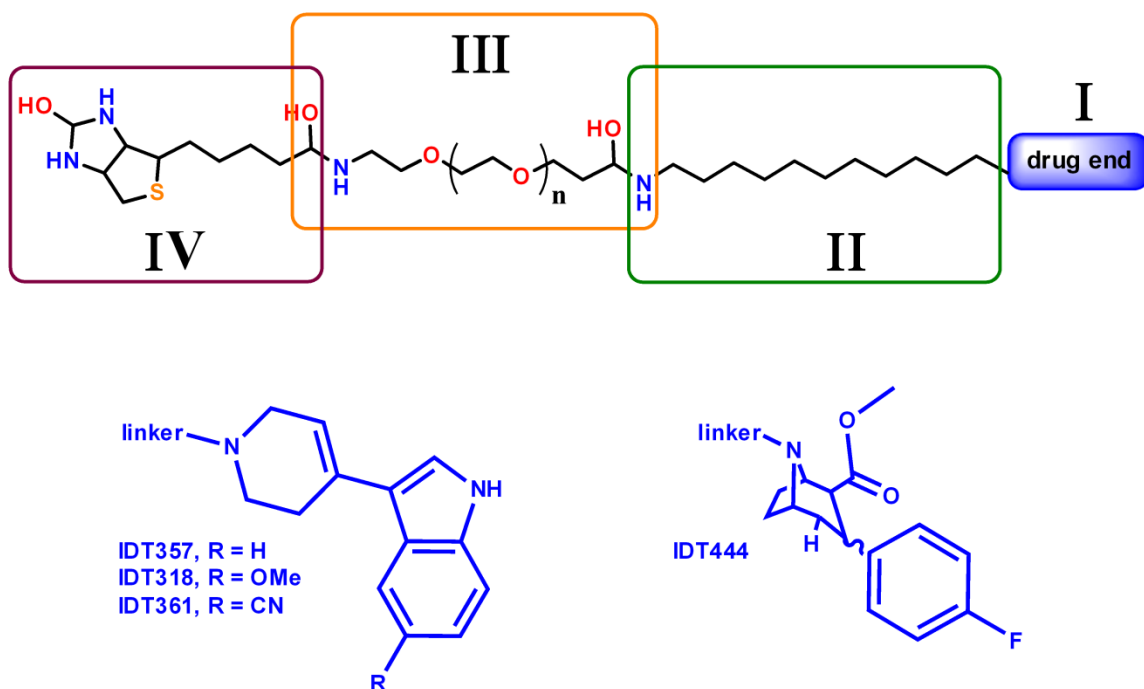


Figure A.2. Structure schematic of tailored organic ligands targeting plasma membrane monoamine transporters. Shown here is the general modular probe design (top) and examples of active drug ends (in blue) successfully conjugated to the biotinylated linker (top). Bottom left: a drug end of SERT-specific ligands based on the indoleamine-derived parent drug; bottom right: a drug end of a DAT-specific ligand based on the phenyltropane-derived parent drug.

conjugated QDs. By using the two-step protocol the biotinylated ligand is not subject to steric hindrance and retains flexibility to bind to the target, whereas pre-forming ligand-QD complexes typically results in multivalent probes with significantly reduced avidity, most likely due to unfavorable interactions between streptavidin molecules and biotinylated ligands (unpublished data). Additionally, it is difficult to control the number and orientation of ligands bound/pre-conjugated to QDs, as commercially available QDs typically present 5-10 tetravalent streptavidins on the surface. The optimal strategy to prevent multivalent interactions between the QD probes and target proteins is to conjugate a single monovalent streptavidin to the QD surface, a method pioneered by Alice Ting and colleagues.^{47,48}

A.3.1. The Displacement Assay

Photostability, exceptional optical properties, and excellent specificity of these antagonist-conjugated QDs enable several fluorescence-based, pharmacological assay formats that utilize a target-based, active configuration (Figure A.3a). In an active continuous (displacement) assay format, living cells/oocytes expressing membrane transporters are initially labeled with QD conjugates resulting in the “on” fluorescence signal. Next, a drug candidate, which may bind to an allosteric binding site, is added, and continuous, real-time fluorescence signal measurement is initiated. A positive drug candidate hit induces a protein conformational change and initiates QD conjugate displacement upon binding to the transporter. Consequently, fluorescence signal is significantly reduced and attains the “off” state. The key requirements for the QD conjugates to be successfully employed in a displacement assay format are (i) the reversibility of the binding interaction and (ii) micromolar affinity of the organic ligand for the transporter. As a validation of the displacement assay format, Chang *et al.* focused on an oocyte model expressing human SERT (hSERT), a primary target for drugs used to treat major depressive disorder (Figure A.4).⁴⁴ A QD-tagged indoleamine derivative (IDT318), which is structurally similar to serotonin, was used to access the primary neurotransmitter binding site of hSERT. Then, paroxetine, an antidepressant drug known as PaxilTM and hypothesized to bind to the allosteric site, was used to trigger displacement of the QD conjugates in a dose-dependent manner. Continuous signal measurement via widefield fluorescence microscopy readily

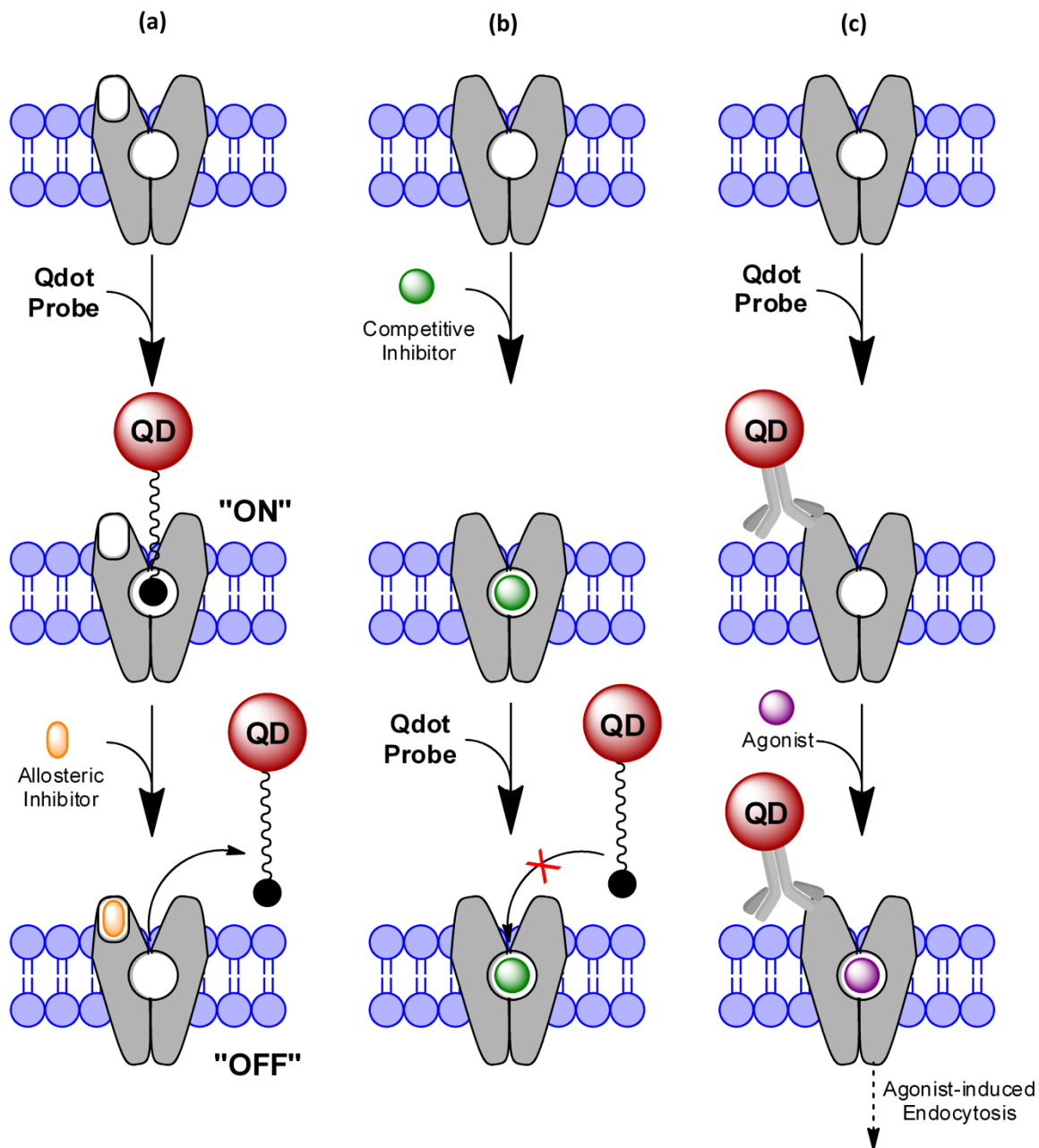


Figure A.3. Possible configurations of a target-based drug screening assay employing QDs. (a) In an active continuous format, target protein-expressing cells are initially incubated with antagonist-conjugated QD probes, resulting in an “ON” fluorescence signal. A competitive or an allosteric inhibitor candidate is then added, and the induced displacement of antagonist-conjugated probes is indicated by fluorescence loss, resulting in the “OFF” signal. (b) In an active endpoint format, target-protein expressing cells are initially exposed to a drug candidate, which may block subsequent QD probe binding, resulting in the “OFF” signal. In contrast, the parallel control sample is characterized by the “ON” fluorescence signal. (c) In a passive format, a QD probe initially targets the extracellular domain of the target protein, removed from the primary binding site. Agonist-induced Endocytosis

Administration of an agonist leads to target protein-QD complex internalization, resulting in the endosomal accumulation of QDs. The extent of internalization is quantified via assessing the amount of bright endosomal puncta accumulated.

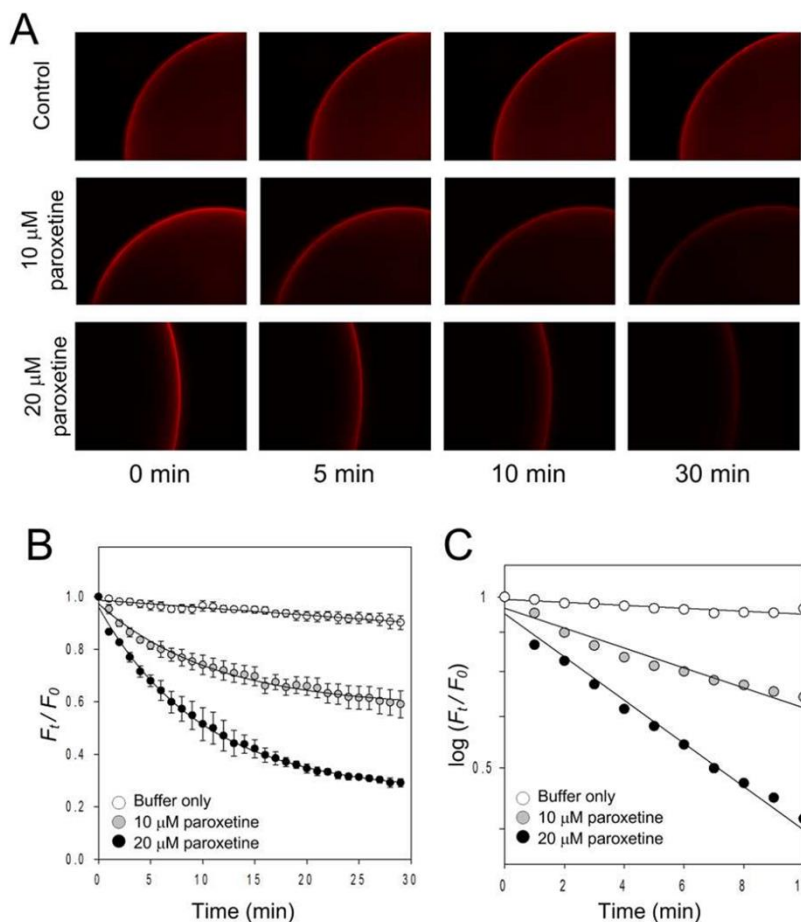


Figure A.4. QD-based fluorescence displacement assay aimed at the discovery of allosteric antidepressants. (a) Representative fluorescence time series, (b) time-dependent fluorescence intensity plots, and (c) dissociation kinetics plot show the effect of paroxetine, suggested to be an allosteric selective serotonin reuptake inhibitor (SSRI), on the interaction between ligand-conjugated QD probes and membrane SERT molecules. QD probes are readily displaced in the presence of 10 μM and 20 μM doses of paroxetine as opposed to the buffer control. Compound activity is determined based on the drug-induced dissociation kinetics. Reprinted with permission from Ref 44. Copyright 2011 American Chemical Society.

allowed extraction of an apparent dissociation rate constant, an important parameter in antidepressant drug screening. This QD-based displacement platform was found to possess sensitivity necessary for antidepressant drug screening; its throughput can be increased more

than 100-fold when used in conjunction with a commercially available, multiwell-plate imaging system.

A.3.2. The Active Endpoint Assay

When the binding interaction between the QD conjugates and membrane transporters is pseudo-irreversible and is characterized by nanomolar affinity, an active endpoint assay format is feasible (Figure A.3b). In this format, live cells expressing membrane transporters are initially incubated with a drug candidate and subsequently labeled with antagonist-conjugated QD probes in the presence of the drug candidate. A positive drug candidate hit causes the loss of surface transporters available for QD conjugate binding either via blocking the binding site (orthosteric or allosteric) or eliciting transporter endocytosis. Consequently, fluorescence signal is significantly reduced and attains the “off” state as opposed to the “on” signal exhibited by the parallel control (untreated) cell population. As a validation of the active endpoint assay format, Kovtun *et al.* employed a biotinylated, pegylated, high-affinity dopamine transporter (DAT) antagonist β -CFT (2- β -carbomethoxy-3- β -(4-fluorophenyl)tropane (IDT444), characterized by structural rigidity, pharmacological properties resembling those of cocaine, and the IC_{50} value of ~ 50 nM.⁴² DAT is a major target for the psychostimulants (cocaine, amphetamine), and abnormalities in DAT structure have been linked to a variety of neurodegenerative and psychiatric disorders, including schizophrenia, bipolar disorder, Parkinson’s disease, and attention deficit/hyperactivity disorder.⁴⁹⁻⁵⁴ Consequently, discovery of novel DAT function modulators is a high-priority task, as they represent a promising category of therapeutics in the light of increasing global incidence and socioeconomic burden of mental disorders linked

to dopamine signaling dysregulation. To this end, Kovtun *et al.* exploited excellent specificity, high affinity, and pseudo-irreversible binding mode of the IDT444-conjugated QDs to develop an active endpoint assay targeting DAT.⁴⁵ As a proof of principle, live, DAT-expressing HEK293 cells were initially titrated with increasing concentrations of GBR12909 (a high-affinity DAT antagonist) and phorbol 12-myristate 13-acetate (PMA; a protein kinase C activator) and subsequently exposed to IDT444-conjugated QDs. A commercially available benchtop flow cytometer was used for fluorescence signal detection and permitted a rapid, multiwell, single-cell analysis of multiple, large populations (thousands) of individual, QD-labeled cells in parallel. As expected, the fluorescence signal was significantly reduced in the presence of GBR12909 and PMA due to the direct antagonism and acute DAT surface loss respectively. The QD median intensity parameter was used to generate inhibitory dose-response curves of DAT modulators, and the extracted IC₅₀ values were found to be in excellent agreement with literature values. Furthermore, the use of a commercially available flow cytometer system readily allows the miniaturization of the assay to the 384-well plate format and represents a promising tool to aid in the initial stages of high throughput screening of novel DAT modulators.

A.3.3. The Passive Assay

In the case of a target-based passive configuration, a central QD scaffold is conjugated to an antibody against the extracellular domain sequence or a genetically engineered surface fusion tag of a membrane protein (Figure A.3c). In this configuration, it is possible to monitor agonist-induced internalization of the target protein with minimal interference from the QD tag, hence the descriptor “passive”. The endosomal accumulation

of QD-protein complexes leads to the appearance of bright, intracellular fluorescence puncta that can be readily quantified via automated image analysis. Recently, Lee and colleagues reported a QD-based platform that allowed for real-time monitoring of the agonist-induced endocytosis of G-protein coupled κ -opioid receptors (κ -OR), a clinical cancer marker overexpressed in several types of carcinomas (Figure A.5).⁵⁵ The κ -opioid receptor was

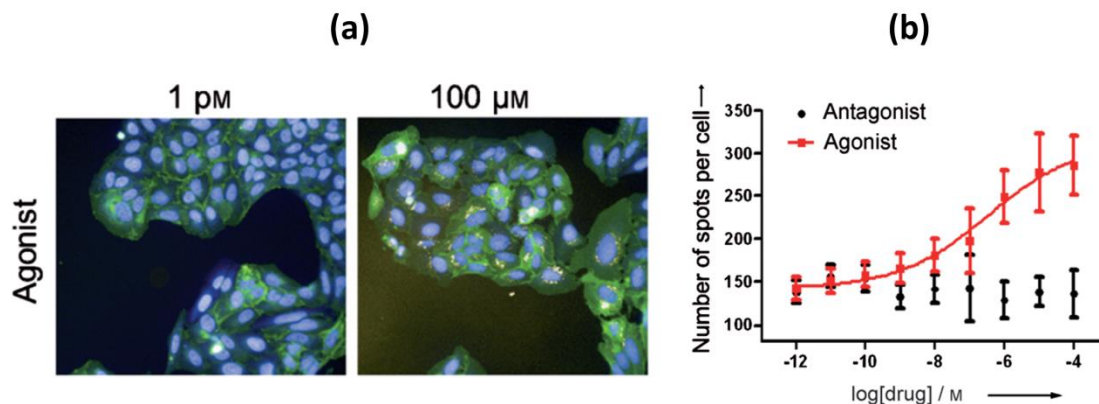


Figure A.5. High-content screening of the agonist-induced internalization of κ -opioid receptor in human osteocarcinoma cells. (a) Representative human osteocarcinoma cell images treated with 1 pM and 100 μ M of κ -opioid receptor agonist. (b) The number of spots (Qdot fluorescence) within the cytoplasmic region was calculated per cell using automated image analysis software, and the resulting EC_{50} values were obtained from concentration-dependent plots. Reprinted with permission from Ref 55. Copyright 2012 WILEY-VCH Verlag GmbH & Co.

engineered to contain an extracellular influenza hemagglutinin peptide tag, which can be specifically recognized by the anti-hemagglutinin antibody, and then overexpressed in human osteosarcoma (U2OS) cells. In turn, the hemagglutinin antibody was covalently conjugated to the central QD scaffold via SMCC methodology to enable specific, passive labeling of the membrane receptors. When exposed to a selective κ -OR agonist, QD-bound receptors underwent acute endocytosis within 30 minutes of agonist application. Intracellular accumulation of QD-receptor complexes was monitored using an automated fluorescence microscope system (Operetta, PerkinElmer, USA), and the obtained dose-response curves were used to quantify agonist potency. This report illustrates how a combination of a QD-

based screening platform with an automated fluorescence imaging system represents a promising platform for further drug-screening applications.

A.4. Multiplexed Quantum Dot-Based Biosensing via Förster Resonance Energy Transfer

The ability of the QD nanoscaffold to accommodate multiple copies of biomolecular probes and form multivalent, multimodal constructs has been actively exploited in the field of biosensing. As a biosensor, QD no longer acts as a passive, persistently “on” tag; instead, it participates in a signal transduction cascade via Förster resonance energy transfer (FRET) or charge transfer (CT), whereby QD emission intensity is modulated in the presence of appropriate donor/acceptor molecules.⁷ FRET has become a dominant mechanism for QD-based biosensing, as it is rigorously characterized and exploits key advantages of QDs over traditional fluorophores: (i) high quantum yields and large molar extinction coefficients that maximize FRET, (ii) narrow, size-tunable emission spectra and broad excitation spectra that allow multicolor sensor configurations and minimize spectral cross-talk, and (iii) multivalent presentation of donors/acceptors on the central QD scaffold that directly enhances FRET efficiency. As such, QDs are ideal FRET donors, and the typical QD-FRET configuration includes an organic dye molecule serving as the acceptor fluorophore. Such QD-dye FRET pairs have been successfully employed by many groups to sense nucleic acid hybridization, detect the presence of ions/analytes in solution, monitor proteolytic enzyme activity, and assess competitive receptor binding kinetics.⁵⁶⁻⁶³ Until recently, QD use as the acceptor has been limited, as it is difficult to circumvent direct optical excitation of QDs due to their broad absorption spectra and large molar extinction coefficients. Another complicating factor is the long-lived (>10 ns) excited state of QDs compared to that of conventional

molecular fluorophores (<5 ns).²³ One elegant solution to this challenge has been the use of luminescent lanthanide ion donors with millisecond excited state lifetimes.⁶⁴ Furthermore, lanthanide-QD FRET pairs are characterized by excellent FRET efficiency and large Förster radii (~10 nm). Incorporation of the lanthanide ions into the biosensor architecture enables efficient energy transfer to the QD acceptor after the QD excited state is allowed to decay following direct optical excitation. Taking advantage of the compatibility of excited state lifetimes of QDs, dyes, and lanthanides, it has become possible to assemble multistep QD/dye/lanthanide FRET relays around the central QD nanoscaffold, whereby QD core functions as both a FRET donor and acceptor (Figure A.6).⁶⁵⁻⁶⁸ Recently, Algar *et al.* reported

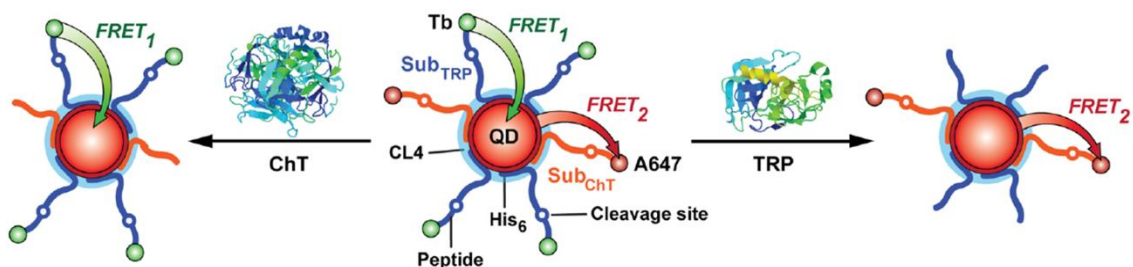


Figure A.6. Schematic of a time-gated FRET relay for multiplexed protease sensing. A central CdSe/ZnS core/shell Qdot is coated with compact zwitterionic ligands (CL4) and assembled with polyhistidine (His6)-appended peptide substrates. The peptides, labeled with either Tb lanthanide or Alexa647 dye, serve as substrates, SubTRP and SubChT, for trypsin (TRP) and chymotrypsin (ChT) proteolytic enzymes, respectively. The cleavage sites are highlighted in the peptide sequences. Proteolytic activity disengages FRET₁ and FRET₂ pathways and alters the prompt/gated photoluminescence ratios, which are used as analytical signals. Reprinted with permission from Ref 66. Copyright 2012 American Chemical Society.

the use of QDs as a time-gated FRET relay intermediary to achieve multiplexed, spectrotemporal detection of proteolytic and nucleic acid binding events.^{66, 67} In a prototypical architecture, multiple copies of Tb³⁺ ions and AlexaFluor dyes are concentrically assembled around the QD nanoscaffold. Tb-to-QD time-gated FRET pathway 1 (FRET₁) and QD-to-AlexaFluor FRET pathway 2 (FRET₂) serve as sensors of parallel, independent binding events. In contrast to previous multiplexed QD formats which rely on several colors

of QDs, binding event information in this configuration is derived from two independent FRET processes and provides the unprecedented ability to simultaneously monitor several biological processes using a single color of QD, a significant advancement in the field of nanoparticle-based biosensing.

A.5. Conclusion and Future Outlook

Recent advances in bioconjugation and bioorthogonal chemistry will considerably improve the utilization of the large QD surface area, wherein the QD serves as the central nanoscaffold for the multivalent assembly of multifunctional biomolecular probes in a concentric fashion. Such QD surface functionalization versatility combined with reduced size and compact amphiphilic surfactants is the reason multiplexed biosensing of intracellular signaling cascades is a swiftly approaching reality. As advanced, high-content imaging systems are becoming increasingly commercially available and users are adopting QD technology globally, QD-based drug screening and multiplexed biosensing have the potential to revolutionize the early stages of the drug discovery process. Furthermore, with recent breakthroughs in microfluidic technology, it is no longer merely a fruit of imagination that QD-based lab-on-a-chip devices will be routinely used for point-of-care diagnostics. Nevertheless, the most pressing issues currently hindering widespread QD use are (i) batch-to-batch variability in the preparation of application-ready QD constructs, (ii) limited QD probe reusability, as most documented applications are conducted in bulk solutions, (iii) potential toxicity concerns associated with QD core constituent materials, and (iv) a relatively high cost of quantum dot synthesis. Efforts are under way to overcome these significant challenges and develop a new generation of low-cost, non-toxic, reproducible, and reusable QD-based drug screening assays and bioanalytical sensing technologies.

A.6. References

- (1) W. C. Chan, and S. Nie, *Science*, 1998, 281, 2016-2018.
- (2) M. Bruchez, Jr., M. Moronne, P. Gin, S. Weiss and A. P. Alivisatos, *Science*, 1998, 281, 2013-2016.
- (3) A. P. Alivisatos, W. Gu and C. Larabell, *Annu Rev Biomed Eng*, 2005, 7, 55-76.
- (4) I. L. Medintz, H. T. Uyeda, E. R. Goldman and H. Mattoussi, *Nat Mater*, 2005, 4, 435-446.
- (5) S. J. Rosenthal, J. C. Chang, O. Kovtun, J. R. McBride and I. D. Tomlinson, *Chemistry & Biology*, 2011, 18, 10-24.
- (6) F. Pinaud, S. Clarke, A. Sittner and M. Dahan, *Nat Meth*, 2010, 7, 275-285.
- (7) I. L. Medintz and H. Mattoussi, *Phys Chem Chem Phys*, 2009, 11, 17-45.
- (8) X. Michalet, F. F. Pinaud, L. A. Bentolila, J. M. Tsay, S. Doose, J. J. Li, G. Sundaresan, A. M. Wu, S. S. Gambhir and S. Weiss, *Science*, 2005, 307, 538 - 544.
- (9) J. Delehanty, H. Mattoussi and I. Medintz, *Analytical and Bioanalytical Chemistry*, 2009, 393, 1091-1105.
- (10) J. C. Chang, O. Kovtun, R. D. Blakely and S. J. Rosenthal, *Wiley Interdisciplinary Reviews: Nanomedicine and Nanobiotechnology*, 2012, 4, 605-619.
- (11) M. Dahan, S. Levi, C. Luccardini, P. Rostaing, B. Riveau and A. Triller, *Science*, 2003, 302, 442-445.
- (12) H. Tada, H. Higuchi, T. M. Wanatabe and N. Ohuchi, *Cancer Research*, 2007, 67, 1138-1144.
- (13) S. Courty, C. Luccardini, Y. Bellaiche, G. Cappello and M. Dahan, *Nano Letters*, 2006, 6, 1491-1495.
- (14) X. Gao, Y. Cui, R. M. Levenson, L. W. K. Chung and S. Nie, *Nat Biotech*, 2004, 22, 969-976.
- (15) B. Cui, C. Wu, L. Chen, A. Ramirez, E. L. Bearer, W.-P. Li, W. C. Mobley and S. Chu, *Proceedings of the National Academy of Sciences*, 2007, 104, 13666-13671.
- (16) D. S. Lidke, P. Nagy, R. Heintzmann, D. J. Arndt-Jovin, J. N. Post, H. E. Grecco, E. A. Jares-Erijman and T. M. Jovin, *Nat Biotech*, 2004, 22, 198-203.
- (17) X. Wu, H. Liu, J. Liu, K. N. Haley, J. A. Treadway, J. P. Larson, N. Ge, F. Peale and M. P. Bruchez, *Nat Biotech*, 2003, 21, 41-46.
- (18) D. R. Larson, W. R. Zipfel, R. M. Williams, S. W. Clark, M. P. Bruchez, F. W. Wise and W. W. Webb, *Science*, 2003, 300, 1434-1436.
- (19) B. R. Smith, Z. Cheng, A. De, A. L. Koh, R. Sinclair and S. S. Gambhir, *Nano Lett*, 2008, 8, 2599-2606.
- (20) P. Zrazhevskiy and X. Gao, *Nat Commun*, 2013, 4, 1619.
- (21) S. J. Rosenthal, J. McBride, S. J. Pennycook and L. C. Feldman, *Surface Science Reports*, 2007, 62, 111-157.
- (22) J. McBride, J. Treadway, L. C. Feldman, S. J. Pennycook and S. J. Rosenthal, *Nano Letters*, 2006, 6, 1496-1501.
- (23) U. Resch-Genger, M. Grabolle, S. Cavaliere-Jaricot, R. Nitschke and T. Nann, *Nat Meth*, 2008, 5, 763-775.
- (24) W. R. Algar, K. Susumu, J. B. Delehanty and I. L. Medintz, *Analytical Chemistry*, 2011, 83, 8826-8837.
- (25) P. K. Chattopadhyay, D. A. Price, T. F. Harper, M. R. Betts, J. Yu, E. Gostick, S. P. Perfetto, P. Goepfert, R. A. Koup, S. C. De Rosa, M. P. Bruchez and M. Roederer, *Nat Med*, 2006, 12, 972-977.

- (26) W. R. Algar, D. E. Prasuhn, M. H. Stewart, T. L. Jennings, J. B. Blanco-Canosa, P. E. Dawson and I. L. Medintz, *Bioconjugate Chemistry*, 2011, 22, 825-858.
- (27) B. O. Dabbousi, J. Rodriguez-Viejo, F. V. Mikulec, J. R. Heine, H. Mattoussi, R. Ober, K. F. Jensen and M. G. Bawendi, *The Journal of Physical Chemistry B*, 1997, 101, 9463-9475.
- (28) C. B. Murray, D. J. Norris and M. G. Bawendi, *Journal of the American Chemical Society*, 1993, 115, 8706-8715.
- (29) M. A. Hines and P. Guyot-Sionnest, *The Journal of Physical Chemistry*, 1996, 100, 468-471.
- (30) E. L. Bentzen, I. D. Tomlinson, J. Mason, P. Gresch, M. R. Warnement, D. Wright, E. Sanders-Bush, R. Blakely and S. J. Rosenthal, *Bioconjugate Chemistry*, 2005, 16, 1488-1494.
- (31) A. F. Hezinger, J. Tessmar and A. Gopferich, *Eur J Pharm Biopharm*, 2008, 68, 138-152.
- (32) T. Pellegrino, L. Manna, S. Kudara, T. Liedl, D. Koktysh, A. L. Rogach, S. Keller, J. Randler, G. Natile and W. J. Parak, *Nano Letters*, 2004, 4, 703-707.
- (33) X. Gao, Y. Cui, R. M. Levenson, L. W. K. Chung and S. Nie, *Nat Biotech*, 2004, 22, 969-976.
- (34) E. R. Goldman, E. D. Balighian, H. Mattoussi, M. K. Kuno, J. M. Mauro, P. T. Tran and G. P. Anderson, *Journal of the American Chemical Society*, 2002, 124, 6378-6382.
- (35) P. C. Weber, D. H. Ohlendorf, J. J. Wendoloski and F. R. Salemme, *Science*, 1989, 243, 85-88.
- (36) S. Kim and M. G. Bawendi, *Journal of the American Chemical Society*, 2003, 125, 14652-14653.
- (37) S. J. Rosenthal, I. Tomlinson, E. M. Adkins, S. Schroeter, S. Adams, L. Swafford, J. McBride, Y. Wang, L. J. DeFelice and R. D. Blakely, *Journal of the American Chemical Society*, 2002, 124, 4586-4594.
- (38) I. D. Tomlinson, J. N. Mason, R. D. Blakely and S. J. Rosenthal, *Bioorganic & Medicinal Chemistry Letters*, 2005, 15, 5307-5310.
- (39) H. A. Gussin, I. D. Tomlinson, D. M. Little, M. R. Warnement, H. Qian, S. J. Rosenthal and D. R. Pepperberg, *Journal of the American Chemical Society*, 2006, 128, 15701-15713.
- (40) I. D. Tomlinson, J. N. Mason, R. D. Blakely and S. J. Rosenthal, *Bioorganic & Medicinal Chemistry Letters*, 2006, 16, 4664-4667.
- (41) I. D. Tomlinson, J. Chang, H. Iwamoto, L. J. D. Felice, R. D. Blakely and S. J. Rosenthal, *Targeting the human serotonin transporter (hSERT) with quantum dots*, SPIE, 2008.
- (42) O. Kovtun, I. D. Tomlinson, D. S. Sakrikar, J. C. Chang, R. D. Blakely and S. J. Rosenthal, *ACS Chemical Neuroscience*, 2011, 2, 370-378.
- (43) I. D. Tomlinson, H. Iwamoto, R. D. Blakely and S. J. Rosenthal, *Bioorganic & Medicinal Chemistry Letters*, 2011, 21, 1678-1682.
- (44) J. C. Chang, I. D. Tomlinson, M. R. Warnement, H. Iwamoto, L. J. DeFelice, R. D. Blakely and S. J. Rosenthal, *Journal of the American Chemical Society*, 2011, 133, 17528-17531.
- (45) O. Kovtun, E. J. Ross, I. D. Tomlinson and S. J. Rosenthal, *Chemical Communications*, 2012, 48, 5428-5430.

- (46) J. C. Chang, I. D. Tomlinson, M. R. Warnement, A. Ustione, A. M. D. Carneiro, D. W. Piston, R. D. Blakely and S. J. Rosenthal, *The Journal of Neuroscience*, 2012, 32, 8919-8929.
- (47) M. Howarth, D. J-F Chinnapen, K. Grove, P.C Dorrestein, M.R Grandy, N. L. Kelleher, A. El-Husseini and A.Y Ting, *Nature Methods*, 2006, 3, 267 – 273.
- (48) M. Howarth and A.Y Ting, *Nature Protocols*, 2008, 3, 534-545.
- (49) U. D. McCann, D. F. Wong, F. Yokoi, V. Villemagne, R. F. Dannals and G. A. Ricaurte, *J Neurosci*, 1998, 18, 8417-8422.
- (50) D. D. Dougherty, A. A. Bonab, T. J. Spencer, S. L. Rauch, B. K. Madras and A. J. Fischman, *The Lancet*, 1999, 354, 2132-2133.
- (51) C. Saunders, J. V. Ferrer, L. Shi, J. Chen, G. Merrill, M. E. Lamb, L. M. F. Leeb-Lundberg, L. Carvelli, J. A. Javitch and A. Galli, *Proceedings of the National Academy of Sciences*, 2000, 97, 6850-6855.
- (52) D. J. Brunswick, J. D. Amsterdam, P. D. Mozley and A. Newberg, *American Journal of Psychiatry*, 2003, 160, 1836-1841.
- (53) M. A. Kurian, J. Zhen, S.-Y. Cheng, Y. Li, S. R. Mordekar, P. Jardine, N. V. Morgan, E. Meyer, L. Tee, S. Pasha, E. Wassmer, S. J. R. Heales, P. Gissen, M. E. A. Reith and E. R. Maher, *The Journal of Clinical Investigation*, 2009, 119, 1595-1603.
- (54) D. Sakrikar, M. S. Mazei-Robison, M. A. Mergy, N. W. Richtand, Q. Han, P. J. Hamilton, E. Bowton, A. Galli, J. Veenstra-VanderWeele, M. Gill and R. D. Blakely, *The Journal of Neuroscience*, 2012, 32, 5385-5397.
- (55) J. Lee, Y.-J. Kwon, Y. Choi, H. C. Kim, K. Kim, J. Kim, S. Park and R. Song, *ChemBioChem*, 2012, 13, 1503-1508.
- (56) C.-Y. Zhang, H.-C. Yeh, M. T. Kuroki and T.-H. Wang, *Nat Mater*, 2005, 4, 826-831.
- (57) I. L. Medintz, A. R. Clapp, H. Mattoussi, E. R. Goldman, B. Fisher and J. M. Mauro, *Nat Mater*, 2003, 2, 630-638.
- (58) R. Gill, I. Willner, I. Shweky and U. Banin, *The Journal of Physical Chemistry B*, 2005, 109, 23715-23719.
- (59) R. Bakalova, H. Ohba, Z. Zhelev, T. Nagase, R. Jose, M. Ishikawa and Y. Baba, *Nano Letters*, 2004, 4, 1567-1573.
- (60) T. Pons, I. L. Medintz, X. Wang, D. S. English and H. Mattoussi, *Journal of the American Chemical Society*, 2006, 128, 15324-15331.
- (61) C. Y. Zhang and L. W. Johnson, *J Am Chem Soc*, 2006, 128, 5324-5325.
- (62) K. Boeneman, B. C. Mei, A. M. Dennis, G. Bao, J. R. Deschamps, H. Mattoussi and I. L. Medintz, *Journal of the American Chemical Society*, 2009, 131, 3828-3829.
- (63) J. B. Delehanty, C. E. Bradburne, K. Susumu, K. Boeneman, B. C. Mei, D. Farrell, J. B. Blanco-Canosa, P. E. Dawson, H. Mattoussi and I. L. Medintz, *Journal of the American Chemical Society*, 2011, 133, 10482-10489.
- (64) D. Geißler, L. J. Charbonnière, R. F. Ziessel, N. G. Butlin, H.-G. Löhmannsröben and N. Hildebrandt, *Angewandte Chemie International Edition*, 2010, 49, 1396-1401.
- (65) W. R. Algar, M. G. Ancona, A. P. Malanoski, K. Susumu and I. L. Medintz, *ACS Nano*, 2012, 6, 11044-11058.
- (66) W. R. Algar, A. P. Malanoski, K. Susumu, M. H. Stewart, N. Hildebrandt and I. L. Medintz, *Analytical Chemistry*, 2012, 84, 10136-10146.
- (67) W. R. Algar, D. Wegner, A. L. Huston, J. B. Blanco-Canosa, M. H. Stewart, A. Armstrong, P. E. Dawson, N. Hildebrandt and I. L. Medintz, *Journal of the American Chemical Society*, 2012, 134, 1876-1891.

- (68) D. Geißler, S. Stufler, H.-G. Löhmannsröben and N. Hildebrandt, *Journal of the American Chemical Society*, 2012, 135, 1102-1109.
- (69) V. Pardo-Yissar, E. Katz, J. Wasserman and I. Willner, *Journal of the American Chemical Society*, 2002, 125, 622-623.
- (70) R. Gill, L. Bahshi, R. Freeman and I. Willner, *Angewandte Chemie International Edition*, 2008, 47, 1676-1679.
- (71) J. Liu, J. H. Lee and Y. Lu, *Analytical Chemistry*, 2007, 79, 4120-4125.
- (72) Z.-M. Zhou, Y. Yu and Y.-D. Zhao, *Analyst*, 2012, 137, 4262-4266.
- (73) Z. Chen, G. Li, L. Zhang, J. Jiang, Z. Li, Z. Peng and L. Deng, *Analytical and Bioanalytical Chemistry*, 2008, 392, 1185-1188.
- (74) Y. Choi, Y. Cho, M. Kim, R. Grailhe and R. Song, *Analytical Chemistry*, 2012, 84, 8595-8601.
- (75) K. E. Sapsford, J. Granek, J. R. Deschamps, K. Boeneman, J. B. Blanco-Canosa, P. E. Dawson, K. Susumu, M. H. Stewart and I. L. Medintz, *ACS Nano*, 2011, 5, 2687-2699.
- (76) D. E. Prasuhn, A. Feltz, J. B. Blanco-Canosa, K. Susumu, M. H. Stewart, B. C. Mei, A. V. Yakovlev, C. Loukou, J.-M. Mallet, M. Oheim, P. E. Dawson and I. L. Medintz, *ACS Nano*, 2010, 4, 5487-5497.
- (77) I. L. Medintz, A. R. Clapp, F. M. Brunel, T. Tiefenbrunn, H. Tetsuo Uyeda, E. L. Chang, J. R. Deschamps, P. E. Dawson and H. Mattoussi, *Nat Mater*, 2006, 5, 581-589.
- (78) K. Boeneman, B. C. Mei, A. M. Dennis, G. Bao, J. R. Deschamps, H. Mattoussi and I. L. Medintz, *Journal of the American Chemical Society*, 2009, 131, 3828-3829.
- (79) M. Suzuki, Y. Husimi, H. Komatsu, K. Suzuki and K. T. Douglas, *Journal of the American Chemical Society*, 2008, 130, 5720-5725.
- (80) C.-y. Zhang and L. W. Johnson, *Analytical Chemistry*, 2009, 81, 3051-3055.
- (81) R. Cui, Y.-P. Gu, L. Bao, J.-Y. Zhao, B.-P. Qi, Z.-L. Zhang, Z.-X. Xie and D.-W. Pang, *Analytical Chemistry*, 2012, 84, 8932-8935.
- (82) W. Ma, L.-X. Qin, F.-T. Liu, Z. Gu, J. Wang, Z. G. Pan, T. D. James and Y.-T. Long, *Sci. Rep.*, 2013, 3.
- (83) D.-W. Li, L.-X. Qin, Y. Li, R. P. Nia, Y.-T. Long and H.-Y. Chen, *Chemical Communications*, 2011, 47, 8539-8541.
- (84) J. M. Ingram, C. Zhang, J. Xu and S. J. Schiff, *Journal of Neuroscience Methods*, 2013, 214, 45-51.